THE ROLE OF INSIG-MEDIATED CHOLESTEROL HOMEOSTASIS IN

MOUSE HAIR DEVELOPMENT

APPROVED BY SUPERVISORY COMMITTEE

Michael Brown, M.D.
Joseph Goldstein, M.D.
Luis Parada, Ph.D
Melanie Cobb, Ph.D.
Andrew Zinn, M.D., Ph.D.

DEDICATION

To those who took the time to teach me, I thank you

THE ROLE OF INSIG-MEDIATED CHOLESTEROL HOMEOSTASIS IN MOUSE HAIR DEVELOPMENT

by

MIDHAT SALEEM FAROOQI

DISSERTATION

Presented to the Faculty of the Graduate School of Biomedical Sciences

The University of Texas Southwestern Medical Center at Dallas

In Partial Fulfillment of the Requirements

For the Degree of

DOCTOR OF PHILOSOPHY

The University of Texas Southwestern Medical Center at Dallas

Dallas, Texas

May, 2012

THE ROLE OF INSIG-MEDIATED CHOLESTEROL HOMEOSTASIS IN MOUSE HAIR DEVELOPMENT

MIDHAT SALEEM FAROOQI

The University of Texas Southwestern Medical Center at Dallas, 2012

MICHAEL BROWN, M.D. & JOSEPH GOLDSTEIN, M.D.

Insig-1 and Insig-2, two very homologous proteins, are indispensable for feedback inhibition of cholesterol biosynthesis. Mice null for both Insigs drastically overproduce cholesterol and its precursor sterol intermediates and exhibit many developmental abnormalities such as cleft palate. In this work, we generate and characterize a line of mice lacking both Insigs in the hair and skin. These epidermal-specific, Insig-double knockout mice have many skin abnormalities, but their most striking defect is a complete lack of body hair. Epidermal-specific, Insig-double knockout mice also have a significant buildup of cholesterol precursors in skin, as they are unable to check endogenous cholesterol production. However, topical treatment of these mutant

mice with simvastatin, an inhibitor of cholesterol biosynthesis, can reduce these sterol intermediates and completely correct the skin defects and alopecia.

Further studies of epidermal-specific, Insig-double knockout mice showed that they had a dramatic decrease in the expression of many keratin-associated proteins relative to their control littermates. In the case of certain keratin-associated proteins, this loss of mRNA was especially severe; keratin-associated protein 28-13 expression, for example, was reduced by more than twenty-fold. Electron microscopy revealed that the hair shafts of mutant mice had grossly abnormal cuticles, and topical treatment of mutant mice with simvastatin rescued keratin-associated protein expression. We conclude that epidermal-specific, Insig-double knockout mice have a hair eruption defect due to improper formation of the hair shaft cuticle likely caused by a lack of keratin-associated protein expression. These findings are relevant to the multiple skin and hair abnormalities seen in human diseases where sterol precursors accumulate due to inborn errors in cholesterol biosynthesis.

TABLE OF CONTENTS

DEDICATION ii

ABSTRACT iv

PRIOR PUBLICATIONS vii

LIST OF FIGURES viii

LIST OF TABLES x

LIST OF DEFINITIONS xi

CHAPTER ONE 1

Introduction

CHAPTER TWO 36

Hair Growth Defects in Insig-Deficient Mice Caused by Cholesterol Precursor Accumulation and Reversed by Simvastatin

CHAPTER THREE 63

Alopecia in Insig-deficient Mice Preceded by Loss of Keratin-associated Protein mRNA Expression and Abnormal Hair Cuticle Formation

CHAPTER FOUR 96

Conclusion

BIBLIOGRAPHY 104

PRIOR PUBLICATIONS

Schneider JW, Gao Z, Li S, Farooqi M, Tang TS, Bezprozvanny I, Frantz DE, Hsieh J (2008) Small-molecule activation of neuronal cell fate. Nat Chem Biol 4:408-410.

LIST OF FIGURES

FIGURES: CHAPTER ONE 28

FIGURE 1-1 Inborn Errors of Cholesterol Metabolism 28

FIGURE 1-2 The SREBP Proteolytic Pathway 29

FIGURE 1-3 The Degradation of HMG-CoA Reductase 30

FIGURE 1-4 The Effects of Insig Loss 31

FIGURE 1-5 Types of Mouse Coat Hair 32

FIGURE 1-6 The Hair Follicle and its Layers 33

FIGURE 1-7 Follicular morphogenesis 34

FIGURE 1-8 The Hair Cycle 35

FIGURES: CHAPTER TWO 55

FIGURE 2-1 Generation of mice lacking *Insigs* in the epidermis 55

FIGURE 2-2 Gross morphology of control and Epi-*Insig*-DKO mice 56

FIGURE 2-3 Histology of skin from control and Epi-*Insig*-DKO mice 57

FIGURE 2-4 Hair follicle morphogenesis and cycling in control and Epi-*Insig*-DKO mice 58

FIGURE 2-5 Staining of lipids and immunological visualization of HMG-CoA reductase in skin from control and Epi-*Insig*-DKO mice 59

FIGURE 2-6 Sterol content in the skin of control and Epi-*Insig*-DKO mice treated with or without simvastatin 60

FIGURE 2-7 Gross morphology and histology of control and Epi-*Insig*-DKO mice treated with or without simvastatin 61

FIGURE 2-8 Morphology and skin sterol content of control and Epi-*Insig*-DKO mice at 3 and 5.5 months after stopping simvastatin 62

FIGURES: CHAPTER THREE 84

FIGURE 3-1 Loss of expression of *Insig-1* mRNA and protein 84

FIGURE 3-2 Overall appearance of control and Epi-*Insig*-DKO mice 85

FIGURE 3-3 Proliferation and apoptosis of hair follicle cells 86

FIGURE 3-4 *In situ* hybridization of *Sonic hedgehog* mRNA 89

FIGURE 3-5 mRNA expression of different Krtap family members 91

FIGURE 3-6 Transmission electron microscopy of hair follicles 92

FIGURE 3-7 Scanning electron microscopy of hair follicles 93

FIGURE 3-8 Sterol content in the skin of control and Epi-*Insig*-DKO mice 94

FIGURE 3-9 mRNA expression of different Krtap family members in control and Epi-*Insig*-DKO mice treated with or without simvastatin 95

FIGURES: CHAPTER FOUR 101

FIGURE 4-1 RORα does not transactivate Krtap5 family promoters linked to luciferase *in vitro* 101

FIGURE 4-2 Insig-deficiency does not affect the transcriptional activity of RORα *in vitro* 102

FIGURE 4-3 Select metabolic parameters of control and Epi-*Insig*-DKO mice ... 103

LIST OF TABLES

TABLES: CHAPTER THREE 87

TABLE 3-1 mRNA Levels of Developmental Pathway Genes in Epi-*Insig*-DKO Mice Relative to Control Mice, Fold Change 87

TABLE 3-2 mRNA Levels of Developmental Pathway Genes in Epi-*Insig*-DKO Mice Relative to Control Mice, C_T Values 88

TABLE 3-3 List of Genes Down-regulated in the Skin of Epi-*Insig*-DKO Mice Versus Control Mice 90

LIST OF DEFINITIONS

18-MEA – 18-methylecosanoic acid

bHLH-Zip – Basic helix-loop-helix–leucine zipper

CDPX2 – Chondrodysplasia punctata, X-linked dominant, type 2

CHILD syndrome – Congenital hemidysplasia, icthyosiform erythroderma, and limb defects

Ce – Cuticle (of the inner root sheath)

Co – Cortex (of the hair shaft)

Cu – Cuticle (of the hair shaft)

CoA – Coenzyme A

CTS – Connective tissue sheath

DP – Dermal papilla

Dpc – Days post coitum

EM – Electron microscopy

ER – endoplasmic reticulum

ERAD – ER-associated degradation

Epi-*Insig*-DKO – epidermal-specific, Insig-double knockout

GC-MS – Gas chromatography-mass spectroscopy

He – Henle's layer

HIDS – Hyperimmunoglobulinemia D syndrome

HMG-CoA – 3-hydroxy-3-methylglutaryl-CoA

Hx – Huxley's layer

Insig-DKO – *Insig*-double knockout

Insig-1$^{f/f}$ – Floxed *Insig-1*

Insig-2$^{-/-}$ – Null *Insig-2*

IRS – Inner root sheath

K14-Cre – Keratin14-Cre

Krtap – keratin-associated proteins

LDL – low-density lipoprotein

ORS – Outer root sheath

PFA – Paraformaldehyde

PND – Postnatal day

RIP – Regulated intramembrane proteolysis

RORα – Retinoic acid receptor-related orphan receptor α

S1P – Site-1 protease

S2P – Site-2 protease

SEM – Standard error of the mean

Shh – Sonic Hedgehog

SLOS – Smith-Lemli-Opitz syndrome

SRE – Sterol regulatory element

SREBP – Sterol regulatory element-binding protein

SSD – Sterol-sensing domain

TEM – Transmission electron microscopy

tRNA – transfer RNAs

TUNEL – Terminal deoxynucleotidyl transferase dUTP nick end labeling

VCP – Valosin-containing protein

CHAPTER ONE
Introduction

SECTION ONE

Mammalian Cholesterol Homeostasis

On Cholesterol

In the late 18th century, a French chemist by the name of François Poulletier de la Salle identified a firm, waxy substance present in human gallstones; a finding replicated a few years later by Antoine François de Fourcroy (McNamara *et al.*, 2006). However, it was not until 1816, when this compound came under the study of one of their fellow countrymen, Michel-Eugène Chevreul, that a recognizable name was given to it: 'cholesterine', using the Greek words for bile, *cholē*, and solid, *stereos*. It was only when Marcellin Pierre Eugène Berthelot demonstrated some forty years later that cholesterine was, in fact, an alcohol that the name of this substance changed to the one widely known today: cholesterol.

Since then, cholesterol has become both famous and infamous for its role in mammalian life. An excess of cholesterol is almost certain to lead to cardiovascular disease, the primary cause of death worldwide (Mathers and Loncar, 2006). However, it also serves as the starting point for the synthesis of bile acids, oxysterols, and steroid hormones; it modulates the function of hedgehog proteins, a family of signaling molecules essential to development; and it is a critical component of mammalian cell membranes, needed to maintain their permeability and fluidity (Kelley and Herman, 2001; Espenshade and Hughes, 2007). As such, all nucleated mammalian cells synthesize

cholesterol, and this process is one of those most intensely regulated in all biology (Brown and Goldstein, 2009).

On Cholesterol Biosynthesis

Cholesterol, formally termed (3β)-cholest-5-en-3-ol, is composed of twenty-seven carbons, forty-six hydrogens, and one oxygen molecule (Panico and International Union of Pure and Applied Chemistry, 1993). Of note, all of the carbons in cholesterol can be traced back to a simple precursor: acetate; and it is with this substrate that cholesterol biosynthesis begins (Murray *et al.*, 2006).

First, two molecules of acetyl-Coenzyme A (-CoA) condense to form acetoacetyl-CoA, which then combines with a third acetyl-CoA to produce 3-hydroxy-3-methylglutaryl-CoA (HMG-CoA). Next, the enzyme HMG-CoA reductase reduces HMG-CoA to generate mevalonate. This reaction in the cholesterol biosynthetic pathway is important for four reasons: first, it is the rate-limiting step for the whole process; second, it is irreversible; third, it is where much of the overall feedback inhibition for the pathway occurs; and fourth, it is the site of action for statins, a class of drugs that are competitive inhibitors of HMG-CoA reductase, e.g., compactin (Endo, 2010).

Once formed, mevalonate is sequentially phosphorylated thrice in a series of ATP-utilizing reactions, then decarboxylated to ultimately yield the five-carbon (C_5) compound called isopentenyl diphosphate (Murray *et al.*, 2006). This isoprene unit is termed ‘active’ as it can readily polymerize. It begins by combining with its isomer, dimethylallyl diphosphate (C_5), giving rise to geranyl diphosphate (C_{10}). This molecule condenses with another unit of isopentenyl diphosphate to yield farnesyl diphosphate

(C_{15}), which then reacts with itself at the diphosphate end in a tail-to-tail fashion to produce squalene (C_{30}).

These reactions are noteworthy because the precursor isoprenoids they create are used to produce many other important compounds besides cholesterol (Goldstein and Brown, 1990). Isopentenyl diphosphate, for instance, directly modifies adenosine nucleosides in a subset of transfer RNAs (tRNAs) to modulate translational fidelity (Persson *et al.*, 1994). Farnesyl diphosphate serves as the precursor molecule for the synthesis of dolichol, Coenzyme Q_{10} (ubiquinone) and heme A; dolichol being important in the *N*-linked glycosylation of proteins, while the other two are components of the electron transport chain (Goldstein and Brown, 1990).

Farnesyl diphosphate and its derivative geranylgeranyl diphosphate also attach covalently to proteins in a process termed prenylation (Seabra *et al.*, 1993). This modification is especially important to the Rab family of G-proteins, monomeric GTPases involved primarily in vesicle trafficking, as the inability to prenylate Rab leads to progressive retinal degeneration and vision loss, a disease known as choroideremia. Conversely, the blocking of Rab prenylation in osteoclasts is believed to underlie the beneficial effects of nitrogenous bisphosphonates, inhibitors of farnesyl diphosphate synthase, in the treatment of diseases of bone loss like osteoporosis (Buhaescu and Izzedine, 2007).

The final stage of cholesterol biosynthesis begins with the formation of an epoxide group on squalene; a moiety that aids in the subsequent step: the cyclization of squalene to form lanosterol (Murray *et al.*, 2006). A series of reactions then convert lanosterol to cholesterol. Three methyl groups are removed producing zymosterol; the

double bond of the cyclohexene migrates to a different position within the ring yielding desmosterol, and the side chain double bond is reduced to make cholesterol (Bloch, 1965).

These last few steps may also occur in a different order, creating a second set of intermediate sterols (Kelley and Herman, 2001). If the reduction of the side chain double bond occurs first, lanosterol becomes dihydrolanosterol. Subsequently, removal of the three methyl groups forms lathosterol; the creation of a second double bond in the cyclohexene ring yields 7-dehydrocholesterol; and a reduction of the first double bond gives rise to cholesterol. Shown in Figure 1 are both of the chemical routes to cholesterol and the different sterol intermediates generated along the way.

These molecules are not just precursors to cholesterol but have cellular functions in their own right. The dimethyl sterols stimulate meiosis and thus are found at comparatively high levels in gonads (Herman, 2003). In the skin, 7-dehydrocholesterol is directly photolyzed by ultraviolet light, yielding pre-vitamin D_3. Finally, all of these precursor sterols along with cholesterol can be converted to oxysterols, which are potent suppressors of cholesterol biosynthesis and ligands for a sub-family of transcription factors known as nuclear receptors.

Endogenous synthesis of cholesterol is not the only mechanism by which cells maintain adequate levels of this molecule. They can also acquire it from the environment in the form of low-density lipoprotein (LDL) via the LDL receptor, a process known as receptor-mediated endocytosis (Goldstein and Brown, 2009). These two abilities, synthesis and uptake, ensure that cells can maintain proper levels of cholesterol in their membranes. The capacity to take up LDL also helps to compensate for lack of cholesterol

in cases where synthesis cannot occur properly. Though this ability may mitigate some of the adverse consequences of defective cholesterol synthesis, the inability to properly complete certain steps in the cholesterol biosynthetic pathway has severe effects on health and development, which will now be outlined.

On the Inborn Errors of Cholesterol Metabolism

Inherited defects in the enzymes involved in cholesterol biosynthesis result in two types of illnesses: autoinflammatory disorders or 'multiple congenital anomaly / mental retardation' syndromes, depending on which part of the cholesterol biosynthetic pathway is affected (Kelley and Herman, 2001) (Figure 1). Mutations in the first half of the pathway, specifically in the enzyme mevalonate kinase, cause the autoinflammatory disorders: hyperimmunoglobulinemia D syndrome (HIDS) and mevalonic aciduria.

Both of these disorders are, in essence, one disease manifesting at two different levels of severity. HIDS is marked by febrile crises lasting three to seven days recurring once every one or two months; the onset of these symptoms occurs within the first year of the patient's life. Mevalonic aciduria is more severe; the periodic fevers accompanied by psychomotor retardation, dysmorphic features, a 'measles-like' skin rash, anemia, and cataracts. Both groups of patients have elevated levels of polyclonal IgD in their serum, and increased amounts of urinary mevalonic acid.

Mutations in the second half of the pathway, i.e., in the enzymes responsible for the conversion of lanosterol to cholesterol, result in the 'multiple congenital anomaly / mental retardation' syndromes, of which seven are known to date. These human malformation syndromes are all associated with a buildup of sterol precursors (prior to

the enzymatic block) and cholesterol deficiency. They are shown in Figure 1 as well and will be described briefly in the order they occur in the pathway (Porter, 2002; Porter, 2003).

- **Antley-Bixler syndrome** is characterized by craniosynostosis (premature fusion of cranial sutures), ulnar and femoral bowing, renal and genital anomalies, and choanal atresia (obstructed nasal passages). Patients with this syndrome have high levels of lanosterol and dihydrolanosterol due to a defect in lanosterol 14-α-demethylase. Of note, maternal exposure to fluconazole, an antifungal drug that inhibits this same enzyme, causes malformations in an ABS-like pattern.
- **Greenberg dysplasia** is typified by hydrops fetalis (accumulation of fluid, or edema, in parts of the fetus), abnormal calcifications in the larynx and trachea, patchy bone loss giving long bones a "moth-eaten" appearance, and abnormal ossification, occurring to excess in the spine and deficient in the skull. Hence, it is also known as hydrops-ectopic calcification-moth-eaten skeletal dysplasia. Patients with this syndrome have high levels of the first set of dimethyl sterols because of defects in sterol Δ^{14}-reductase.
- **CHILD syndrome** is so named because patients with this disease have congenital hemidysplasia (one side of their body is underdeveloped), ichthyosiform erythroderma (a large patch of very red skin on the affected side of the body with concomitant scaling and hair loss), and limb defects due to deficiencies in C4 sterol decarboxylase; accordingly, dimethyl sterol levels are elevated.

- **Conradi-Hunermann-Happle syndrome** also known as chondrodysplasia punctata, X-linked dominant, type 2 (CDPX2) is somewhat similar to CHILD syndrome. Indeed, mutations in the enzyme causing CDPX2—sterol Δ^8,Δ^7-isomerase—can also cause CHILD syndrome, and both diseases are almost exclusively seen in females. Like patients with CHILD syndrome, CDPX2 patients suffer from icthyosiform erythroderma and patchy alopecia though, in their case, these skin problems are not restricted to one half of the body but occur in a linear, blotchy manner. CDPX2 further differs from CHILD syndrome in that patients develop cataracts. The most characteristic feature of the disease is 'epiphyseal stippling': punctate calcifications found at the ends of long bones.
- **Lathosterolosis,** as the name implies, is a build up of lathosterol due to a defect in lathosterol 5-desaturase. Few patients have been reported with this disease, but those who have it suffer from progressive cholestatic liver disease, deafness, osteoporosis, dysmorphic facial features, and psychomotor retardation.
- **Smith-Lemli-Opitz syndrome** was the first of these syndromes to be described and is by far the most common. Afflicted individuals have very typical craniofacial attributes: ptosis (drooping upper eyelids), small upturned noses, microcephaly (small heads), prominent foreheads, and cleft palate (in half of all patients). Other common malformations seen are atrioventricular septal defects, limb abnormalities, underdeveloped genitalia and kidneys, and structural defects of the central nervous system. Patients also have eczema and display marked photosensitivity. The enzymatic defect is in sterol Δ^7-reductase and, consequently, patients have high levels of 7-dehydrocholesterol.

- **Desmosterolosis** is the last of the known syndromes; to date, only two cases have been reported. Individuals with the disorder have abnormal head sizes, cleft palate, ambiguous genitalia, and heart defects. Cutis aplasia (focal absence of epidermis and hair) and osteosclerosis (increased bone density) have been noted as well. Patients have increased amounts of desmosterol due to poor function of sterol Δ^{24}-reductase.

On the Regulation of Cholesterol Biosynthesis

Since the cholesterol biosynthetic pathway produces so many important metabolites and since aberrant cholesterol biosynthesis has such drastic effects on mammalian development, higher order eukaryotic cells have evolved an intricate system to keep the pathway under control. Enzymes within the pathway can be differentially phosphorylated, transcribed, translated, or degraded depending on cellular conditions; the best illustration of this is HMG-CoA reductase, the rate-limiting enzyme for the entire process (Goldstein and Brown, 1990).

In the short-term, cells can reversibly phosphorylate, and thereby inhibit, HMG-CoA reductase. This event occurs in response to glucagon through the action of AMP-activated protein kinase (Gibson *et al.*, 1982). Furthermore, the enzymatic activity of HMG-CoA reductase in cells can be modulated by both cholesterol and mevalonate; addition of the former (via LDL) decreases HMG-CoA reductase activity by more than 90% (Goldstein and Brown, 1990). This feedback is how the cell balances the amount of cholesterol gained from external sources with that obtained from internal synthesis. However, to completely abolish HMG-CoA reductase activity, one must also add

mevalonate. This dual regulation is necessary because it allows the cell to maintain the synthesis of mevalonate and its nonsterol end-products without producing cholesterol.

In addition, the cell can compensate for abnormal situations, such as when cholesterol and other mevalonate end-products are needed, but HMG-CoA reductase is inhibited unnaturally. When one incubates cells with one such inhibitor, compactin (a statin drug), it results in a two hundred-fold increase in the amount of reductase protein in a few hours! This sharp rise is due to the synergism of multilevel effects; namely, upon compactin addition, reductase protein is degraded five-fold more slowly, its mRNA translated five times as fast, and its gene transcribed eight times as much.

Moreover, the increase in transcription is not limited to HMG-CoA reductase. It also occurs coordinately for the other enzymes in the cholesterol biosynthetic pathway, as well as proteins involved in cholesterol uptake like the LDL receptor (Horton *et al.*, 2002). This rise is achieved through a 10-base pair sequence (5'-ATCACCCCAC-3') that confers regulation of expression by sterols (aptly termed the 'sterol regulatory element' or 'SRE'). It is found in the promoters of all the genes for the proteins mentioned above and can occur one or more times (Smith *et al.*, 1990). The proteins that bind such elements, named sterol regulatory element-binding proteins (SREBPs), are a unique class of transcription factors that serve as master regulators of the genetic network of proteins involved in cholesterol synthesis and uptake (Horton *et al.*, 2002).

On SREBPs

SREBPs are part of the basic helix-loop-helix–leucine zipper (bHLH-Zip) family of transcription factors but differ from the majority of these proteins in two ways. First, a

highly conserved arginine residue found in the DNA-binding region of most bHLH-Zips is instead a tyrosine in SREBPs (Kim *et al.*, 1995). This replacement allows SREBPs to bind the nonpalindromic SRE mentioned above. In contrast, typical binding sites for bHLH transcription factors are palindromic E-boxes ('CANNTG'). A second difference is that SREBPs are tethered to the endoplasmic reticulum (ER) as soon as they are made; i.e., upon synthesis, they are fully capable of activating transcription in the nucleus but unable to get there (Horton *et al.*, 2002).

Each SREBP protein consists of about 1,150 amino acids ordered into three domains: (1) a 480 amino acid DNA-binding bHLH-Zip domain at the amino-terminus; (2) a membrane domain composed of two hydrophobic transmembrane–spanning segments interspaced by a short loop of about thirty hydrophilic amino acids projecting into the ER lumen; and (3) a 590 amino acid regulatory domain at the carboxy-terminus.

Currently, there are two known SREBP genes: *srebp-1* and *srebp-2*. The latter produces the protein SREBP-2 while the former, through the use of two different promoters and alternative splicing, yields two proteins, denoted SREBP-1a and SREBP-1c. These two proteins differ only at their amino-termini, as they arise from different first exons. In the case of SREBP-1a, its first exon encodes a longer transcriptional activation region (in the bHLH-Zip domain), making SREBP-1a a more potent transcription factor than SREBP-1c. Indeed, where SREBP-1c specifically activates transcription of genes essential for fatty acid synthesis and SREBP-2 does so preferentially for genes involved in cholesterol synthesis, SREBP-1a can transcribe both sets of genes with equal efficiency.

Another difference between SREBP-1a and -1c lies in their expression pattern: SREBP-1a is usually only expressed to a significant degree in cultured cell lines (Shimomura *et al.*, 1997). *In vivo*, it is constitutively expressed at low levels in a majority of tissues. SREBP-1c is usually not expressed by cells in culture but predominates in the liver and most other intact tissues. SREBP-2 is expressed equally well both *in vitro* and *in vivo* and, to return to an earlier point, responsible for the coordinated increase in transcription of genes such as HMG-CoA reductase that is seen when cells are incubated with compactin (Horton *et al.*, 2002).

The question then becomes how SREBPs can activate transcription when they are bound to the ER membrane. The answer, shown in Figure 2, is that they undergo a sterol-regulated proteolytic cleavage process controlled by four molecules: Scap, Insig, Site-1 protease (S1P), and Site-2 protease (S2P) (DeBose-Boyd, 2008). All four of these proteins, like SREBPs, are membrane-bound (Goldstein *et al.*, 2006). Scap and Insig even reside in the ER, though the two proteases are found in the Golgi apparatus. Thus, in order to reach S1P and S2P, SREBPs must be transported by Scap from the ER to the Golgi where they are sequentially cleaved in such a way that frees the bHLH-Zip region from the rest of the membrane-embedded molecule. This bHLH-Zip domain can now travel to the nucleus and activate transcription. Insig proteins regulate this cleavage process in a sterol-responsive manner. When cellular sterol levels are high, Insigs bind to Scap and force it to stay in the ER, blocking the ER-to-Golgi migration of SREBPs.

On the SREBP Proteolytic Pathway

Scap (which at one point stood for SREBP-cleavage activating protein) is an integral membrane protein that is about 1,270 amino acids long organized into two domains: one, an amino-terminal hydrophobic domain (~ 730 residues) that spans the ER membrane eight times and two, a carboxy-terminal hydrophilic domain (~ 540 residues) that extends into the cytosol (Nohturfft *et al.*, 1998). The latter is composed of sequences known as WD repeats that are important in protein-protein interactions. Accordingly, the COOH-terminus of Scap interacts with the COOH-terminal regulatory domain of SREBP. At the NH_2-terminus of Scap, transmembrane helices 1-6 form what is known as a 'sterol-sensing domain' (SSD). This region is also present in a few other proteins, notably HMG-CoA reductase; Neimann-Pick type C1 (NPC1), a lysosomal protein; Patched, the receptor for the morphogen Sonic Hedgehog (Shh); Dispatched, the transporter of Shh from inside to outside the cell; and sterol Δ^7-reductase, the enzyme whose mutant form causes Smith-Lemli-Opitz syndrome (Radhakrishnan *et al.*, 2004). Of interest, certain point mutations in the SSD of Scap can render the proteolysis of SREBPs insensitive to regulation by cholesterol.

Scap transports SREBPs to the Golgi apparatus in COPII-coated vesicles, the formation of which is typically dependent on six key proteins: Sec12, Sar-1, the Sec23/Sec24 complex, and the Sec13/Sec31 complex (Sun *et al.*, 2007). Sec12 begins COPII coat formation by exchanging the GDP bound to Sar-1 for GTP. This allows Sar-1 to bind to the ER membrane and recruit the Sec23/Sec24 complex. The latter recognizes the proteins needing to be transported by directly binding to them and promoting their clustering within budding vesicles. In this case, Sec24 recognizes a six residue long sequence known as MELADL (Met–Glu–Leu–Ala–Asp–Leu) found in the loop between

transmembrane helices six and seven of Scap. Addition of the Sec13/Sec31 complex completes the coat, and the SREBP-Scap complex travels to the Golgi apparatus.

Here it meets Site-1 protease, another integral membrane protein roughly 1,050 amino acids long with a single transmembrane helix and a large protease domain that resides in the ER lumen (Espenshade *et al.*, 1999). S1P is a member of the subtilisin superfamily (subtilisin being a serine endopeptidase isolated from *Bacillus subtilis*) and functionally resembles kexin proteases (also known as furins in mammals). Like other furins, S1P is synthesized as a pre-protein that must be cleaved proteolytically in order to be active; in the case of S1P, this process is autocatalytic. However, it also differs from furin proteases in two ways: its substrate recognition and its cellular location (Sakai *et al.*, 1998). S1P cuts SREBP after the amino acid sequence RSVL, whereas furins typically cleave substrates after RX(R/K)R. Moreover, furins usually operate in post-Golgi secretory vesicles whereas S1P works in the earlier Golgi compartments.

Overall, S1P recognizes the Scap-SREBP complex, binds to it, and cuts the luminal hydrophilic loop in between the two transmembrane helices of SREBP. This cleavage separates the NH_2-terminus of SREBP (with its bHLH-Zip domain) from the regulatory COOH-terminus (bound to SCAP), but still leaves the former (termed the intermediate fragment) attached to the membrane. A second protease, termed Site-2 protease (S2P), is required to completely release the bHLH region from the membrane.

Site-2 protease is another integral membrane protein about 520 amino acids in length (Zelenski *et al.*, 1999). Most of the protein is extremely hydrophobic but, interestingly, contains an active site (HEIGH) that identifies it as a zinc metalloprotease (the consensus sequence is HEXXH); usually, this active site is found within hydrophilic

domains in this family of proteases. Even more interestingly, S2P cleaves the intermediate fragment of SREBPs three residues into the transmembrane helix, i.e. the cut occurs within the plane of the membrane. This phenomenon of two sequential cleavages—a primary cut that removes most of the protein followed by a secondary cut that occurs within the membrane—is known as regulated intramembrane proteolysis (RIP) (Brown *et al.*, 2000). This process ultimately frees cytosolic fragments of transmembrane proteins that then enter the nucleus and modulate gene transcription.

In regards to SREBPs, the proteolysis is regulated by sterols, which shut down this process. Fascinatingly, the key point of regulation occurs not at either S1P or S2P, but instead at the exit of the Scap-SREBP complex from the ER. Indeed, if one artificially moves S1P to the ER, proteolysis of SREBPs occurs just as it would in the Golgi; there is no need for Scap-mediated transport, and sterols no longer have the ability to regulate this system (DeBose-Boyd *et al.*, 1999).

This point highlights the importance of Scap and its SSD. Cholesterol blocks the cleavage of SREBPs by binding to the SSD of Scap. This causes Scap to bind to Insigs, which prevents the Scap-SREBP complex from leaving the ER (Radhakrishnan *et al.*, 2004). Interestingly, oxysterols also block RIP of SREBP (and do this even more potently than cholesterol) but do not bind to Scap (Adams *et al.*, 2004; Radhakrishnan *et al.*, 2007). So what, if not Scap, senses oxysterols? The answer: Insig proteins.

On Insigs

Currently, two such proteins are known: Insig-1 and Insig-2 (Goldstein *et al.*, 2006). They are about 260 and 225 amino acids long respectively and both are very

hydrophobic proteins that span the ER membrane six times. The membrane domains of both proteins are very similar (>85%) but some differences come to light when the ends of both proteins are compared: Insig-1, for example, has an NH2-terminus that is 50 amino acids longer than that of Insig-2. The two Insigs differ more strikingly in the regulation of their expression. Insig-1 is an SREBP target gene, which means that its transcription is negatively regulated by sterols. Insig-2 transcription is not dependent on SREBPs and is constitutive (except for in the liver where its mRNA is reduced in response to insulin). In general though, Insigs have redundant functions.

Both proteins bind to Scap when cholesterol is in excess and induce in it a conformational change; this prevents Sec24 from binding to the MELADL sequence and prompts the Insig-Scap-SREBP complex to remain in the ER (Sun *et al.*, 2007). Both cholesterol and oxysterols act in this fashion except that cholesterol binds Scap and prompts it to bind to Insig, whereas oxysterols bind Insig and prompt it to bind to Scap (Radhakrishnan *et al.*, 2007). When sterols are not present, Insigs and Scap do not interact, allowing the Scap-SREBP complex to go to the Golgi (Goldstein *et al.*, 2006).

Remarkably, Insigs also bind to HMG-CoA reductase. This enzyme is also embedded in the membrane of the ER by virtue of a ~340 amino acid long, NH2-terminal domain that forms into eight transmembrane helices interspersed by short loops. The COOH-terminal domain is composed of around 550 amino acids and serves as the catalytic portion of the enzyme. When cells are incubated with sterols, the degradation of HMG-CoA reductase protein is accelerated (Gil *et al.*, 1985). This increase in rate is achieved through the actions of Insig-1, oxysterols, and the sterol intermediate, 24,25-dihydrolanosterol (DeBose-Boyd, 2008).

The breakdown of HMG-CoA reductase protein occurs through an Insig-mediated process termed ER-associated degradation (ERAD) (DeBose-Boyd, 2008). When 24,25-dihydrolanosterol and oxysterols accumulate, they promote Insig-1 binding to HMG-CoA reductase. Once bound, Insig-1 recruits both gp78 and Valosin-containing protein/p97 (hereafter VCP) to this site. Gp78 is the E3 ligase that ubiquitinates HMG-CoA reductase and attaches to Insig-1 directly. VCP on the other hand is an ATPase that recruits proteasomes to the ER membrane (Figure 3); it binds Insig-1 indirectly through gp78.

When cells are incubated with compactin, the decrease in cholesterol, its precursors, and its derivatives promotes the dissociation of Insig-1 from HMG-CoA reductase (Ikeda *et al.*, 2009). In such conditions, Insig is itself ubiquitinated and undergoes ERAD. This is mediated through the same effector proteins gp78 and VCP. Again, gp78 binds Insig-1 directly, while VCP binds indirectly through Ubxd8, a protein not fully characterized.

There are three interesting aspects to the ERAD of Insig-1 and HMG-CoA reductase. The first is that unsaturated fatty acids block Insig-1 binding to Ubxd8·VCP; the second is that oxysterols are ligands for Insig-1 and so their levels can be sensed directly (Radhakrishnan *et al.*, 2007); and the third is that degradation of all reductase molecules does not occur unless a nonsterol mevalonate metabolite (geranylgeraniol) is present as well, guaranteeing that production of mevalonate still continues for necessary nonsterol end-products (Sever *et al.*, 2003).

In summary, Insigs are the focal point in the feedback regulation of the cholesterol biosynthetic pathway (Goldstein *et al.*, 2006). When sterols rise to a sufficient

level in the cell, they trigger binding of Insigs to Scap (and HMG-CoA reductase). This action prevents the escort of SREBPs by Scap to the Golgi; hence, SREBPs cannot be proteolytically cleaved by S1P and S2P and their bHLH-Zip domains remain bound to the membrane. As these domains serve to activate the transcription of all genes involved in the synthesis and uptake of cholesterol, lack of these molecules in the nucleus causes transcription of said genes to decline (Horton *et al.*, 2002). Furthermore, Insigs promote the ubiquitination and ER-associated degradation of the rate-limiting enzyme of the pathway, HMG-CoA reductase. These dual actions of Insigs define them as key regulators of cholesterol homeostasis (Goldstein *et al.*, 2006).

On the Studies of Insigs In Vivo

As many of these discoveries were made in cultured cells, a formal demonstration of Insig function *in vivo* was necessary and came with the generation of a conditional *Insig*-double knockout (Insig-DKO) mouse (Engelking *et al.*, 2005). This strain was homozygous null for *Insig-2* and carried two floxed *Insig-1* alleles, which were removed specifically in the liver by an inducible Cre recombinase. The dramatic effects of Insig loss are shown best in Figure 4. Unable to check the synthesis and uptake of both cholesterol and fatty acids, *Insig*-DKO mice developed severe hepatic steatosis (fatty liver). Immunoblot analysis showed highly elevated levels of HMG-CoA reductase, nuclear SREBP-1c, and nuclear SREBP-2, which were constitutively present even when the animals were fed cholesterol. These findings demonstrate once more the regulatory importance of Insigs. The authors mention in the paper that while germline knockouts of

both *Insig-1* and *Insig-2* alone were viable, double-knockout animals died either *in utero* or at birth; hence, the need for a conditional knockout.

Subsequent investigations into the cause of this lethality led to the discovery that nearly all *Insig*-DKO embryos had craniofacial abnormalities: 52% had cleft palate and 44% had both cleft face and palate (Engelking *et al.*, 2006). As such defects are also present in syndromes arising from inborn errors of cholesterol metabolism, the authors postulated a teratogenic role for sterols in causing the clefting phenotype. Measurement of both cholesterol and sterol intermediates in the palate and maxilla of these embryos (right before palatal fusion occurs) showed that *Insig*-DKO embryos had seven times the amount of sterol precursors than control animals and, surprisingly, equivalent amounts of cholesterol. This finding implied that the craniofacial defects seen in these mice were due to an abnormal amount of sterol intermediates; a notion strengthened by the discovery that facial clefting in *Insig*-DKO mice decreased when pregnant females were treated with lovastatin, another statin that inhibits HMG-CoA reductase.

Ensuing studies tested whether these craniofacial abnormalities could be replicated by removing Insigs solely from the palate. Accordingly, mice lacking both Insigs in palatal epithelial cells or neural crest cells, which make up the palatal mesenchyme, were generated; these studies are discussed in further detail elsewhere (Evers, 2009). Animals lacking Insigs in the palatal epithelium also had both proteins knocked out in the epidermis. These mutant mice had defects in hair growth and will be the subject of this dissertation. Accordingly, a description of the formation and growth of the hair follicle along with the mechanisms underlying this process will now be given.

SECTION TWO

The Development and Growth of the Hair Follicle

On Hair

Hair is a distinguishing feature of mammals (Schneider *et al.*, 2009). More importantly, it serves a wide variety of key functions. Hair plays a role in an animal's physical protection, sensory and tactile abilities, thermoregulation, dispersion of sweat and sebum, camouflage, and social interactions. As such, different types of hair can be found in different regions of an animal. In mice, two examples of specialized hair are vibrissae (whiskers) and eyelashes (Tauchi *et al.*, 2010). Even the pelage (body) hair of mice can be subdivided into four types based on length and curvature: the large guard hairs, the intermediate awl and auchene hairs, and the downy zigzag hairs (Figure 5) (Schlake, 2007). The majority of the coat is composed of zigzag hairs (60-70%), followed by awl hairs (20-30%), then auchene hairs (5-10%), and lastly guard hairs (2-5%) (Fraser, 1951).

Despite these differences, the basic structure underlying hair is nearly always composed of the same key elements: a hair follicle (generator of the hair shaft), a sebaceous gland (important for the eruption of hair from the skin) and an arrector pili muscle (a smooth muscle which 'raises' the hair when contracted); collectively, these structures are called the 'pilosebaceous unit' (Schneider *et al.*, 2009). Of these three, the hair follicle is the most complex. It is comprised of a connective tissue sheath and papilla of dermal origin, pigment-producing cells derived from neural crest cells, as well as three

major concentric cylindrical layers of epithelial origin: the outer root sheath (ORS), inner root sheath (IRS), and hair shaft (Figure 6).

On the Layers of the Hair Follicle

The ORS serves to separate the epithelial layers from the dermis and is contiguous with the epidermis; as such, it is stationary (Morioka, 2004; Bourne and Danielli, 1979). This is not the case with the inner root sheath (IRS). It functions to guide the hair shaft out of the skin and thus grows upwards together with the hair shaft. The movement of the IRS against the ORS is buffered by the intermediate companion layer. The IRS itself is composed of three different cell types: Henle's layer (which gives the IRS structural rigidity), Huxley's layer (which helps to provide nutritive metabolites via the ORS to the hair shaft and compensates for any changes in hair shaft thickness by inversely changing its own width), and the IRS cuticle (which is structured as overlapping scales that interlock with the hair shaft ensuring synchronous movement).

The layer that the IRS cuticle intermeshes with is the cuticle of the hair shaft. Its scales are oriented opposite to the IRS cuticle such that the two together look like mirrored saw teeth (Kiso *et al.*, 2009). Though it serves a joint purpose with the IRS cuticle initially, once the hair has erupted, the cuticle is essential for protecting the remaining two layers of the hair shaft: the cortex (which consists of dead cells filled with keratin and makes up the majority of the hair shaft) and the medulla (which also consists of keratinized cells oriented perpendicular to the cortex and separated by large air spaces (fusi); it further bulks and strengthens the hair shaft) (Morioka, 2004).

The components of the hair follicle that are of dermal origin–namely, the connective tissue sheath (CTS) and papilla–also play a vital role in its growth and development (Yang and Cotsarelis, 2010). The CTS and dermal papilla (DP) are contiguous with one another but separated from the epithelial layers of the hair follicle by a basement membrane. The CTS consists of three layers of collagen fibers as well as fibroblasts, which can usually be found in the middle layer. It is a reservoir of DP cells (specialized fibroblasts) and, in cases of papillary loss or dysfunction, can regenerate the DP. Interestingly, cells in the papilla are not solely mesenchymally-derived, but also of neural crest cell origin. These cells are essential as they induce hair follicle formation from epithelial cells. As such, the dermal papilla is one of the oldest parts of the entire hair follicle, present (albeit, in rudimentary form) since the follicle's very inception.

On Hair Follicle Morphogenesis

Hair follicle development (also known as morphogenesis) begins in the embryo on the 13th embryonic day (e13.0) when the epidermis is fairly undifferentiated, its few layers of epithelial stem cells lying atop the many mesenchymal cells of the dermis (Schmidt-Ullrich and Paus, 2005) (Figure 7). Termed Stage 0, it is the point when various epithelial-mesenchymal interactions coalesce to induce hair follicle formation, though it is unmarked by major histological changes (Paus *et al.*, 1999).

Though it is not known what signal (or gradient field of signals) instructs parts of the epithelial layer to start forming a hair follicle, it is known that canonical Wnt signaling and/or Ectodysplasin function (operating through NFκB) are essential for the initiation of Stage 1 (e14.0) (Schmidt-Ullrich and Paus, 2005). At this stage, one sees the

epidermis thicken at specific regions of hair follicle induction as epithelial cells change their orientation, aligning vertically, and dermal fibroblasts cluster in close proximity to them; this structure is known as the 'hair placode'. Mice with abnormally low Wnt or Eda signaling do not develop hair placodes since such signaling is required to repress the cell-to-cell adhesion molecule, E-cadherin (Jamora *et al.*, 2003). Loss of this protein must occur as it allows the epithelial cells to orient themselves vertically. Nearly as important to hair placode formation and especially to the progression to Stage 2 is the repression of BMP signaling by secreted protein inhibitors such as noggin and follistatin (Botchkarev and Sharov, 2004). Mice lacking these proteins have deficiencies in hair placode formation and arrest partway through Stage 1.

In stage 2 (e15.5), the hair placode begins to grow downward into the dermis in a bud-like shape, still capped by a cluster of dermal cells, termed the 'hair germ' (Paus *et al.*, 1999). The latter continues to elongate and grow, becoming a solid column of epithelial cells known as the 'hair peg'. At this point, the specialized dermal cells collect themselves into a ball and are begun to be enveloped by the hair peg, forming essentially what is named the 'dermal papilla' and marking Stage 3 (e16.5). A molecule important for these stages is Sonic Hedgehog (Shh) as activation of its pathway is critical for proper development of the hair peg (Schmidt-Ullrich and Paus, 2005). Shh signaling is also required for the dermal papilla to organize correctly, as it activates expression of dermal Wnt-5a, necessary for proper papilla growth. As such, mice lacking Shh or essential components of its signaling pathway arrest between Stages 2 and 3 (St-Jacques *et al.*, 1998; Chiang *et al.*, 1999).

In Stage 4 (e17.0), the hair peg encloses the dermal papilla even more and begins to thicken around it, giving the peg a bulb-like appearance (Paus *et al.,* 1999). This bulb is where the majority of the dividing cells in the peg localize; they are known as matrix cells. At this point, these cells are continuously proliferating not only to extend the hair peg downwards, but also to begin the process of differentiation into the different cell layers of the hair follicle upwards. Accordingly, a cone-shaped structure, the IRS, starts to form above the papilla at this stage.

By Stage 5 (e17.5), the IRS extends halfway up the follicle, the dermal papilla is almost completely encased, and the first sebocytes and melanin granules begin to appear (Paus *et al.*, 1999). Since by now the bulb-like form of the hair peg is quite pronounced, Stage 5 is known as the 'bulbous peg' stage. Stage 6 (e18.5) finds the IRS having reached the eventual point of exit for the hair shaft, the now-visible hair canal. At this stage, the sebocytes have organized themselves into a sebaceous gland and the hair follicle has grown to the point where it now lies in the subcutis. Most importantly, the hair follicle finally contains a hair shaft.

In these stages, many different molecules are important to the growth and cell differentiation processes that occur (reviewed in detail here: Schneider *et al.*, 2009). In brief, a transcription factor central to ORS development is Sox-9. Gata-3 function is essential for the IRS to form; the Notch signaling pathway is needed for maintaining IRS cell fate, and proteins like Hox-C13 and Fox-N1 are critical for correct hair shaft formation.

In Stage 7 (postnatal day (PND) 1–5), the hair shaft has lengthened to where its tip is no longer surrounded by the IRS and now lies in the hair canal at the level of the

sebaceous gland (Paus *et al.*, 1999). The gland itself is now positioned to the side of the hair follicle. This growth has been made possible by the continuous proliferation of the matrix cells (Alonso and Fuchs, 2006). Daughter cells from the matrix have continued to differentiate as they moved upwards, turning into the different cells of the IRS and hair shaft. Moreover, upon reaching an even higher level in the hair follicle, these daughter cells have terminally differentiated—extruding their organelles and filling up with keratin proteins—in a process known as keratinization.

In the IRS, keratinization serves to rigidify the structure, allowing it to support and guide the hair shaft out of the skin; the IRS itself though degenerates at the level of the sebaceous gland (Rogers, 2004). It should be mentioned that in between the keratin bundles are aggregates of keratin-associated proteins (Krtaps) that act as a scaffold for those filaments. In the hair fiber, both keratin filaments and keratin-associated proteins are especially rich in cysteine which allows them to cross-link heavily to one another, lending the hair shaft strength and flexibility.

Stage 8 (PND6 – 16) is the final stage of hair follicle morphogenesis (Paus *et al.*, 1999). At long last, the hair shaft emerges through the epidermis. Also in this stage, the hair follicle achieves full maturity as well as its maximal length—now lying adjacent to the subcutaneous muscle layer (the panniculus carnosus). This final stage of follicular morphogenesis can easily be seen in mice as pups go from having bare skin at five to six days of age, to a downy covering of fur the next day, followed by a well-developed coat of hair a day or two after that (Muller-Rover *et al.*, 2001).

On the Hair Cycle

Surprisingly, once a hair follicle has undergone morphogenesis and produced a hair shaft, it disassembles itself into a quiescent hair follicle remnant (Alonso and Fuchs, 2006). So while everything in the follicle at the level of the arrector pili muscle and above stays permanent, the lower half of the follicle degenerates and remains in that state until another hair shaft needs to be produced. At that point, the bottom part of the follicle regenerates itself and begins to make the next hair shaft.

Key to this ability is a reservoir of epithelial stem cells in a region of the hair follicle known as the 'bulge' which is necessary to the reformation of the lower follicle (Blanpain and Fuchs, 2006). Once a new hair shaft is produced, the bottom section of the hair follicle will break down once more and so on and so forth for the rest of its life (Muller-Rover *et al.*, 2001). This pattern is known as the hair cycle; its three stages (described above) are termed: anagen (regrowth), catagen (regression), and telogen (rest) (Figure 8). Each hair follicle will perpetually cycle through these phases and give rise to many hair shafts over its lifetime.

The stage of the adult hair cycle that the hair follicle resembles at the end of morphogenesis (around PND15) is late anagen. By PND17, the hair follicle moves into catagen, the stage in which the lower portion of the hair follicle degenerates. In catagen, the IRS is lost, the dermal papilla condenses out of the hair bulb and the epithelial cells in the hair bulb, along with the cells of the ORS, undergo apoptosis. The apoptotic remnants of the lower hair shaft form what is called the epithelial strand; a structure specific to catagen that runs between the dermal papilla and the degenerating hair follicle (Alonso and Fuchs, 2006). Overall, the hair follicle recedes in length from the subcutis to the level of the dermis (Muller-Rover *et al.*, 2001). The bottom of the hair shaft seals off by

forming a hollow brush of mature keratinocytes (called club hair) and fills much of what is left of the hair follicle bulb.

This much smaller follicle then enters telogen, a resting phase, in which it sits quiescently until the need for a new hair shaft. When the time arrives, hair follicle stem cells emerge from the bulge region and the follicle enters anagen. The epithelial stem cells differentiate into matrix cells, recreating the proliferative hair bulb. This hair bulb goes on to re-envelope the cluster of dermal fibroblasts, forming the dermal papilla once more; and the lower part of the hair follicle proliferates until it reaches well down into the subcutis. Concomitantly, the IRS regenerates, and the hair follicle begins to form a new hair shaft.

Remarkably, this hair can erupt even without loss of the old hair formed by the same follicle (Alonso and Fuchs, 2006). In mice, it is quite common to have two to three hairs in one follicle at the same time, though only one is growing; the new hair simply forms in a pocket adjacent to the one containing the club hair and both hairs share the same point of exit. Loss of older hairs occurs randomly, but they can also be shed actively in a relatively little understood process termed ‘exogen’. Typically, in mice, catagen lasts on the order of days, telogen–weeks, and anagen–months, though the time a hair follicle spends in telogen increases as the animal ages (Muller-Rover *et al.*, 2001).

The same molecular controls of follicular morphogenesis hold for hair follicle cycling, albeit with a few differences (Stenn and Paus, 2001). Instead of initiating placode formation, Wnt signaling activates the stem cells of the bulge through the stabilization of β-catenin, beginning anagen (Blanpain and Fuchs, 2009). Shh function is critical to hair follicle regeneration in the adult as well. It is expressed in a polar fashion

by matrix cells, with cells on one side expressing the ligand but not those on the opposite side (Oro and Higgins, 2003). The reason for this is unclear, but its function is not: agonists of Shh signaling hasten entry into anagen from telogen, while anti-Shh antibodies given to postnatal hair follicles block progression of anagen (Blanpain and Fuchs, 2006).

When it comes to the molecular control of the hair cycle, though, Shh and Wnt are but the tip of the iceberg and a comprehensive review of all the pathways and target genes involved is beyond the scope of this work (for that see Stenn and Paus, 2001 as well as Schmidt-Ullrich and Paus, 2005). On the whole, though hair follicle formation and cycling are complex subjects, knowledge of basic hair anatomy and the key developmental molecules and milestones outlined here, will greatly aid in the understanding of the experimental work to follow.

Summa summarum

Cholesterol is an essential molecule for mammalian life. Cells have evolved a complex regulatory network to tightly maintain levels of cholesterol in themselves and, hence, the body. Central to the feedback regulation of cholesterol are Insig proteins. When these proteins are lost, cells are unable to check cholesterol biosynthesis or uptake and accumulate cholesterol and its precursor sterol intermediates. In this work, we generate mice that lack Insig proteins in the epidermis. These mutant mice have deficiencies in hair growth. We hypothesize that these hair growth defects are due to the teratogenic effects of sterol intermediates and that buildup of these precursors causes abnormal development of the hair shaft.

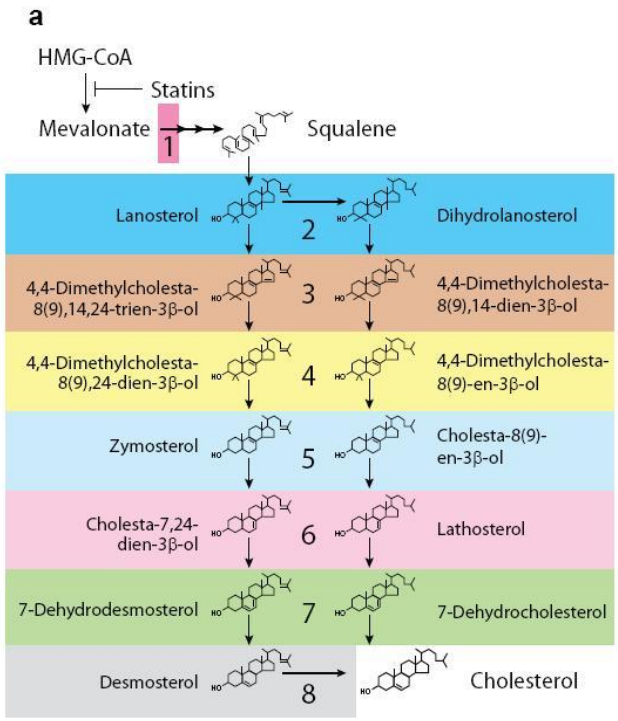

b

	Enzyme Deficiency	Human Disease	Skin Affected
1	Mevalonate Kinase	Mevalonic Aciduria; HIDS	+
2	Lanosterol 14-α-demethylase	Antley-Bixler	−
3	Sterol Δ^{14}- reductase	Greenberg Dysplasia	−
4	C4 Sterol decarboxylase	CHILD	+
5	Sterol Δ^{8}, Δ^{7}- isomerase	CDPX2; CHILD	+
6	Lathosterol 5-desaturase	Lathosterolosis	−
7	Sterol Δ^{7}- reductase	SLOS	+
8	Sterol Δ^{24}- reductase	Desmosterolosis	+

Figure 1-1 Inborn Errors of Cholesterol Metabolism. Human diseases occurring due to defects in cholesterol biosynthetic enzymes cluster in the post-squalene part of the pathway (A). Syndromes that have a component of skin disease are noted (B). The production of zymosterol (and cholesta-8(9)-en-3β-ol) is actually catalyzed by a group of three enzymes–C4 sterol methyloxidase, C4 sterol decarboxylase (NSDHL), and 3-ketoreductase–known as the C4 demethylation complex; of these, mutations associated with CHILD syndrome have only been found in the gene for the decarboxylase. Reduction of the side-chain double bond can occur at any step of the pathway; it is only shown occurring for lanosterol and desmosterol for the sake of simplicity.
(Figure adapted from Engelking *et al.*, 2006)

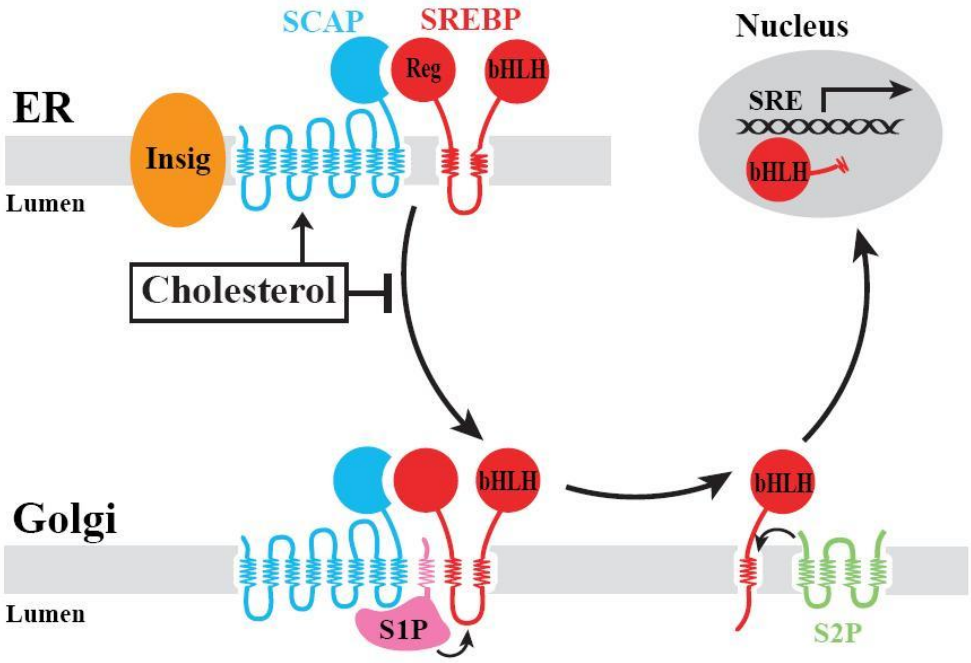

Figure 1-2 The SREBP Proteolytic Pathway. When the cell needs to synthesize cholesterol, it increases the protein levels of all the enzymes in the cholesterol biosynthetic pathway. The cell achieves this rise through SREBP. Under conditions of sterol-depletion, Scap transports SREBP from the ER to the Golgi apparatus, where two proteases, S1P and S2P, act sequentially to release the NH2-terminal domain of SREBP from the membrane. This domain of SREBP is bHLH transcription factor. No longer tethered, it travels to the nucleus, binds to SREs in the promoter region of target genes, and activates their transcription. The cleavage of SREBPs is feedback-inhibited by cholesterol, which binds to Scap and causes it to change in conformation. This shift, together with Insig binding to Scap, retains the Scap-SREBP complex in the ER. (Figure adapted from DeBose-Boyd, 2008)

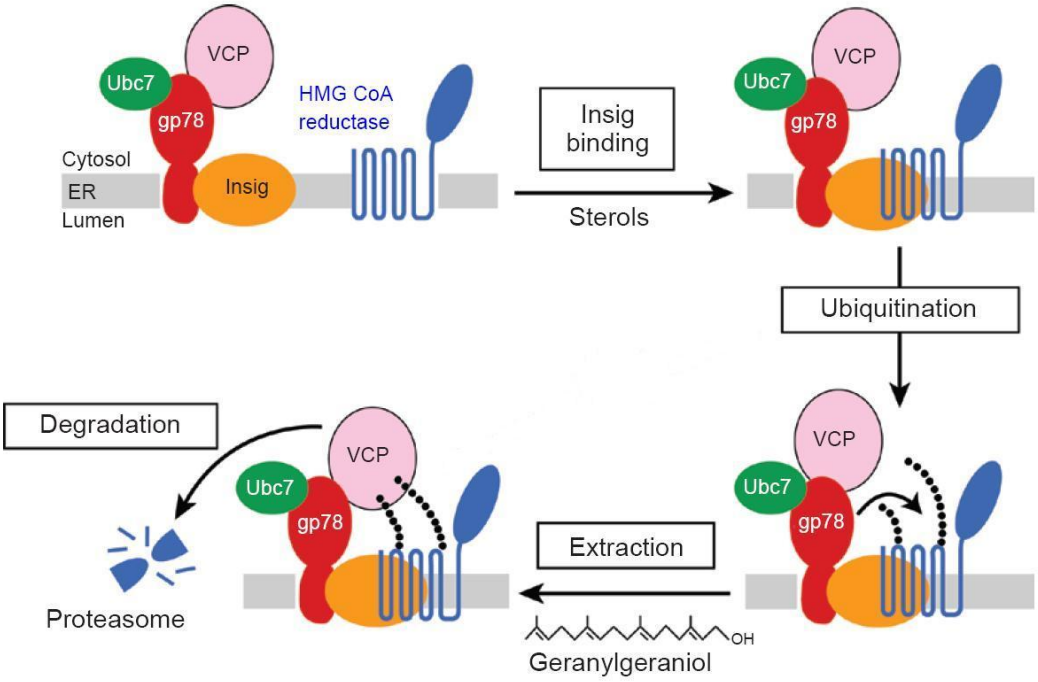

Figure 1-3 The Degradation of HMG-CoA Reductase. Buildup of oxysterols and 24,25-dihydrolanosterol prompts the binding of Insig to HMG-CoA reductase. Attached to Insig are gp78, Ubc7, and VCP – three proteins which carry out the ERAD of reductase. Ubc7 is an E2, which possesses the ubiquitin chain. Gp78, the E3, transfer this chain (represented as a string of closed circles) from Ubc7 to HMG-CoA reductase. The ATPase VCP then extracts reductase from the membrane and delivers it to proteasomes for degradation. This process can be enhanced by the presence of geranylgeraniol. (Figure adapted from DeBose-Boyd, 2008)

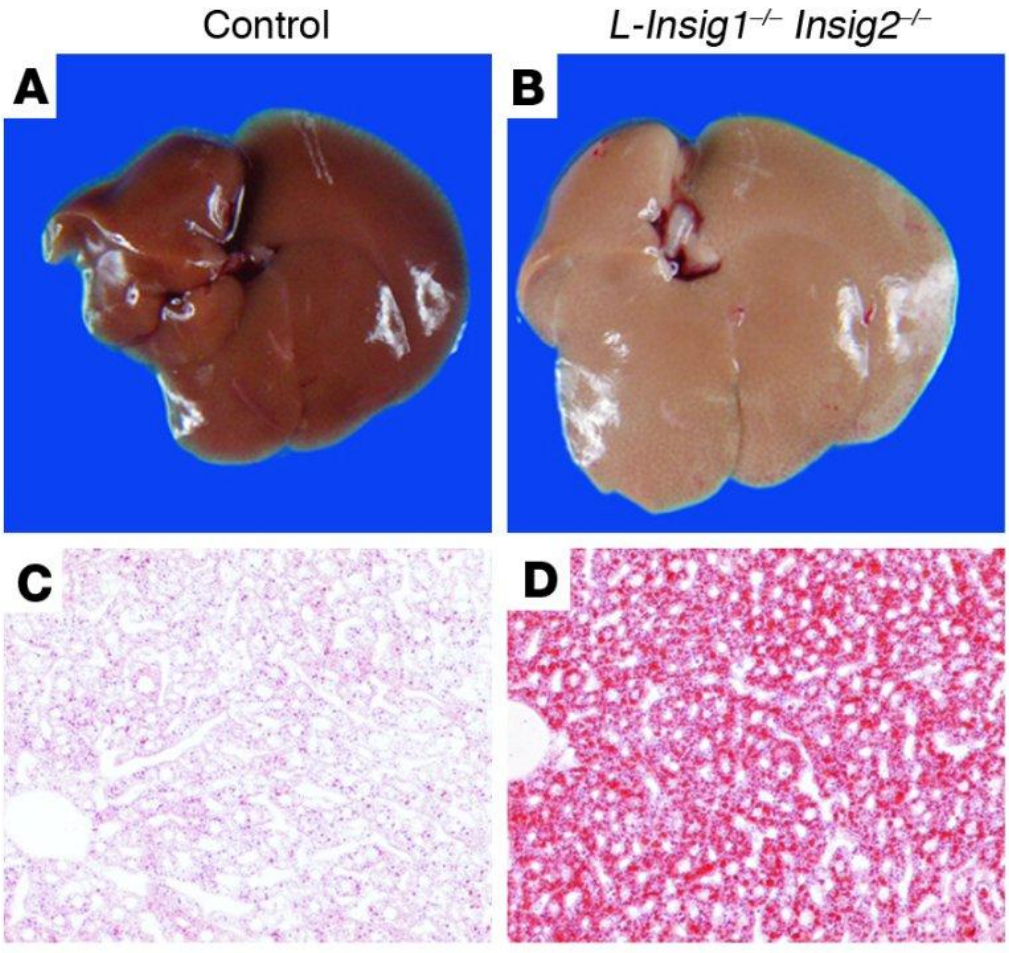

Figure 1-4 The Effects of Insig Loss. Removal of both Insig-1 and Insig-2 specifically from the liver of mice results in a striking accumulation of lipids in that organ. Though both mice were fed a normal chow diet, the Insig knockout liver is pale and engorged with fat (B) relative to the liver from a control mouse (A). Histologic sections from both of these livers stained with Oil Red O, a lipophilic dye, reinforce this observation (C, D).
(Figure adapted from Engelking *et al.*, 2005)

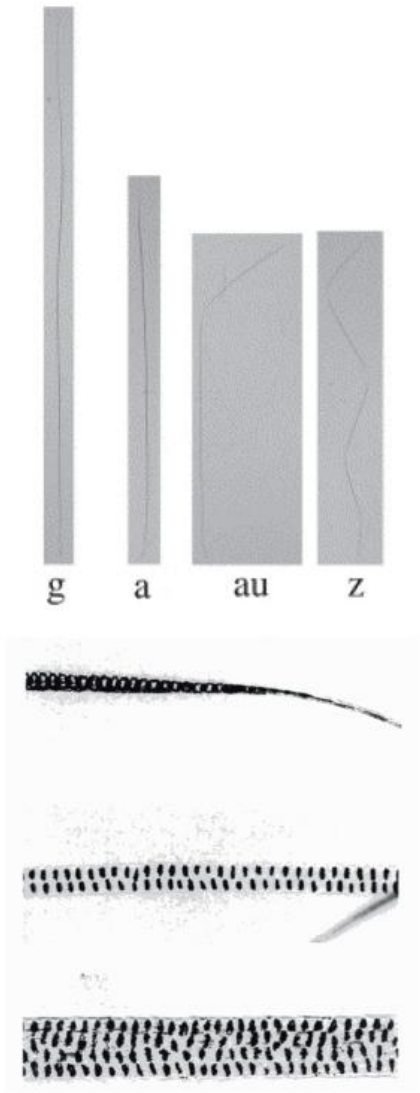

Figure 1-5 Types of Mouse Coat Hair. The four different types of murine pelage hair are shown to scale. Guard hairs (also called monotrich, tylotrich, or primary hairs) are the longest. Awl hairs are slightly shorter than guard hairs but, like them, are still straight. Auchene hairs have one bend in the hair while zigzag hairs have multiple bends. These bends in the hair shaft are associated with a constriction of the hair, which can be seen with light microscopy. This technique also demonstrates a second distinguishing characteristic between these hair types: the number of columns of air spaces (fusi) in the medulla of the hair shaft. Zigzag hairs have only one such column, whereas guard hairs have two. In skin sections, guard hairs can be further distinguished by the presence of two sebaceous glands instead of one. Awl and auchene hairs have two or more columns of medullary air spaces. Of note, human hair fibers do not have fusi in their medullas. (Figure adapted from Schalke, 2007 and Sundberg, 1994)

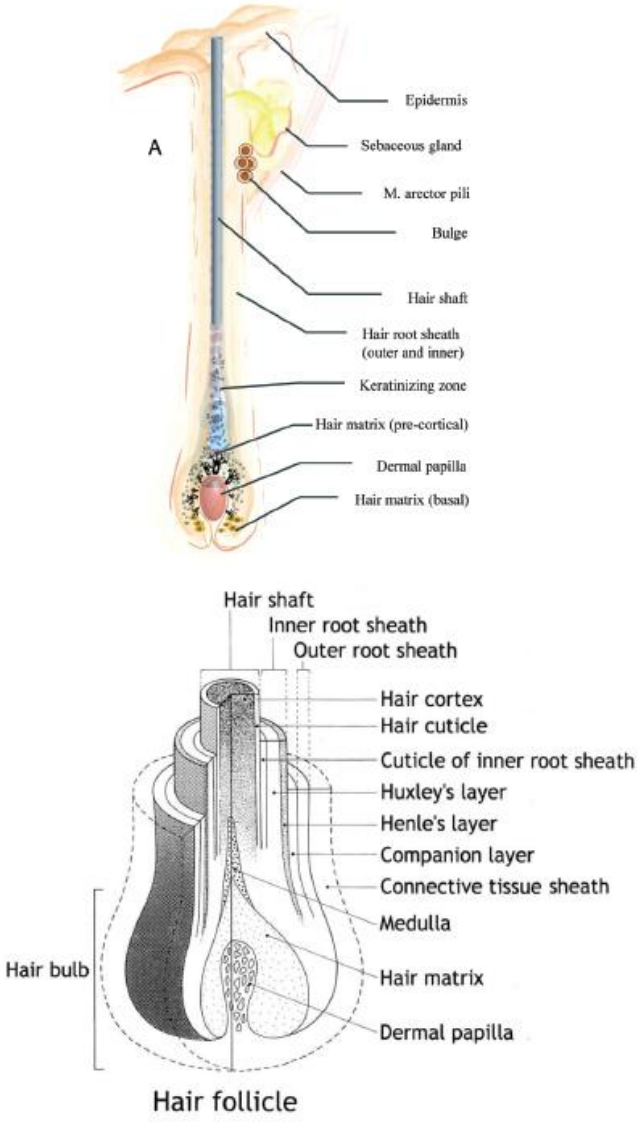

Figure 1-6 The Hair Follicle and its Layers. The arrector pili muscle, sebaceous gland, and hair follicle together form the pilosebaceous unit. Note the presence of epithelial stem cells in the bulge. The hair follicle itself consists of proliferating matrix cells at its base, which differentiate into the outer and inner root sheaths as well as the hair shaft as they move upwards. These layers are concentric cylinders that can be subdivided further. The inner root sheath is made up of Henle's layer, Huxley's layer, and the IRS cuticle, while the hair shaft is composed of the hair cuticle, cortex, and medulla. Jutting into the hair follicle is a small peg of tissue known as the dermal papilla. The follicle is enveloped by another dermal component, the connective tissue sheath. (Figure adapted from Ohnemus *et al.*, 2006 and Morioka, 2004)

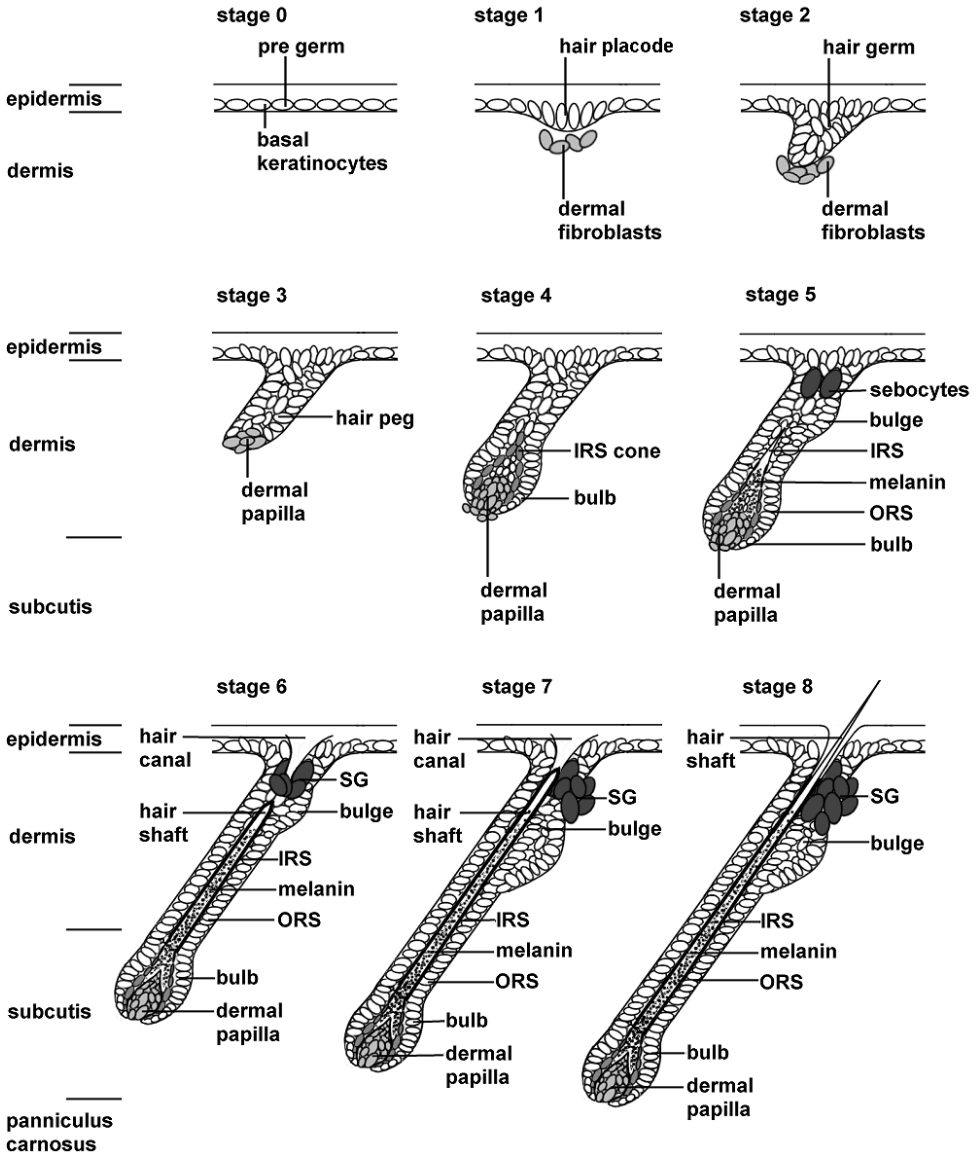

Figure 1-7 Follicular morphogenesis. The development of the hair follicle begins *in utero* and continues after birth, taking place in eight stages. The length of the hair follicle in relation to the different layers of the skin is indicated.
(Adapted from Paus *et al.*, 1999)

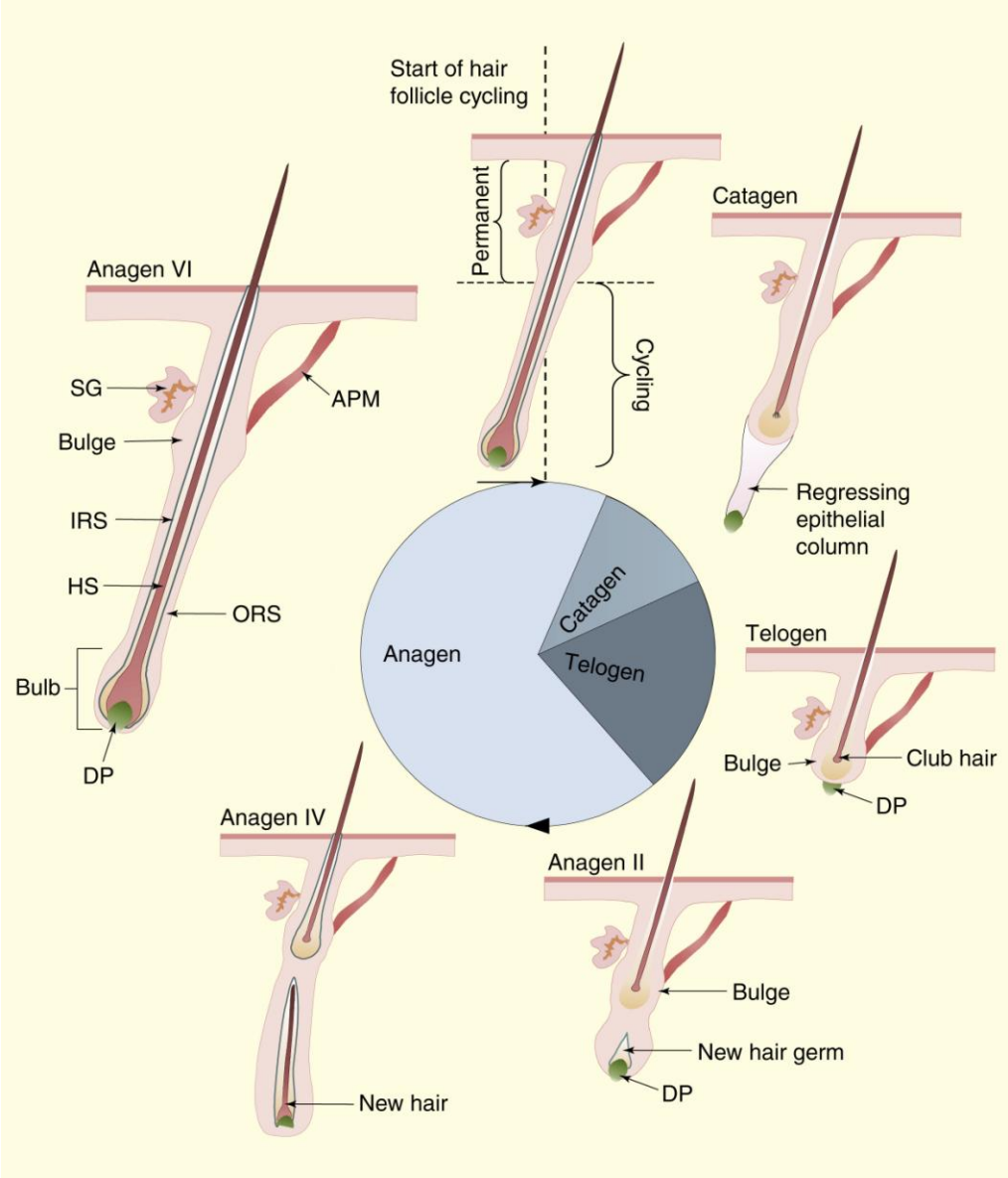

Figure 1-8 The Hair Cycle. Upon completion of morphogenesis, the new hair follicle most closely resembles an adult follicle in late anagen; this is then its point of entry into the hair cycle (black arrow, dotted vertical line). From there, it quickly proceeds into catagen, where its lower half collapses into a quiescent structure. Following a period of rest (telogen), the lower bulb portion of the follicle regenerates and begins to create a new hair shaft (anagen).
(Adapted from Schneider *et al.*, 2009)

CHAPTER TWO
Hair Growth Defects in Insig-Deficient Mice Caused by Cholesterol Precursor Accumulation and Reversed by Simvastatin

Adapted from: Evers BM, Farooqi MS, Shelton JM, Richardson JA, Goldstein JL, Brown MS, Liang G (2010) J. Invest. Dermatol 130:1237-1248

Introduction

Cholesterol has an essential role in mammalian development, and its concentration is tightly regulated by a feedback system that senses the level of cholesterol in cell membranes and modulates the rates of cholesterol synthesis (Brown and Goldstein, 2009). At the core of this feedback regulation are Insig-1 and Insig-2, two closely related endoplasmic reticulum membrane proteins. Under conditions of sterol excess, Insigs limit cholesterol synthesis by enhancing the ubiquitination and degradation of 3-hydroxy-3-methylglutaryl coenzyme A reductase (HMG-CoA reductase), the rate-limiting enzyme of cholesterol biosynthesis. In addition, excess sterols cause Insigs to inhibit the action of Scap, a polytopic membrane protein that transports sterol regulatory element-binding proteins (SREBPs) from the endoplasmic reticulum to the Golgi apparatus (Goldstein *et al.*, 2006).

Sterol regulatory element-binding proteins are membrane-bound transcription factors required for transcription of all of the known genes encoding enzymes of the cholesterol biosynthetic pathway (Horton *et al.*, 2002). To enter the nucleus, inactive SREBP precursors must be transported by Scap to the Golgi, where they are processed proteolytically to yield active nuclear fragments (nSREBPs). When sterols accumulate to high levels within cells, Insigs bind and retain the Scap/SREBP complex in the

endoplasmic reticulum, preventing the generation of active nSREBPs and thereby reducing transcription of cholesterol biosynthetic genes. By controlling both the stability of HMG-CoA reductase protein and the generation of active nSREBPs, the net result of Insig action is to decrease cholesterol synthesis whenever sterol levels are high (Brown and Goldstein, 2009).

The essential role of Insig-mediated regulation of cholesterol homeostasis *in vivo* was shown by our previous studies of mice lacking both Insig-1 and Insig-2 (Engelking *et al.*, 2005, 2006). In these Insig double knockout (*Insig*-DKO) mice, Insig deficiency caused an overproduction of cholesterol and a marked buildup of cholesterol precursors, which led to craniofacial abnormalities. The teratogenic role of sterol intermediates in causing the craniofacial defects was supported by the observation that facial clefting in *Insig*-DKO mice decreased when pregnant females were treated with lovastatin, an inhibitor of HMG-CoA reductase that lowers the level of cholesterol and its sterol precursors (Engelking *et al.*, 2006). We postulated that the teratogenic effects were caused by the accumulation of sterol precursors, but the mechanism remained unknown. The neonatal lethality of the *Insig*-DKO mice precluded us from examining whether excess sterol precursors impair developmental processes that occur after birth.

Inasmuch as palatal development requires the interaction between epithelial and mesenchymal cells (Gritli-Linde, 2007), we set out to examine whether the clefting defects in *Insig*-DKO mice are caused by excess sterol precursors in epithelial and/or mesenchymal cells of the palate. Accordingly, in this study we generated a tissue-specific line of knockout mice lacking both Insig-1 and Insig-2 in the oral epithelium. These mice also lacked Insigs in the epidermis of the skin (termed Epi-*Insig*-DKO mice). Epi-*Insig*-

DKO mice did not manifest any craniofacial abnormalities, indicating that loss of Insigs in the oral epithelium is not sufficient to produce cleft palate. Instead, Epi-*Insig*-DKO mice exhibited defects in hair growth and other skin abnormalities, associated with a marked accumulation of sterol precursors in the skin. The causal role of sterol precursors is supported by the observation that the hair and skin defects were completely corrected by topical application of a statin inhibitor of HMG-CoA reductase that lowered the elevated sterol precursors in the skin. These findings have implications for the pathogenesis of skin abnormalities seen in several inborn errors of cholesterol synthesis, such as the CHILD syndrome (congenital hemidysplasia with ichthyosiform nevus and limb defects) and the CDPX2 syndrome (X-linked dominant chondrodysplasia punctata type 2), both of which exhibit a buildup of sterol precursors in skin.

RESULTS

Generation of mice lacking Insig-1 and Insig-2 in the epidermis

Mice carrying floxed *Insig-1* and null *Insig-2* alleles (*Insig-1*$^{f/f}$;*Insig-2*$^{-/-}$) were bred to *Keratin14-Cre* (*K14-Cre*) transgenic mice in which Cre recombinase driven by the human *Keratin14* promoter was expressed in the oral epithelium, epidermis, and hair follicles (Dassule *et al.*, 2000; Gritli-Linde *et al.*, 2007). The *K14-Cre* mediated deletion of *Insig-1* (Figure 1a), in combination with the germline deletion of *Insig-2*, rendered the resulting *Insig-1*$^{f/f}$;*Insig-2*$^{-/-}$;*K14-Cre* mice deficient in both Insig-1 and Insig-2 in these tissues. For simplicity, we designated these *Insig-1*$^{f/f}$;*Insig-2*$^{-/-}$;*K14-Cre* mice as epidermal-specific *Insig*-double knockout (Epi-*Insig*-DKO) mice. For all experiments

described here, we bred *Insig-1*$^{f/wt}$;*Insig-2*$^{-/-}$;*K14-Cre* male and *Insig-1*$^{f/f}$;*Insig-2*$^{-/-}$ female mice to obtain control *Insig-1*$^{f/f}$;*Insig-2*$^{-/-}$ and Epi-*Insig*-DKO littermates. At 18.5 days post coitum (dpc), Epi-*Insig*-DKO mice were observed in the expected 1:1:1:1 Mendelian ratio (based on 42 litters). At birth, mutant mice were grossly indistinguishable from wild-type littermates.

In Figure 1b, we used real-time PCR to quantify the relative amount of Insig-1 mRNA in the skin and liver from postnatal day 14 (PND 14) control and Epi-*Insig*-DKO mice. Compared with control mice, the amount of Insig-1 mRNA in the skin of Epi-*Insig*-DKO mice was reduced by 93%. Liver Insig-1 mRNA levels were comparable between control and Epi-*Insig*-DKO mice. Therefore, the *K14-Cre*-mediated recombination led to an efficient and skin-specific ablation of *Insig-1* in Epi-*Insig*-DKO mice, consistent with previous studies in which the same *K14-Cre* was used to delete other floxed genes in the skin (Wang *et al.*, 2006; Gritli-Linde *et al.*, 2007).

Although Epi-*Insig*-DKO mice were grossly indistinguishable from control littermates at birth, they failed to thrive, and none survived beyond 6 weeks after birth. The cause of death remains to be determined, but did not appear to result from any detectable gross abnormality in the oral epithelium. Figure 1c shows the body weights of control and Epi-*Insig*-DKO mice at various ages before death. At 18.5 dpc, Epi-*Insig*-DKO embryos weighed the same (1.21g; mean of 99 embryos) as control littermates (1.22g; mean of 101 embryos). In experiments not shown, both control and mutant 18.5-dpc embryos exhibited an intact epidermal barrier as measured by the X-gal staining assay (Hardman *et al.*, 1998). At PND 4, the mutant mice (1.77g) were 27% smaller than controls (2.44g) (Figure 1c). As the mice aged, this difference became more dramatic

such that by PND 28 mutant mice (5.93g) were 63% smaller than controls (15.83g) (Figure 1c).

Most strikingly, Epi-*Insig*-DKO mice failed to grow body hair. At PND 14, all of the control mice (44 out of 44) had a full coat of body hair, whereas none of the Epi-*Insig*-DKO mice (0 out of 48) had any body hair (Figure 2a). Other gross abnormalities in the mutant mice included hyperkeratosis, kinking of the vibrissae (whiskers), and exophthalmos (compare Figure 2c and b). Histological examination revealed abnormalities in the eyes and the meibomian glands. In the former, three out of five Epi-*Insig*-DKO mice had keratitis; in the latter, five out of five showed gland enlargement. No gross abnormalities were found in the teeth, nails, and internal organs on necropsy.

Histological analyses of skin from control and Epi-Insig-DKO mice

Figure 3 shows histological sections of skin from control and Epi-*Insig*-DKO mice at PND 14. Whereas the hair follicles of control mice were aligned normally (Figure 3a and inset), those of Epi-*Insig*-DKO mice were misaligned, unevenly distributed, ectatic, plugged with keratin, and contained distorted hair shafts (Figure 3b and inset). Epi-*Insig*-DKO mice also showed a loss of hypodermal adipocytes (Figure 3b) and exhibited epidermal hyperplasia and orthokeratotic hyperkeratosis with hypergranulosis (Figure 3d). The hyperplastic epidermis of Epi-*Insig*-DKO mice was 5- to 7-cell layers thick, whereas the epidermis of control mice was only 2- to 3-cell layers thick. In controls, the dermal papillae were enveloped by follicular epithelial cells to form normal hair bulbs (Figure 3e). In contrast, the dermal papillae of Epi-*Insig*-DKO mice were condensed and separated from the follicular epithelial cells, associated with degeneration

of the hair bulbs (Figure 3f). A slight infiltration of neutrophils was noted in the dermis, but not in the hair follicles.

Growth of hair follicles is divided into two distinct stages: (1) follicular morphogenesis in which the hair follicle develops and grows from embryonic precursors, and (2) the follicular cycle (or hair cycle) whereby hair follicles grow (anagen), regress (catagen), and rest (telogen), producing new hairs throughout the mammalian lifetime (Alonso and Fuchs, 2006; Schneider *et al.*, 2009). In mice, follicular morphogenesis begins on the upper back at 14.5 dpc. The ectoderm elongates and invaginates, and mesenchymal cells beneath the invaginated ectoderm condense to form the hair placode. The invaginated ectoderm will differentiate into the hair follicle and adjacent epidermis, whereas the mesenchymal cell condensation will become the dermal papilla. After birth, between PNDs 6 and 8, the hair follicles of the back become fully mature, and the cells within the hair bulb continue to proliferate and differentiate, causing the hair shaft to erupt from the skin surface. Around PND 16, when follicular morphogenesis is complete, hair follicles enter the catagen phase of the first follicular cycle and begin to regress. By PND 19, the hair follicles progress to telogen that lasts for 1–2 days. At the end of telogen, the hair follicles enter the first anagen phase of the follicular cycle and remain in this phase until catagen begins again roughly 6 weeks after birth, after which the follicular cycle repeats anew.

To further characterize the hair follicle defects of Epi-*Insig*-DKO mice, we compared hair follicle development between control and Epi-*Insig*-DKO mice at PNDs 4, 7, 14, 21, and 28 (Figure 4). At PND 4, hair follicles were histologically similar in control (Figure 4a) and Epi-*Insig*-DKO (Figure 4f) mice. At PND 7, some hair shafts in

Epi-*Insig*-DKO mice had become kinked (Figure 4g and inset). Near the completion of follicular morphogenesis at PND 14, the hair follicles of control mice were aligned (Figure 4c), whereas the hair follicles of Epi-*Insig*-DKO had become misaligned and unevenly dispersed (Figure 4h). The hair follicles from these mutant mice also exhibited ectasia, kinked hair shafts, dermal papillae condensation, and hair bulb degeneration. Epi-*Insig*-DKO mice also showed a loss of hypodermal adipocytes compared with control mice. At PND 21, when hair follicles of control mice were in the telogen phase of the follicular cycle (Figure 4d), those of Epi-*Insig*-DKO mice were arrested and exhibited progressive ectasia, with keratin accumulation within the follicles (Figure 4i). This arrest of hair follicle cycling persisted in the Epi-*Insig*-DKO mice at PND 28 with further enlargement of the hair follicles along with minimally detectable scarring (Figure 4j). Because the hair follicles were extremely ectatic at this stage, it was difficult to determine whether follicular drop out had occurred. In control mice at PND 28, hair follicles proceeded into the anagen phase normally (Figure 4e).

Elevation in cholesterol precursors in skin of Epi-Insig-DKO mice and reduction by simvastatin treatment

In our previous studies of germ-line *Insig*-DKO mice, we showed that Insig deficiency caused an overproduction and marked buildup of sterol precursors of cholesterol that led to craniofacial abnormalities (Engelking *et al.*, 2006). We therefore explored the possibility that the skin abnormalities in Epi-*Insig*-DKO mice were also due to the accumulation of sterol precursors. As a first step to test this hypothesis, we used oil red O to stain the neutral lipids in skin sections from control and Epi-*Insig*-DKO mice

(Figure 5). At PND 14, sebaceous glands were enlarged and filled with lipids in Epi-*Insig*-DKO (Figure 5c) compared with those of control (Figure 5a) mice. Quantification of sebaceous gland area revealed that the sebaceous glands of Epi-*Insig*-DKO mice were 1.7-fold larger in cross-section than those of control mice (2,045±101 vs. 1,236±35μm^2, $P<0.001$). Lipids also accumulated in the epidermal compartment of the hair bulbs in Epi-*Insig*-DKO mice (Figure 5d), but not in those of control mice (Figure 5b).

We next carried out immunoblot analysis to determine the protein levels of HMG-CoA reductase in the skin of PND 14 control and Epi-*Insig*-DKO mice. As shown in Figure 5e, the relative amount of HMG-CoA reductase protein in the skin of Epi-*Insig* DKO mice was 10-fold higher than that in control mice (mean of four values in each group). These relative values were determined by densitometric quantification of the reductase protein band relative to that of the transferrin protein band (loading control). Figure 5g shows the marked overabundance of reductase protein in the sebaceous glands of the mutant mice, as revealed by immunohistochemistry.

Figure 6a shows an abridged diagram of the cholesterol biosynthetic pathway, depicting the major sterol precursors. Also shown is the enzyme HMG-CoA reductase, which converts HMG-CoA to mevalonate and is the target for the statin class of drugs that inhibit cholesterol synthesis (Goldstein and Brown, 1990). We determined the levels of cholesterol and its precursors in skin from control and Epi-*Insig*-DKO mice using gas chromatography-mass spectroscopy (GC-MS). In the experiments shown in Figure 6b–g, we treated entire litters of mice daily from PND 2 to PND 13 with topical applications of vehicle or the cholesterol synthesis inhibitor simvastatin. We used a protocol in which acetone is rubbed on the skin to disrupt the permeability barrier before application of the

vehicle or simvastatin (Feingold *et al.*, 1990). The drug was applied to a patch of skin 0.5–1cm^2 located between the shoulder blades. At PND 14, after the mice were photographed, skin from the upper back was harvested for sterol measurements, and tail tissues were used for genotyping. The skin of vehicle-treated Epi-*Insig*-DKO mice had elevated levels of cholesterol and its precursors compared with that of vehicle-treated control mice. As indicated by the black bars in Figure 6, the fold increases ranged from 1.7-fold for desmosterol (Figure 6f) to 7.1-fold for lathosterol (Figure 6e). When treated with simvastatin, the cholesterol content in the skin of control mice was not reduced, whereas the cholesterol content in the skin of Epi-*Insig*-DKO mice was reduced to a level close to that of control mice (gray bars in Figure 6g). In the skin of control mice, simvastatin treatment significantly reduced the levels of all of the sterol precursors (gray bars in Figure 6b-f). An even greater relative reduction was observed in the skin of the Epi-*Insig*-DKO mice with the exception of desmosterol, which was not affected by simvastatin treatment (Figure 6f).

Simvastatin-mediated correction of hair defects in Epi-Insig-DKO mice

Figure 7 shows the overall appearances and histological analyses of control and Epi-*Insig*-DKO mice treated with either vehicle or 1mg simvastatin. As described earlier, entire litters of mice were treated daily from PND 2 to PND 13 with topical applications of either vehicle or simvastatin. At PND 14, the mice were photographed and scored for hair growth by two independent observers before genotyping. The hair growth and body weights of control mice were not affected by simvastatin treatment (20 out of 20, Figure 7b). All (11 out of 11) of the vehicle-treated Epi-*Insig*-DKO mice were hairless, the same

phenotype exhibited by untreated Epi-*Insig*-DKO mice (Figure 2). Simvastatin treatment completely corrected the hairless phenotype such that 100% (16 out of 16) of the treated mutant mice had normal hair growth (Figure 7d), no meibomian gland enlargement, and no keratitis. Normalization of hair was observed throughout the body, and not just in the region where the drug was applied. Simvastatin treatment also corrected the low body weight phenotype of Epi-*Insig*-DKO mice, consistent with a widespread systemic effect. Whereas vehicle-treated Epi-*Insig*-DKO mice weighed 39% less than vehicle-treated control littermates (4.84 vs. 7.97g), simvastatin-treated Epi-*Insig*-DKO and control mice had similar body weights (6.11 vs. 6.90g). A lower dose of simvastatin (30μg per day from PND 2 to PND 13) only partially corrected the phenotype; the coat was frizzled and tattered (100% of mutant mice) and the number of hair follicles was markedly reduced and showed abnormalities of the type seen in Figure 3b, d, and f.

To further evaluate the effect of simvastatin treatment on hair growth, we carried out histological analyses of skin from all four groups of mice described above (Figure 7e–p). Neither vehicle nor simvastatin treatment had any effect on the hair and skin histology of control mice (Figure 7e, f, i, and j). Vehicle-treated Epi-*Insig*-DKO mice (Figure 7g and k) showed the same gross and histological defects in hair and skin observed in untreated Epi-*Insig*-DKO mice (Figure 3). All these defects were corrected in simvastatin-treated Epi-*Insig*-DKO mice (Figure 7h and l). Furthermore, the accumulation of oil red O-stained lipids seen in the epidermal compartment of the hair bulbs of Epi-*Insig*-DKO mice (Figure 7o) was prevented by simvastatin treatment (Figure 7p). Sebaceous gland hyperplasia seen in Epi-*Insig*-DKO mice was also ameliorated by simvastatin treatment (data not shown).

Analyses of control and Epi-Insig-DKO mice at different times after stopping simvastatin treatment

In the experiments shown in Figure 7, the mice were treated daily with simvastatin from PND 2 to PND 13 and analyzed at PND 14. To determine whether the mice would regress after cessation of statin treatment, we carried out another study in which control and Epi-*Insig*-DKO mice were first treated with vehicle or 1mg simvastatin from PND 2 to PND 13 and then left untreated for the next 5.5 months. The mice were monitored weekly by two independent observers. None (0 out of 4) of the vehicle-treated Epi-*Insig*-DKO mice survived beyond 6 weeks of age. In contrast, simvastatin-treated Epi-*Insig*-DKO mice lived to the 6-month end point. Strikingly, though they were only treated with simvastatin from PND 2 to PND 13, the Epi-*Insig*-DKO mice maintained a full coat of body hair, normal body weight, and normal claws for ~3.5 months (Figure 8a). After 3.5 months, the mutant mice began to lose hair, and body weight decreased. By 6 months of age, the mutant mice showed a near-total loss of body hair (Figure 8b), and their body weight was severely reduced (23.4±0.82 vs. 32.1±1g in controls, $P<0.001$). The claws of these mice were deformed and the vibrissae were shortened and kinked. Histological analysis of the skin from Epi-*Insig*-DKO mice at 6 months of age revealed abnormalities similar to those in Figure 3. Figure 8c-h shows the sterol content of the skin from 6-month old control and Epi-*Insig*-DKO mice that were treated with simvastatin only from PND 2 to PND 13 and left untreated thereafter. The levels of 24-dihydrolanosterol, zymosterol, lathosterol, and cholesterol were all significantly elevated in the Epi-*Insig*-DKO mice (Figure 8d–f and h). Lanosterol and desmosterol levels did not differ significantly between control and Epi-*Insig*-DKO mice (Figure 8c and g).

DISCUSSION

The present studies show that epidermal-specific ablation of the genes encoding Insig-1 and Insig-2, two proteins required for the feedback inhibition of cholesterol synthesis, leads to accumulation of sterol precursors in the skin. The excess sterol precursors impair normal hair development, producing a hairless phenotype along with other skin abnormalities. The causal role of sterol precursors is supported by the observation that the hair and skin defects in the mutant mice were completely corrected by topical application of a statin inhibitor of cholesterol synthesis that lowered the levels of sterol precursors in the skin.

Cholesterol has an essential role in the formation and maintenance of the epidermal permeability barrier (Feingold *et al.*, 1990; Feingold, 2009). To date, four human malformation syndromes caused by inherited enzyme defects in the cholesterol biosynthetic pathway exhibit skin defects (Porter, 2003; Anstey, 2006). These syndromes are CHILD, CDPX2, SLOS, and desmosterolosis. Inasmuch as the enzymes defective in these syndromes catalyze different steps in the conversion of lanosterol to cholesterol (see Figure 6a), each of these defects leads to a deficiency in cholesterol with a concomitant buildup of various sterol precursors proximal to the defective enzyme. Roughly two-thirds of all SLOS patients suffer from eczema and/or a severe photosensitivity that results in a sunburn-like erythema upon exposure to UV light (Elias *et al.*, 1997; Anstey, 2006). CHILD and CDPX2 patients as well as the corresponding *Bpa/Str* and *Td* mice exhibit similar skin defects, including ichthyosis, patchy hyperkeratosis, and alopecia (Liu *et al.*, 1999). Among the two reported cases of human

desmosterolosis, one exhibited cutis aplasia (Andersson *et al.*, 2002). The corresponding *Dhcr24*$^{-/-}$ mice showed wrinkleless taut skin and an impaired epidermal permeability barrier; as a result, the mice died within a few hours after birth (Mirza *et al.*, 2006). The skin defects in these three syndromes are caused, either singly or in combination, by cholesterol deficiency or the accumulation of sterol precursors.

Epi-*Insig*-DKO mice differ from the aforementioned syndromes in that the accumulation of sterol precursors is not accompanied by cholesterol deficiency. Instead, at PND 14, the skin cholesterol content is elevated 2.2-fold in the Epi-*Insig*-DKO mice (Figure 6g). Furthermore, the Epi-*Insig*-DKO mice maintain an intact epidermal barrier at 18.5 dpc and do not die until about 6 weeks after birth, suggesting that skin barrier abnormalities associated with cholesterol deficiency do not underlie the skin and hair defects in Epi-*Insig*-DKO mice. Together, these results suggest that the defects in the Epi-*Insig*-DKO mice are caused by a buildup of sterol precursors and not by a deficiency of cholesterol. It is unclear, however, whether these defects are caused by one specific sterol precursor or a combination of sterol precursors.

Hair follicle growth is characterized by two distinct stages: (1) follicular morphogenesis in which the hair follicle develops and grows from embryonic precursors, and (2) the follicular cycle (or hair cycle) whereby hair follicles grow (anagen), regress (catagen), and rest (telogen) to produce new hairs throughout the mammalian lifetime (Alonso and Fuchs, 2006; Schneider *et al.*, 2009). Defects in any one of these steps can lead to anomalies in hair development and growth. The buildup of sterol precursors in the skin of Epi-*Insig*-DKO mice does not affect the initial stages of follicular morphogenesis

(up to PND 7); rather, it appears to interfere with later stages of follicular morphogenesis and the hair cycle (Figure 4).

The mouse mutant, *hairless*, which is deficient in a transcriptional co-repressor for several genes that regulate keratinocyte differentiation (Benavides *et al.*, 2009), has a hair growth phenotype similar to that of Epi-*Insig*-DKO mice. However, there are two main phenotypic differences between these two mutants: (1) the defects in *hairless* appear during the first catagen (after PND 16), whereas those in Epi-*Insig*-DKO appear during follicular morphogenesis (at PND 7); and (2) *hairless* mice exhibit dermal cysts, whereas Epi-*Insig*-DKO mice do not.

The molecular mechanism by which a buildup of sterol precursors interferes with hair follicle growth in the Epi-*Insig*-DKO mice is unknown. One possible target is the Sonic Hedgehog (Shh) signaling pathway, which has been shown to be important in both follicular morphogenesis and follicular cycling (St-Jacques *et al.*, 1998; Chiang *et al.*, 1999). As shown in Figure 4, Epi-*Insig*-DKO mice undergo normal follicular morphogenesis up to PND 7, but fail to progress to later stages. These abnormalities are similar but not identical to those in Shh-deficient ($Shh^{-/-}$) mice that undergo normal follicular morphogenesis up to 15.5 dpc (St-Jacques *et al.*, 1998); (Chiang *et al.*, 1999); whether the accumulation of one or more sterol precursors in Epi-*Insig*-DKO mice is associated with an inhibition of Shh signaling remains to be determined.

The response of Epi-*Insig*-DKO mice to topical simvastatin treatment was dramatic. Unfortunately, we were unable to find conditions in which the response was limited exclusively to the region of application, even when we reduced the volume of simvastatin and the surface area to which it was applied. Inasmuch as the drug was

applied to skin of suckling pups, the mothers licked the fur of the treated pups, possibly distributing the drug to other regions of the skin. It is likely that the drug was absorbed from the skin, released into the circulation, and taken up by the epidermis where it reduced the synthesis of sterol precursors in the epidermis.

Although further studies of this model are clearly indicated, the current data are sufficient to provide insight into the cutaneous abnormalities that accompany genetic diseases in which sterol precursors accumulate, because of the blocks in the cholesterol biosynthetic pathway. Some of these studies are currently underway in our laboratory.

MATERIALS AND METHODS

Generation of mice lacking Insigs in the epidermis

Mice carrying floxed *Insig-1* and null *Insig-2* alleles (*Insig-1*$^{f/f}$;*Insig-2*$^{-/-}$) were generated as described (Engelking *et al.*, 2005). These mice were bred to *K14-Cre* transgenic mice (stock no. 004782; The Jackson Laboratory, Bar Harbor, ME) to generate *Insig-1*$^{f/f}$;*Insig-2*$^{-/-}$;*K14-Cre* mice. For simplicity, we designated these DKO mice lacking Insig-1 and Insig-2 in the epidermis as Epi-*Insig*-DKO mice. For all experiments described in this paper, we bred *Insig-1*$^{f/wt}$;*Insig-2*$^{-/-}$;*K14-Cre* male and *Insig-1*$^{f/f}$;*Insig-2*$^{-/-}$ female mice to obtain control (*Insig-1*$^{f/f}$;*Insig-2*$^{-/-}$) and Epi-*Insig*-DKO littermates. Pregnant females were allowed to pup, and the date of birth was denoted as PND 1. Mice were genotyped by PCR using tail genomic DNA with primers described previously (Dassule *et al.*, 2000; Engelking *et al.*, 2005). The genetic background of the studied mice was C57BL6/129SvEv/CBA. All mice were housed in colony cages with a 12h

light/12h dark cycle and fed *ad libitum* Teklad Mouse/Rat Diet 7002 (Harlan Teklad, Indianapolis, IN). All animal experiments were performed with the approval of the Institutional Animal Care and Research Advisory Committee at The University of Texas Southwestern Medical Center at Dallas.

Histology and oil red O staining

For histological analysis, skin from the upper back was collected from mice at PNDs 4, 7, 14, 21, and 28. The skin was fixed in 10% neutral-buffered formalin (catalog no. HT50-1-320; Sigma-Aldrich, St Louis, MO) for 24–72hours. For hematoxylin and eosin (H&E) staining, skin was embedded in paraffin, sectioned parallel or perpendicular to the hair shaft at 5μm, and stained with H&E. For oil red O staining, skin was incubated in a 30% aqueous sucrose solution overnight at 4°C and embedded in Neg-50 mounting medium (catalog no. 6506; Thermo Fisher Scientific, Waltham, MA) and cryosectioned at 10μm, parallel to the hair shaft. The frozen sections were stained with a 0.18% oil red O solution (catalog no. O0625; Sigma-Aldrich) in 60% (v/v) isopropanol for 10minutes and counterstained with hematoxylin for 1second.

Determination of tissue sterol composition

Skin from the upper back was harvested from mice at PND 14, weighed, and placed individually in Folch's buffer (5ml) containing 5α-cholestane (4μg) and epicoprostanol (4μg) as internal standards. The skins were then homogenized and centrifuged at 260 × *g* for 5minutes at room temperature to remove debris. The supernatants were transferred to new glass tubes and then saponified by heating (100°C)

in ethanolic KOH (100mM) for 2hours. Lipids were extracted with petroleum ether (final volume of 6ml), 1/10th of which (0.6ml) was dried under nitrogen and derivatized with hexamethyldisilazane-trimethylchlorosilane. GC-MS analysis was performed using an Agilent 6890N gas chromatograph coupled to an Agilent 5973 mass selective detector (Agilent Technologies, Santa Clara, CA). The trimethylsilyl-derivatized sterols were separated on a DB-35 (35%-phenyl)-methylpolysiloxane capillary column (30m × 0.25mm internal diameter × 0.25μm film) (catalog no. 122-1932; Agilent Technologies) with carrier gas helium at the rate of $1 ml min^{-1}$. The temperature program was 150°C for 2minutes, followed by increases of 20°C per min up to 280°C, which was then held for 22minutes. For cholesterol, the injector was operated in a 1:10 split mode. For all other sterols, the injector was operated in splitless mode at 280°C. The mass spectrometer was operated in the selective ion-monitoring mode. The mass to charge ratios for the extracted ions were 343.3 (desmosterol), 350.4 (7-dehydrocholesterol), 393.4 (lanosterol), 395.0 (24-dihydrolanosterol), 456.4 (zymosterol), 458.4 (lathosterol), and 458.4 (cholesterol). The retention time for lathosterol and cholesterol differed by 2minutes.

Immunoblot analysis and immunohistochemistry of HMG-CoA reductase

A polyclonal antibody against the C-terminal region (amino acids 426 to 887) of mouse HMG-CoA reductase (GenBank accession no. BC085083) was prepared by immunizing rabbits with purified bacterially expressed $(His)_6$-tagged protein. Immunoblot analysis of mouse reductase was carried out as described (Engelking *et al.*, 2005) except that whole-cell lysates were used. Aliquots of the lysates (30μg) were subjected to 8% SDS–PAGE and immunoblot analysis with $0.3 \mu g ml^{-1}$ anti-reductase (purified IgG fraction). For

loading control, identical filters were incubated with 0.25μgml^{-1} monoclonal mouse anti-human transferrin receptor (catalog no. 13-6800; Invitrogen Corp, Camarillo, CA).

For immunohistochemistry, skin sections (prepared as described for H&E staining) were heated at 58°C for 15minutes, deparaffinized, and quenched in 0.3% hydrogen peroxide for 30minutes at room temperature. After incubating overnight at 4°C with 3μgml^{-1} anti-reductase antibody, sections were stained with ImmPRESS Reagent and Peroxidase Substrate kits (catalog nos. MP-7401 and SK-4100) from Vector Laboratories (Burlingame, CA).

Simvastatin treatment of neonatal mice

A simvastatin stock solution of 6.4mgml^{-1} in propylene glycol/ethanol (PG/E) was prepared in the following manner. Simvastatin (800mg) (Merck, Whitehouse Station, NJ) was first dissolved in ethanol (16ml) at 70°C and converted to its active hydroxyl acid form by the addition of 0.6N NaOH (4ml). The resulting solution was titrated to pH 7.4, and propylene glycol (catalog no. P-1009; Sigma-Aldrich) was added to give a final PG/E ratio of 7:3 (v/v). Topical treatments of mice with simvastatin were carried out as described (Feingold *et al.*, 1990). Briefly, the back skin of each mouse (0.5–1cm^2) was rubbed for 30seconds with an acetone-soaked cotton swab to make the skin permeable. Immediately thereafter, 156μl of PG/E with or without 1mg simvastatin was applied to the acetone-treated interscapular area. These treatments were carried out daily from PND 2 to PND 13, and the mice were genotyped and photographed at PND 14.

Quantification of sebaceous gland area

Skin from the upper back of PND 14 mice was fixed, cryosectioned, and stained with oil red O as described above. Photographs of all of the sebaceous glands in a section were taken, and their area was quantified using ImageJ (http://rsbweb.nih.gov/ij/). To gain an accurate quantification, we measured the areas of all sebaceous glands (more than 150) from 18 individual skin sections (three mice per group, 6 sections per mouse).

Epidermal barrier assay

The epidermal barrier assay was carried out as described (Hardman *et al.*, 1998). Briefly, embryos were submerged overnight at 30°C in a solution of 2mM $MgCl_2$, 5mM $K_3Fe(CN)_6$, 5mM $K_4Fe(CN)_6$, 0.01% (v/v) Triton X, and 1mgml^{-1} X-gal in phosphate-buffered saline. The solution was adjusted to pH 4.5 using HCl. In the absence of an intact epidermal barrier, this acidic solution penetrates the epidermal barrier and activates endogenous β-galactosidase to produce a blue precipitate.

Quantitative real-time PCR

Total RNA was prepared from mouse tissues using RNA STAT-60 (Tel-Test, Friendswood, TX). Equal amounts of RNA were pooled from the tissues of five mice and subjected to quantitative real-time PCR as described (Liang *et al.*, 2002). A threshold line of 0.15 was set at the exponential phase of the PCR amplification to determine the number of PCR cycles required (cycle threshold, C_t) for the sample to reach the threshold level. The relative amount of all mRNAs was calculated using the comparative C_t method with cyclophilin as the invariant control. Primers used for real-time PCR have been described previously (Liang *et al.*, 2002; Yabe *et al.*, 2003).

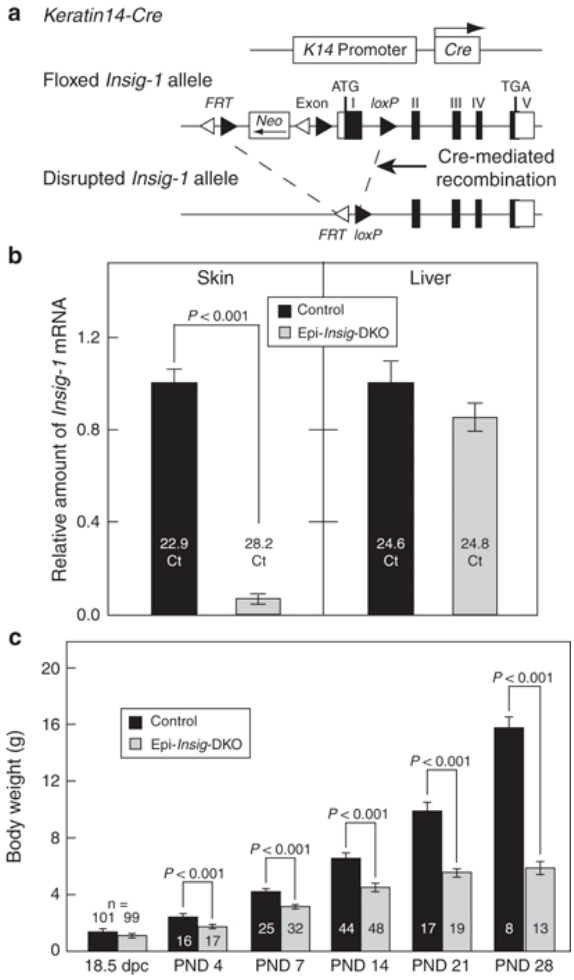

Figure 2-1 Generation of mice lacking *Insigs* in the epidermis. (**a**) Schematic of epidermal-specific deletion of *Insig-1*. The Cre-mediated deletion of *Insig-1*, in combination with the germ-line deletion of *Insig-2*, generated mice that lacked both Insig-1 and Insig-2 in the oral epithelium, epidermis, and hair follicles. Because the epidermis was the major tissue in which Insigs were ablated, we designated these mutant mice as epidermal-specific *Insig*-double knockout (Epi-*Insig*-DKO) mice. (**b**) Total RNA was isolated from back skins and livers of postnatal day 14 (PND 14) littermate control (*Insig-1* $^{f/f}$;*Insig-2* $^{-/-}$) and Epi-*Insig*-DKO mice. Relative amount of *Insig-1* mRNA was determined by quantitative real-time PCR using the comparative C_t method. Each bar represents the mean±SEM of data from five mice. The C_t (cycle threshold) numbers are shown inside the bars. (**c**) Body weights of littermate control and Epi-*Insig*-DKO mice were measured at various ages. Each bar represents the mean±SEM of data from the indicated number of mice. Statistical analysis was performed with the two-tailed Student's *t*-test.

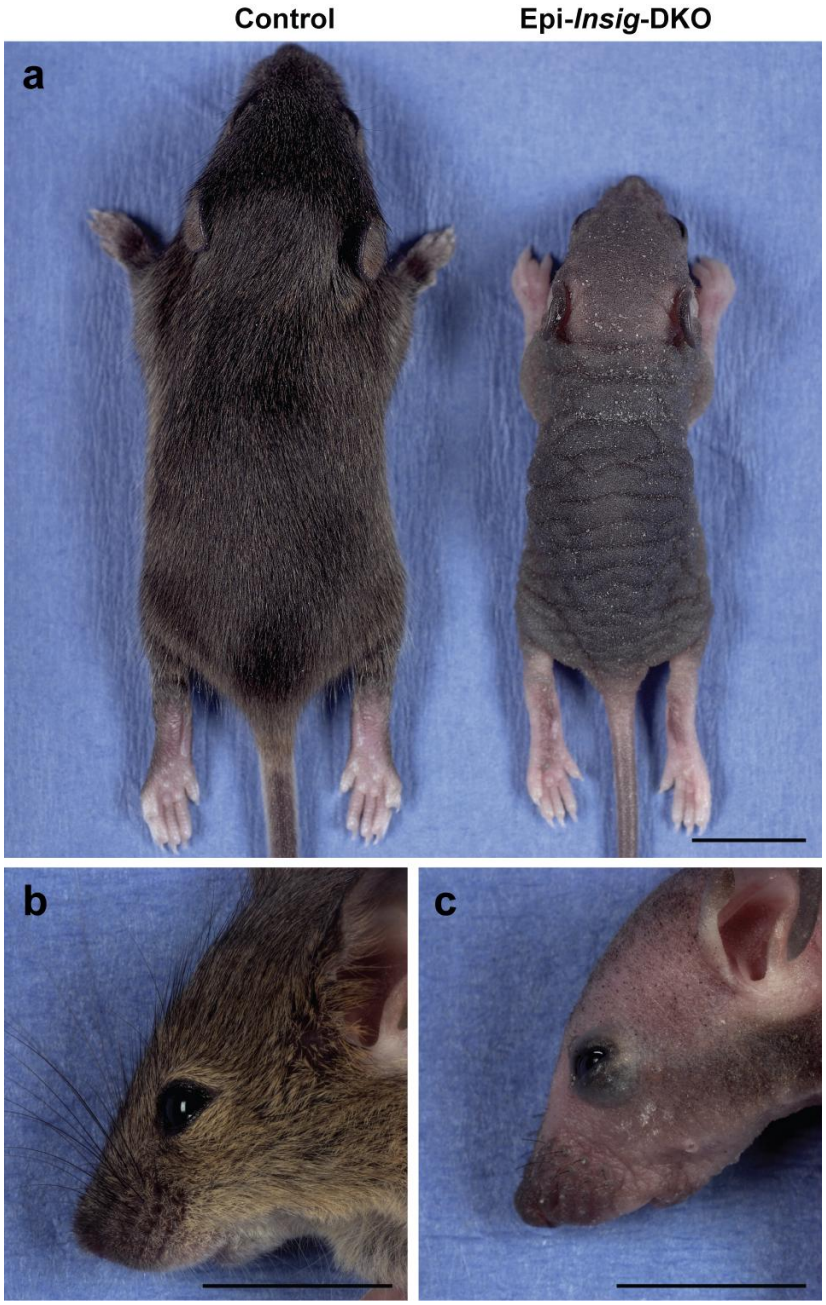

Figure 2-2 Gross morphology of control and Epi-*Insig*-DKO mice. Representative photographs of control and Epi-*Insig*-DKO littermates at postnatal day (PND) 14. Compared with control mice (**a**, left), all mutant mice (**a**, right) were smaller in size, exhibited thickening and flaking of the skin, and failed to grow body hair. Epi-*Insig*-DKO mice (**c**) also exhibited exophthalmos and short, kinked vibrissae compared with control mice (**b**). Scale bars = 1.0cm (**a**–**c**).

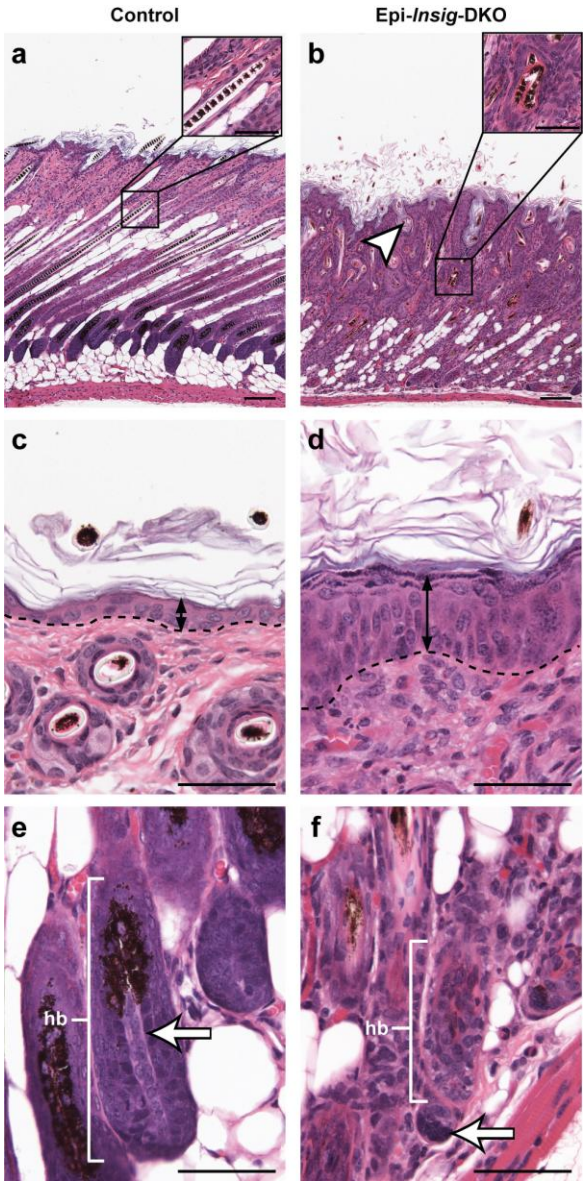

Figure 2-3 Histology of skin from control and Epi-*Insig*-DKO mice. Skin from the upper back of postnatal day (PND) 14 littermate control and Epi-*Insig*-DKO mice was fixed, sectioned parallel (**a**, **b**, **e**, **f**) or perpendicular (**c**, **d**) to the hair shaft, and stained with hematoxylin and eosin. Shown here are sections representative of five mice in each group. (**a**, **b**) Images from control and mutant mice of all three skin layers: epidermis, dermis, and hypodermis. (**c**, **d**) Images taken at a higher magnification focusing on the epidermal layer. The dashed line represents the border between the epidermis and dermis. (**e**, **f**) Images taken at a higher magnification to focus on the hair bulb. Scale bars = 0.1mm (**a**, **b**) and 0.05 mm (**c**–**f**, insets of **a** and **b**).

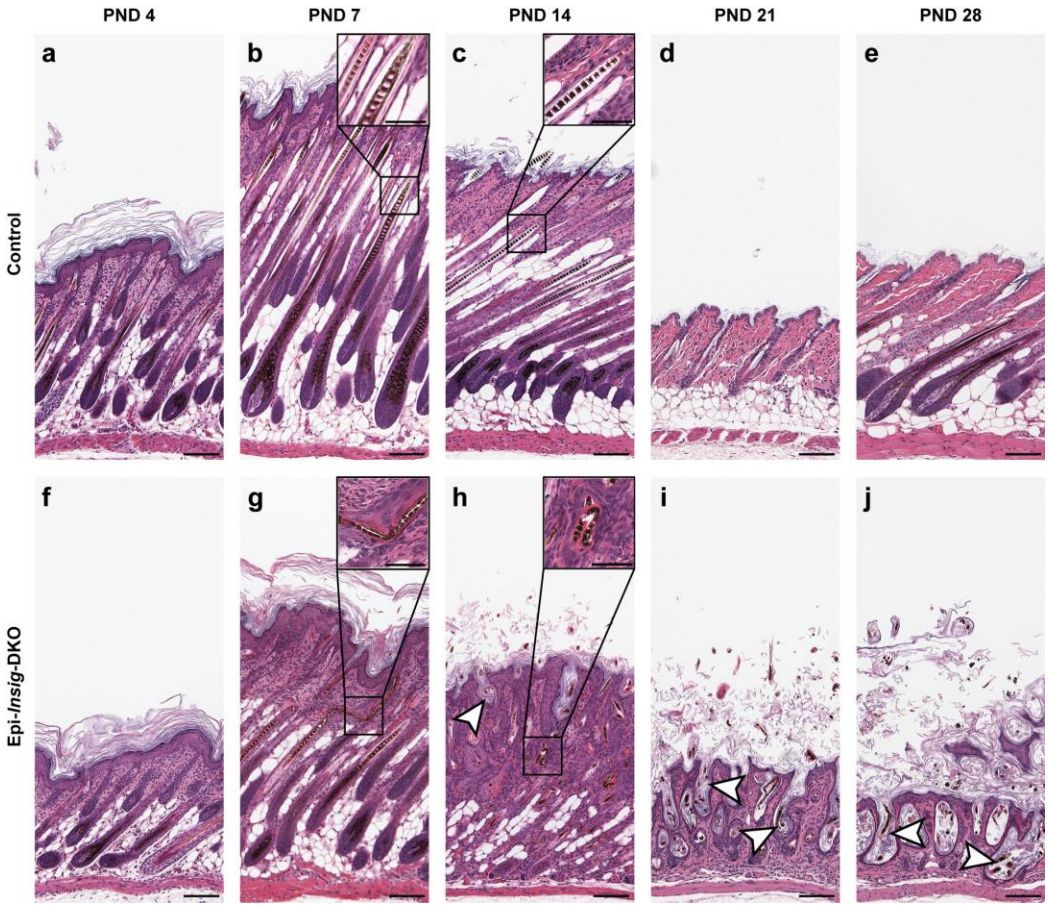

Figure 2-4. Hair follicle morphogenesis and cycling in control and Epi-*Insig*-DKO mice. Skin from the upper back of postnatal days (PNDs) 4, 7, 14, 21, and 28 littermate mice was fixed, sectioned parallel to the hair shaft, and stained with hematoxylin and eosin. (**a**–**j**) Shown here are sections representative of five mice in each group. Scale bars=0.1 mm (**a**–**j**) and 0.05 mm (insets of **b**, **c**, **g**, **h**).

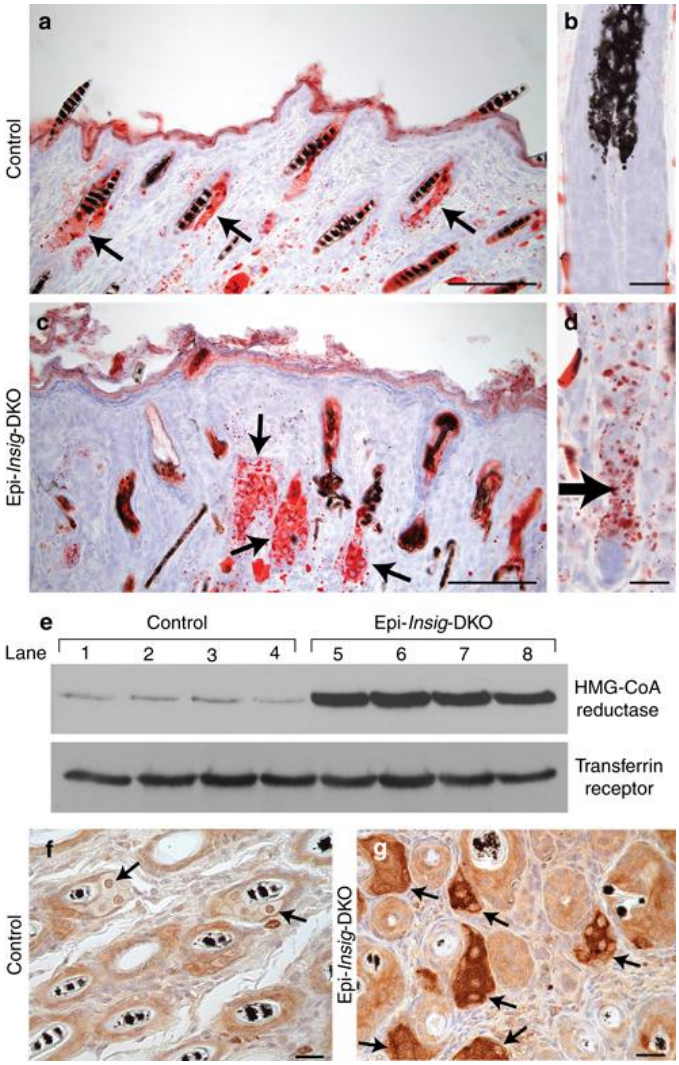

Figure 2-5 Staining of lipids and immunological visualization of 3-hydroxy-3-methylglutaryl coenzyme A (HMG-CoA) reductase in skin from control and Epi-*Insig*-DKO mice. (**a**–**d**) Skin from the upper back of postnatal day (PND) 14 control and Epi-*Insig*-DKO mice was fixed, cryosectioned, and stained with oil red O. Shown here are representative sections from four mice per group. (**e**) Immunoblot analysis of HMG-CoA reductase in skin from the upper back of PND 14 control and Epi-*Insig*-DKO mice. Aliquots of whole-cell lysates (30μg) were subjected to 8% SDS–PAGE and immunoblot analysis with a rabbit polyclonal antibody against mouse HMG-CoA reductase. Transferrin receptor was used as loading control. Shown are results from four control (lanes 1–4) and four Epi-*Insig*-DKO (lanes 5–8) mice. (**f**, **g**) Immunohistochemical analysis of HMG-CoA reductase in skin from upper back of PND 14 control (**f**) and Epi-*Insig*-DKO (**g**) mice. Shown are sections representative of five mice in each group. Scale bars=0.1mm (**a**, **c**), 0.01mm (**b**, **d**), and 0.02mm (**f**, **g**).

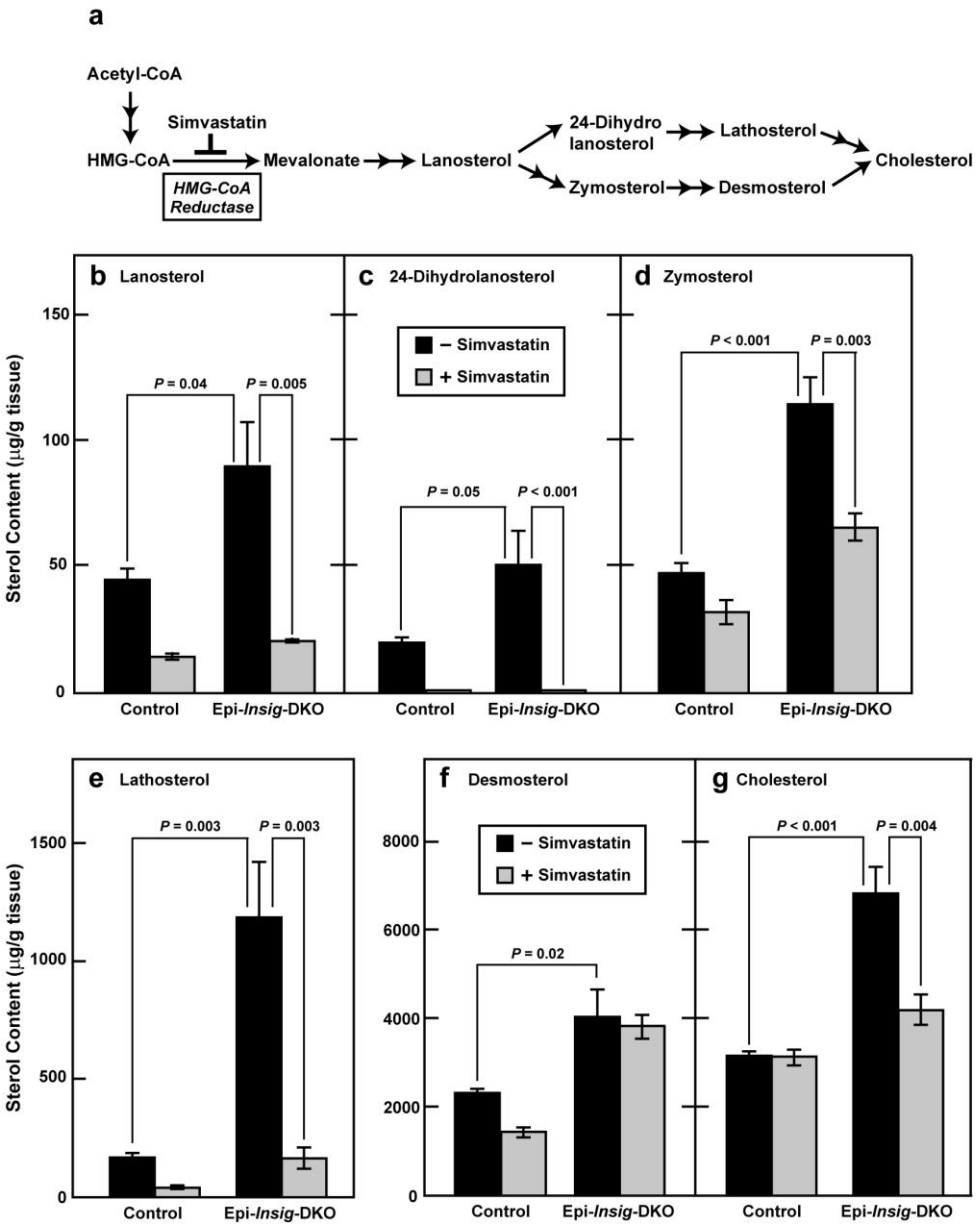

Figure 2-6 Sterol content in the skin of control and Epi-*Insig*-DKO mice treated with or without simvastatin. (**a**) Pathway for cholesterol biosynthesis, showing site of inhibition by simvastatin. (**b**–**g**) Littermate control and mutant mice were treated daily with either 1 mg simvastatin or vehicle from postnatal day (PND) 2 to PND 13. At PND 14, skin from the upper back was harvested and subjected to gas chromatography–mass spectroscopy analysis to measure the levels of various sterols. Each bar represents the mean±SEM of data from five mice. Statistical analysis was performed with the two-tailed Student's *t*-test.

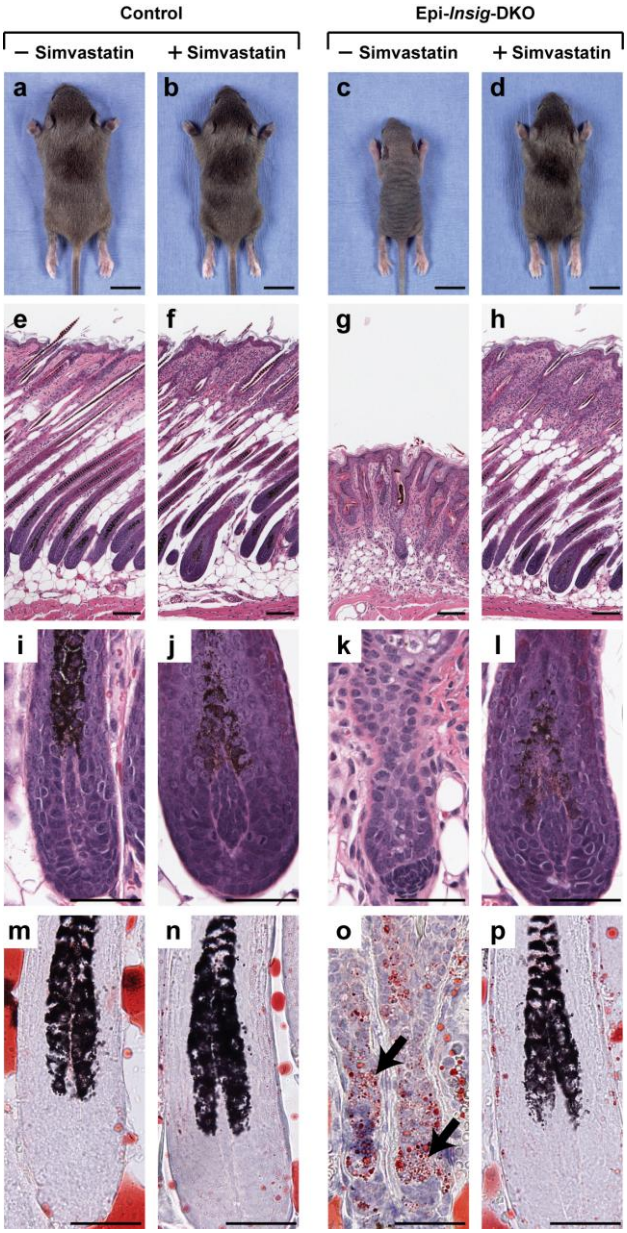

Figure 2-7 Gross morphology and histology of control and Epi-*Insig*-DKO mice treated with or without simvastatin. Littermate control and Epi-*Insig*-DKO mice were treated daily with either 1mg simvastatin or vehicle from postnatal day (PND) 2 to PND 13. (**a**–**d**) At PND 14, animals were photographed and analyzed for hair growth by two independent observers before genotyping. (**e**–**p**) Mice were killed at PND 14, and skin from the upper back was fixed and either sectioned for hematoxylin and eosin staining (**e-l**) or cryosectioned for oil red O staining (**m**–**p**). Shown here are sections representative of three mice (**m**–**p**) or five mice (**e**–**l**) per group. Scale bars=1.0cm (**a**–**d**), 0.1mm (**e**–**p**).

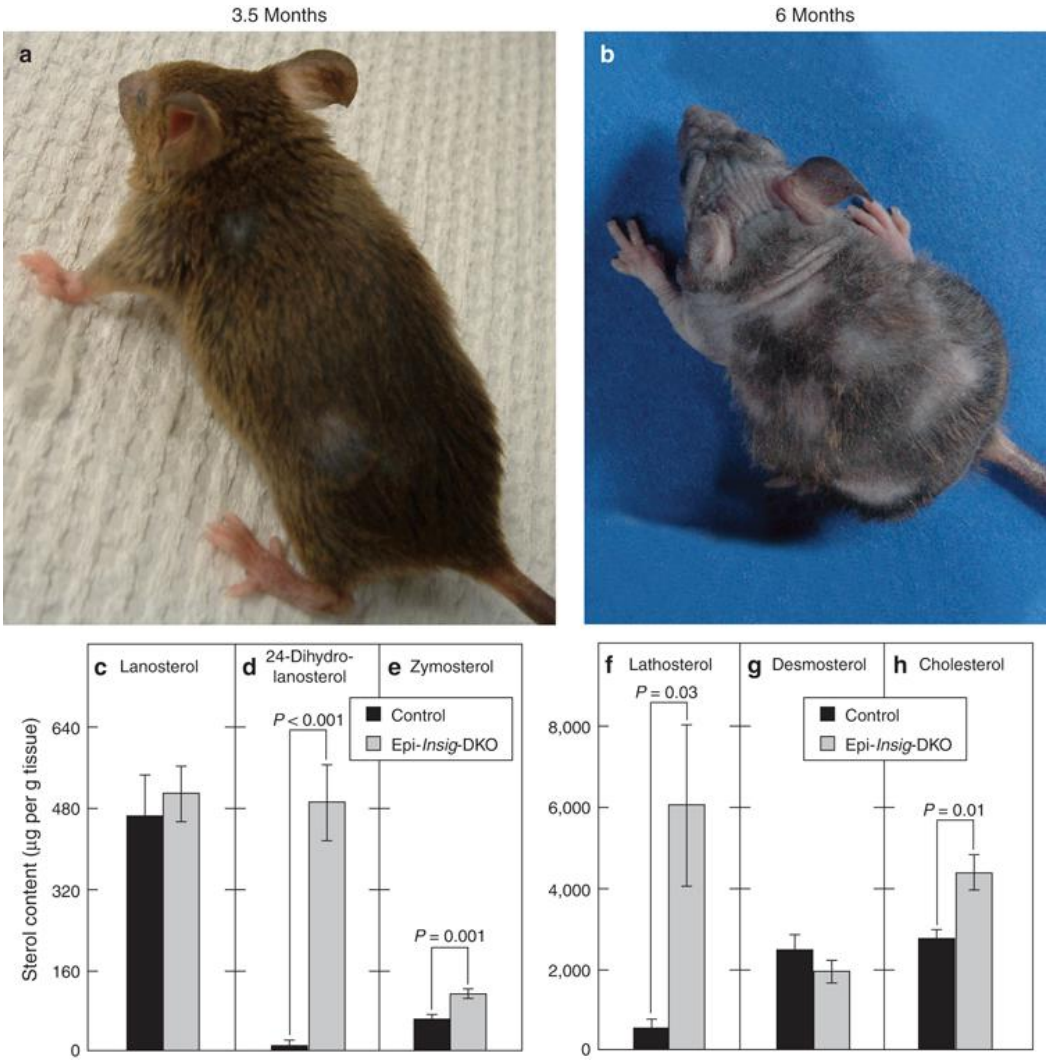

Figure 2-8 Morphology and skin sterol content of control and Epi-*Insig*-DKO mice at 3 and 5.5 months after stopping simvastatin. (**a**, **b**) Five Epi-*Insig*-DKO mice were treated daily with 1 mg simvastatin from postnatal day (PND) 2 to PND 13. Thereafter, the mice were left untreated for 5.5 months. These photographs show the same Epi-*Insig* DKO mouse at 3.5 months (**a**) and 6 months (**b**) of age. The mouse shown here is representative of all five mutant mice studied in this experiment. (**c**–**h**) The sterol content in the back skin from control and Epi-*Insig*-DKO mice at 6 months was measured by gas chromatography–mass spectroscopy. Each bar represents the mean±SEM of data from five mice. Statistical analysis was performed with the two-tailed Student's *t*-test.

CHAPTER THREE
Alopecia in Insig-deficient Mice Preceded by Loss of Keratin-associated Protein mRNA Expression and Abnormal Hair Cuticle Formation

Adapted from Farooqi MS, Evers BM, Owen JL, Zhang Y, Gilpin CJ, Shelton JM, Richardson JA, Goldstein JL, Brown MS, Liang G (2012) In preparation for submission to the Journal of Investigative Dermatology

Introduction

Precise regulation of the levels of cholesterol, its metabolic precursors, and its biosynthesis is absolutely required for mammalian development to occur normally. Humans with inborn errors of cholesterol biosynthesis suffer from a range of multiple congenital anomaly/mental retardation syndromes as they are deficient in cholesterol but accumulate sterol intermediates prior to the enzymatic block (Porter, 2003).

The developing integumentary system is particularly affected by perturbations in cholesterol homeostasis. Skin and hair abnormalities are seen in four types of the malformation syndromes mentioned above: Smith-Lemli-Opitz syndrome (SLOS), desmosterolosis, congenital hemidysplasia with ichthyosiform erythroderma and limb defects (CHILD) syndrome, and X-linked dominant chondrodysplasia punctata type 2 (CDPX2) (Herman, 2003; Anstey, 2006). Patients with these diseases can exhibit cutis aplasia (desmosterolosis); UV light-induced erythema and/or eczema (SLOS); alopecia, hyperkeratosis, and/or ichthyosis (CHILD syndrome and CDPX2). Mice with the corresponding mutations—Dhcr24$^{-/-}$ (desmosterolosis), Bpa/Str (CHILD), and Td (CDPX2)—show similar skin problems (Liu *et al.*, 1999).

Proper control over the amount of cholesterol in a cell is achieved through a network of proteins that sense cellular sterol levels and modulate the rate of cholesterol biosynthesis in turn (Brown and Goldstein, 2009). At the heart of this feedback regulatory system lie Insig-1 and Insig-2, a pair of closely related endoplasmic reticulum (ER) membrane proteins. When concentration of sterols is high, Insigs act in two ways to limit cholesterol synthesis. First, they enhance the ubiquitination and degradation of 3-hydroxy-3-methylglutaryl coenzyme A (HMG-CoA) reductase, the rate-limiting enzyme of cholesterol biosynthesis (Goldstein *et al.*, 2006). Second, Insigs prevent sterol regulatory element-binding proteins (SREBPs) from activating transcription of all cholesterol biosynthetic enzyme genes.

SREBPs are ER membrane-bound transcription factors that have to be freed from this membrane by proteolytic cleavage so that they can travel to the nucleus. For this release to occur, SREBPs have to migrate from the ER to the Golgi apparatus so that they can be cleaved by two proteins only found in the Golgi, Site-1 protease (S1P) and Site-2 protease (S2P) (Horton *et al.*, 2002). SREBPs, though, cannot travel from the ER to the Golgi on their own; they must be escorted by another ER membrane protein: Scap. Insigs block SREBP function by binding to Scap and preventing the ER-to-Golgi transport of SREBPs.

The importance of Insigs to proper embryonic development was made clear when we studied mice with a germline deletion of both Insig-1 and Insig-2 (Engelking *et al.*, 2006). Unable to check HMG-CoA reductase and SREBP function, Insig-double knockout (*Insig*-DKO) mice markedly overproduced cholesterol and significantly accumulated its precursor molecules, leading to a clefting of the face and/or palate

followed by neonatal lethality. Lowering cholesterol biosynthesis in *Insig*-DKO embryos by treating pregnant females with lovastatin, an HMG-CoA reductase inhibitor, reduced levels of sterol intermediates and reversed the facial clefting phenotype. We thus put forth the idea that the developmental defects seen in our mice were caused by the accumulation of sterol precursors.

This concept was further reinforced when we generated mice lacking both Insig proteins specifically in the epidermis and hair follicles (Evers *et al.*, 2010). Epidermal *Insig*-double knockout (Epi-*Insig*-DKO) mice also had a significant build up of cholesterol and its precursor molecules (though this time limited to the skin) and, strikingly, were completely unable to grow body hair. Topical application of simvastatin, another HMG-CoA reductase inhibitor, reduced levels of epidermal sterol intermediates in Epi-*Insig*-DKO mice and completely reversed the hair growth defect. Though this again indicated that abnormally high amounts of pre-cholesterol sterol intermediates have a teratogenic effect, the molecular mechanism by which sterol precursors impaired hair growth remained unknown.

Accordingly, in this study, we investigated the development of hair follicles in Epi-*Insig*-DKO mice at a molecular and ultrastructural level. We found that at postnatal day four (PND4), even though both control and mutant mice were histologically identical, there was a significant decrease in the expression of keratin-associated protein mRNAs in the skin of Epi-*Insig*-DKO mice. This was accompanied by a defect in proper formation of the hair cuticle that could be seen at an ultrastructural level. In addition, there was a marked accumulation of sterol intermediates in the skin of mutant mice at PND4, and treatment with simvastatin was able to rescue Krtap expression. These

findings have implications for the pathogenesis of hair abnormalities seen in diseases that arise from an imbalance of cholesterol homeostasis.

RESULTS

Characterization of mice deficient in Insig-1 and Insig-2 in the epidermis

The generation of Epi-*Insig*-DKO animals has been described previously (Evers *et al.*, 2010). Briefly, female mice harboring floxed *Insig-1* and null *Insig-2* alleles (*Insig-1*$^{f/f}$;*Insig-2*$^{-/-}$) were bred to male mice heterozygous for floxed *Insig-1*, null for *Insig-2*, and carrying a *Keratin14-Cre* (*K14-Cre*) transgene (*Insig-1*$^{f/wt}$;*Insig-2*$^{-/-}$;*K14-Cre*). This cross produces the two sets of mice studied here: control (*Insig-1*$^{f/f}$;*Insig-2*$^{-/-}$) and Epi-*Insig*-DKO (*K14-Cre;Insig-1*$^{f/f}$;*Insig-2*$^{-/-}$).

In our previous work (Evers *et al.*, 2010), we observed that pelage hair did not erupt properly in Epi-*Insig*-DKO mice. As hair erupts between PND 5 and PND 8—i.e., during the eighth stage of hair follicle development (Paus *et al.*, 1999)—we evaluated the hair and skin histologically around this time (PND 7). Skin sections from mutant mice revealed only one difference between their hair follicles and those seen in control mice—10% of mutant hair shafts had kinked within the follicle. Other than this defect, we saw no major follicular abnormalities: there was no dropout of hair follicles, no sign of folliculitis or other pathology, and the follicles developed properly enough to produce pigmented hair shafts. Nonetheless, no body hair erupted in Epi-*Insig*-DKO mice.

To see if we could find a molecular mechanism underlying this phenotype, we decided to investigate these mice at an earlier age: PND 4, a day before hair follicle entry

into Stage 8 of follicular morphogenesis and a point at which control and mutant mice are histologically indistinguishable (Evers *et al.*, 2010). Indeed, they are difficult to tell apart grossly at this age as well (Figure 1). Four-day-old Epi-*Insig*-DKO mice look very similar to control mice, though they are a little smaller in size. This feature is not always present however, nor do mutant mice exhibit the thick, flaky skin and exophthalmos that will mark them later in life. The only visible difference at PND4 is that mutant mice have bent vibrissae that are much shorter than those seen in control mice (Figure 1b and c).

However, Epi-*Insig*-DKO mice are deficient in Insig-1 at this age (Figure 2). Quantitative real-time PCR analysis of the skin and liver from PND 4 control and mutant mice showed approximately an 80% reduction of Insig-1 mRNA levels in the skin of Epi-*Insig*-DKO mice relative to control mice (Figure 2a). The amount of Insig-1 mRNA in the liver between the two groups of mice was very comparable, highlighting the skin-specific ablation of *Insig-1* by *K14-Cre*. Immunoblot analysis of Insig-1 further confirmed its loss in the skin (Figure 2b). The amount of Insig-1 protein was __-fold less in Epi-*Insig*-DKO skins relative to control skins at PND 4. This fold difference was calculated by the densitometric quantification of the Insig-1 protein band relative to its corresponding transferrin protein band (loading control) and is an average of the four values in each group.

Developmental analysis of control and Epi-Insig-DKO hair follicles

We then sought to determine whether there were any differences in hair follicle cell proliferation or apoptosis between control and mutant mice at PND 4. As such, we stained skin sections from both sets of mice with Ki67, a marker for dividing cells

(Figure 3a). We did not observe any disparity in proliferation of skin and hair follicle keratinocytes between control and Epi-*Insig*-DKO mice. Hair bulb matrix cells were just as numerous in mutant mice as control mice and divided just as well. Terminal deoxynucleotidyl transferase dUTP nick end labeling (TUNEL) revealed no differences in keratinocyte cell death either (Figure 3b). Overall, cells of the skin and hair rarely underwent apoptosis in both control and Epi-*Insig*-DKO mice.

We then investigated whether any major developmental signaling pathways involved in hair follicle morphogenesis were abnormal. We began by measuring mRNA levels of proteins involved in the Sonic Hedgehog (Shh) pathway as this developmental ligand is critical throughout hair development (Oro and Higgins, 2003) and is directly modified by both palmitate and cholesterol (Porter *et al.*, 1996). Shh operates by binding to its cell surface receptor, Patched, and preventing this protein from inhibiting Smoothened, a heptahelical membrane protein similar to G protein–coupled receptors (Wang *et al.*, 2007). Smoothened then activates the Gli family of transcription factors. Both *Patched-1* and *Gli-1* are positive targets of Shh signaling and, accordingly, we measured their mRNA expression as well as that of *Shh* and *Smoothened* by qPCR.

There were no differences in the mRNA levels of any of these genes between control and Epi-*Insig*-DKO mice at PND 4 (Tables 1 and 2). As real-time PCR only quantifies the total amount of mRNA and does not provide information regarding the spatial expression of a gene, we conducted *in situ* hybridization to determine any differences in Shh localization (Figure 4). In both control and mutant hair follicles, Shh showed its characteristic asymmetric expression pattern in the hair bulb (Oro and

Higgins, 2003). Similar analysis of *Patched-1* and *Gli-1* mRNA further supported the result that Shh signaling was not perturbed in Epi-*Insig*-DKO skin.

We then measured mRNA levels of Wnt signaling pathway components. Wnt is another protein very important to follicular morphogenesis and, like Shh, has a palmitoyl group covalently attached to it (Logan and Nusse, 2004). Wnt binds to its receptor, Frizzled, on cell surfaces thereby activating the membrane-associated Dishevelled. This molecule then inhibits a trio of proteins (APC, Axin, and GSK-3β) which normally work in concert to promote the degradation of β-catenin. Through the action of Dishevelled, β-catenin increases in amount and enters the nucleus. There, it interacts with the Tcf/Lef transcriptional complex, promoting its activity. We measured the expression of different Wnt ligands and pathway components, including *Wnt-5a*, *Wnt-10b*, *Frizzled-1*, *APC*, *GSK-3β*, *Axin-2*, *β-catenin*, *Tcf-1*, and *Lef-1*, in PND 4 control and mutant skin through real-time PCR; of note, *Tcf-1*, *Lef-1*, and *Axin-2* are positively regulated by Wnt signaling.

Amongst the mRNAs we measured, four—*Wnt-5a*, *Wnt-10b*, *Frizzled-1*, and *Lef-1*—were reduced by around 30-40% in Epi-*Insig*-DKO skin as compared to control skin (Tables 1 and 2). The remaining mRNAs were not significantly decreased. As the significance of this finding was unclear, we asked whether this decline persisted through PND 7; in the case of *Wnt-10b* and *Frizzled-1*, it did not. *Wnt-5a* and *Lef-1*, however, stayed down by approximately 30-40%, and were joined by *Tcf-1* whose expression was decreased by the same amount. Still, the degree of reduction in the levels of these mRNAs seemed slight when compared to the extent of the phenotype. Furthermore, other Wnt signaling targets more specific to hair and skin such as *E-cadherin*, *Ovol-1*, and

Jagged-1 were not changed between control and Epi-*Insig*-DKO mice (data not shown), arguing against the notion of Wnt signaling being significantly different in mutant mice (Jamora *et al.*, 2003; Li *et al.*, 2002; Estrach *et al.*, 2006; Denecke and Kranz, 2009).

Keratin-associated protein expression is significantly decreased in mutant mice

For these reasons, we decided to continue pursuing a molecular basis underlying this hair phenotype and performed comparative microarray analysis of PND 4 control and Epi-*Insig*-DKO skin. Through this technique, we identified a distinct group of genes whose expression was sharply down-regulated in mutant mice (Table 3). Out of the twenty genes that showed the greatest reduction in expression, 80% were either keratin-associated proteins (Krtaps) or transcripts with significant homology to Krtaps. Krtaps are essential for the formation of a rigid, structurally sound hair shaft as they form the matrix in which hair keratin intermediate filaments embed and extensively cross-link to these filaments via cysteine-mediated disulfide bonds (Wu *et al.*, 2008). Our Affymetrix microarray chip had 39 probes specific for unique *Krtap* genes that gave a measurable signal. Of these 39 *Krtaps*, 18 were decreased by more than 50%, 17 by 20-50%, and 4 were not changed.

We confirmed the loss of *Krtap* expression by real-time PCR for a subset of these genes—*Krtap5-2*, *Krtap5-3*, *Krtap6-3*, *Krtap16-9*, and *Krtap28-13* (Figure 5). While the relative amount of *Krtap16*-9 mRNA was reduced by approximately five-fold, the expression of the remaining *Krtap* genes tested decreased by more than 20-fold. As a control, levels of the nuclear hormone receptor *RORα* do not change, though it should be noted that this gene is fairly well-expressed in the skin and hair.

Krtap genes cluster at just a few chromosomal locations relative to their total number (>150 in mouse) and are arrayed in tandem, though different families may be expressed in different regions of the hair follicle even if they are linked in such a fashion (Wu *et al.*, 2008). Krtaps in general can be divided into three major groups by their amino acid composition: high-glycine/tyrosine, high-sulfur (~16–30 mol% cysteine), or ultra-high sulfur (> 30 mol% cysteine) (Shimomura *et al.*, 2003). Of great interest to us was the particular severity of the loss of *Krtap5* family members, a group of ultra-high sulfur proteins found on mouse chromosome 7 that are specifically expressed in the hair shaft cuticle (Rogers, 2004).

Ultrastructure of control and Epi-Insig-DKO hair follicles

Hence, we asked whether the lack of *Krtap5* family expression was due to the absence of a hair cuticle and, for this reason, examined the hair follicles of our mice at an ultrastructural level. Figure 6 shows transmission electron microscopy (TEM) images of ultrathin skin sections from PND 4 control and mutant mice. The first pair of images (Figure 6a and 6b) are taken at a level fairly proximal to the hair bulb as evidenced by the fact that only Henle's layer has keratinized (Morioka, 2004). At this stage, there is no major difference in the organization of the two hair follicles. Both are surrounded by a connective tissue sheath, an outer root sheath, and a companion layer that look very comparable to one another. Both have a properly keratinized Henle's layer, a Huxley's layer that is in the process of keratinizing, and a series of vertically-oriented, oval cells stacked upon one another which comprise the cuticle of the inner root sheath. Finally, both have nucleated cells in the layer immediately next to the IRS cuticle—the cuticle of

the hair shaft, which can be differentiated from the adjacent hair shaft cortex as the latter has cells with larger nuclei and tonofilaments.

Figure 6 also shows TEM images of hair follicles from PND 4 control and Epi-Insig-DKO mice taken at a level more proximal to the skin surface (Figure 6c and 6d). At this point, there is a major difference in the hair shaft cuticle layer. Whereas the cuticle of the control hair shaft keratinizes and organizes into a dark hooked structure, the mutant hair shaft cuticle does not form into such a structure but instead becomes as a thin, indiscriminate layer. The hair cuticle is clearly not absent in this case and has indeed keratinized: hair cuticle cells have lost their mitochondria and nucleus; but no exocuticle or endocuticle can be distinguished. In spite of this, the cells of the IRS cuticle look almost identical between the two follicles: both sets accumulate tonofilaments in a polar fashion and form hooked structures of their own. Note also that the hair shaft cortexes between control and Epi-*Insig*-DKO follicles cannot be told apart; both possesses thick bundles of keratin fibers intermixed with granules of keratohyalin that stain heavily with osmium.

We next wondered if this cuticle defect was also present in vibrissae of Epi-*Insig*-DKO mice. Since these hairs actually erupt from the skin, we were able to observe the surface of the hair fiber in its more native state at an ultrastructural level using scanning electron microscopy (EM). Control vibrissae showed a well-defined cuticle with scales that were sharp, smooth and present in regular intervals (Figure 7a). This cuticular scale was present through the length of the hair fiber examined. Scanning EM revealed an indiscernible cuticular scale in mutant whiskers (Figure 7b); the outer layer of the hair fiber was instead rough and uneven, clumped in some areas and peeling away in others.

The topography of vibrissae from Epi-*Insig*-DKO mice varied by location as well. Near the base and for much of hair fiber (~ 90%), the cuticle was difficult to identify as such. However, as one neared the tip of the hair shaft, a cuticular scale became recognizable. However, the scales themselves were of varying lengths, did not overlap with one another in an even, periodic manner, and were marked with linear striations (Figure 7c and d).

Figure 7 (e and f) also shows a vibrissa from either mouse cut into cross-section (near the middle of the hair shaft) and examined using TEM. This technique confirmed that the cuticle (here composed of multiple cellular layers oriented perpendicularly to the cortex) was grossly distorted in mutant mice (Figure 7f). Compared to the cuticle of the whisker from a control mouse which was organized and formed a scale (Figure 7f), the mutant whisker had uneven and ragged cuticle cells filled with osmium-dense granules and degenerating mitochondrial vesicles.

Elevation of cholesterol precursors and simvastatin-mediated correction of hair defects in Epi-Insig-DKO mice

In our previous study of Epi-*Insig*-DKO mice, we showed that Insig deficiency caused an overproduction and marked buildup of cholesterol and its sterol precursors at PND 14 and postulated that this accumulation led to the skin and hair abnormalities seen in these mice (Evers *et al.*, 2010). Accordingly, we measured the levels of a subset of sterol intermediates and cholesterol using gas chromatography-mass spectroscopy once more, this time in skin from PND 4 control and Epi-*Insig*-DKO mice (Figure 8). Though cholesterol itself was increased slightly, levels of its precursor molecules were elevated to a greater extent in skin from Epi-*Insig*-DKO mice, ranging from 1.9-fold for zymosterol

(Figure 8c) to 4.7-fold for lathosterol (Figure 8b). Overall, total sterol intermediates were higher in Epi-*Insig*-DKO skin relative to control skin to the about the same extent at PND 4 as they were at PND 14 (2.6-fold versus 2.9-fold, respectively).

We then asked whether blocking cholesterol biosynthesis in mutant mice could rescue *Krtap* expression. Hence, we treated control and Epi-*Insig*-DKO mice topically with simvastatin, a compound that competitively inhibits the enzyme HMG-CoA reductase and stops cellular production of cholesterol. This treatment was done as before (Evers *et al.*, 2010) except that mice were dosed daily from PND 1 to PND 4. When treated with vehicle, the epidermal expression of *Krtap* mRNAs was again severely reduced in mutant mice relative to control mice (Figure 9a). However, simvastatin treatment was able to rescue the expression of all of the *Krtap* mRNAs examined in Epi-*Insig*-DKO skin and restored them to levels comparable to those seen in skin from control mice (Figure 9b).

DISCUSSION

In this study, we used comparative microarray analysis to identify a group of keratin-associated proteins whose expression was lost in the skin of Epi-*Insig*-DKO mice. This deficiency preceded the hair eruption defect seen in mutant mice and was associated with a buildup of sterol precursors in mutant epidermis. Topical treatment of Epi-*Insig*-DKO mice with simvastatin, an inhibitor of cholesterol biosynthesis, blocked sterol intermediate accumulation and rescued *Krtap* expression.

The subset of Krtaps most severely affected was the Krtap5 family, a cohort of proteins expressed specifically in the hair cuticle that have a very high sulfur content due to a large number of cysteine residues (Rogers, 2004). Examination of pelage hair follicles with transmission electron microscopy revealed that a keratinizing hair cuticle layer was present in mutant follicles but that it failed to complete this process and organize into its native structure. Analysis of the vibrissae with both scanning and transmission electron microscopy confirmed the presence of a cuticle layer, as well as its abnormal nature in Epi-*Insig*-DKO mice.

The irregular development of the hair cuticle explains the alopecia in our mutant mice. Typically, the cuticle of the hair shaft matures to form an interlocking structure with the cuticle of the inner root sheath (Morioka, 2004). This apposition is critical to preserving synchronous growth between the IRS and hair shaft as it helps maintain the cylindricality and smooth upwards growth of the hair fiber. Furthermore, it is needed to help guide the hair shaft through the skin as evidenced by another mouse model of alopecia—the Sox21-null mouse—which also has a hair shaft cuticle defect (Kiso *et al.*, 2009).

In our model, elevated sterol intermediates lead to improper hair shaft cuticles which prevent pelage hair fibers from erupting. Since the matrix cells in the hair bulb of this follicle are still proliferating, the hair shaft continues to grow but, as it cannot grow outwards, kinks (as seen on PND 7) and later bends back upon itself. By some mechanism, the hair follicle recognizes this aberrant development and begins to degenerate in what we reason is a controlled manner as we do not see any major inflammation, fibrosis, or ancillary cellular destruction associated with this process. We

also think that the relative smoothness and subsequent kinking of the hair fiber is what prevents a phenotype like that seen in the asebia mouse from developing; in that model, the hair shaft, unable to exit through the epidermis, proceeds to extend in reverse towards the dermis, perforating the hair bulb (Sundberg *et al.*, 2000).

These ideas are further corroborated by the fact that mutant vibrissae erupt while pelage hair does not. The whiskers have a cuticle near the tip of the hair fiber, a feature that allows them to emerge from the skin. Though the cuticle cells themselves are irregular—marked with nodules and linear striations—they must still overlap with enough regularity to facilitate eruption of the vibrissae. Most likely, sterol intermediates need to accumulate past some threshold level in order to disrupt cuticle formation. As whisker development begins two days before pelage hair starts to form (Davidson and Hardy, 1952), the oldest cuticular cells (found at the tip of the hair) are able to form somewhat normally. However, as one proceeds down the tip of the whisker fiber towards the skin, a defined cuticular scale becomes absent, in effect marking the point when the amount of sterol precursors reached critical mass.

It is also striking how specific this defect is given the background in which it occurs. The Cre used to delete *Insig-1* is linked to a *Keratin14* promoter, meaning that it expresses at around e14.5 in epithelial progenitor cells (Gritli-Linde *et al.*, 2007). Hence, all of the cells of the epidermis and hair follicle (barring melanocytes and the fibroblasts of the dermal papilla / connective tissue sheath) are deficient in Insigs as they all have an epithelial origin. Yet despite this, development of both the epidermis and the remaining hair follicle layers occurs normally. The outer root sheath and companion layer are present and comparable in both control and Epi-*Insig*-DKO mice. Keratinization of

Henle's layer, Huxley's layer, and hair shaft cortex occurs to completion and happens at proper spatial levels in relation to the follicle in both groups of mice. Most importantly, the cuticle of the IRS develops equally well in Epi-*Insig*-DKO mice as it does in control mice. Nonetheless, the hair shaft cuticle is abnormal.

Perhaps this layer is particularly sensitive to Insig loss due to the fact that its function is intimately related to the presence of certain lipids. For example, many molecules of a unique fatty acid, 18-methyleicosanoic acid (18-MEA), are found covalently attached to the outermost region of the hair shaft cuticle (Jones and Rivett, 1997). This fatty acid is synthesized like others by the enzyme fatty acid synthase but requires a specific precursor formed from the breakdown of isoleucine. Interestingly, patients that are unable to metabolize isoleucine—i.e., those that have Maple Syrup Urine Disease—have defects in their hair shaft cuticles.

In our mice, Insig deficiency leads to an unchecked upregulation of lipid synthesis as amounts of fatty acid synthase protein are increased through the action of SREBP-1c (Engelking *et al.*, 2005a). Hence, it is difficult to envision that 18-MEA would be deficient in Epi-*Insig*-DKO mice; if anything, levels of this compound should be increased. However, detrimental effects associated with an excess of 18-MEA acid have not been reported. Perhaps, excess synthesis of lipids and sterol precursors upset a sensitive balance of lipids needed for proper cuticle formation.

It should also be noted that Insig deficiency does not lead to complete degeneration of the hair shaft cuticle layer. The near complete loss of expression of certain *Krtaps* is not due to the cuticle layer being absent. Indeed, expression of other cuticle-specific proteins—such as Krt32 (Ha2), Krt35 (Ha5) and Krt85(Hb5)— still

occurs, though it is diminished by about 2-fold (according to our microarray analysis). In contrast, compare the 20-fold reduction of expression that occurs in the *Krtap5* family). It is known though that this class of Krtaps is the last to be expressed during keratinization: the typical order is keratin intermediate filaments, followed by high glycine/tyrosine Krtaps, then Krtaps high in sulfur, and finally ultrahigh sulfur Krtaps (Rogers, 2004). This fact further supports the idea that keratinization begins but fails to complete in the cuticle layer of Epi-*Insig*-DKO hair fibers.

What then causes this specific loss of expression? Of the transcription factors known to play a role in Krtap expression—Hox-C13 (Potter *et al.*, 2006), Gata-3 (Kurek *et al.*, 2007), Runx-1 (Soma *et al.*, 2006), c-Maf (Miyai *et al.*, 2010), and Sox-21 (Kiso *et al.*, 2009)—all were present in Epi-*Insig*-DKO mice at a level either equal or slightly decreased to that seen in control mice (microarray, data not shown). Interestingly, three other Hox genes: *Hoxa9*, *Hoxa10*, and *Hoxc10* were decreased by around 70% or more at PND4 (Table 3). These proteins would be expected to follow a highly specific spatial and temporal pattern of expression in the hair shaft cuticle if one or more of them does indeed activate transcription of the *Krtap5* family. As such, our laboratory is following up on these observations by performing immunogold labeling studies with antibodies to these proteins.

Overall, the present studies provide further explanation as to why Epi-Insig-DKO mice have alopecia. They also give insight into the cutaneous abnormalities that are seen in human patients with inborn errors of cholesterol metabolism, diseases in which sterol precursors accumulate due to enzymatic defects in the cholesterol biosynthetic pathway.

MATERIALS AND METHODS

Generation of mice lacking Insigs in the epidermis

Epi-*Insig*-DKO mice, i.e. those carrying a *K14-Cre* transgene, floxed *Insig-1* alleles (*Insig-1*$^{f/f}$) and a germline deletion of *Insig-2* (*Insig-2*$^{-/-}$) were generated as previously described (Evers *et al.*, 2010). As before, the date of birth was designated as PND1 and *Insig-1*$^{f/f}$;*Insig-2*$^{-/-}$ mice were used as controls across all experiments. Animals were genotyped using genomic DNA prepared from tail tissue for PCR with *Insig-1*, *Insig-2*, and *K14-Cre* primers as before (Evers *et al.*, 2010).

All mice were housed in colony cages with a 12-hour light/12-hour dark cycle and ad libitum fed Teklad Global 18% Protein Rodent Diet no. 2018 (Harlan Teklad Global Rodent Diets; Harlan Teklad). All animal experiments were performed with the approval of the Institutional Animal Care and Research Advisory Committee at the University of Texas Southwestern Medical Center at Dallas.

Histology

For histological analysis, skins from the upper back were collected from mice at PND 4 and fixed in 4% paraformaldehyde (PFA) (catalog no. 158127, Sigma-Aldrich, St. Louis, MO) for 24 hours at 4°C. They were then embedded in paraffin and sectioned longitudinally (parallel to the hair shaft) at 5μm. For routine visualization, skin sections were stained with hematoxylin and eosin.

Immunoblot and immunohistochemistry of Insig-1

A polyclonal antibody against the N- and C-terminal regions of mouse Insig-1 (GenBank accession no. AF527630) was prepared by immunizing rabbits with synthesized peptides multiply-conjugated to a branching lysine core (Invitrogen, Carslabad, CA) (Posnett *et al.*, 1988). Immunoblot analysis of mouse Insig-1 was carried out as described (Engelking *et al.*, 2005b) except that samples were not pooled, but run individually. Briefly, aliquots of membrane protein (30 μg) were subjected to 12% SDS–PAGE, transferred onto nitrocellulose filters and then incubated with 1 μg/ml anti-Insig-1 (purified IgG fraction). We used transferrin receptor as a loading control (Evers *et al.*, 2010).

Ki67 staining and TUNEL assay

For immunohistochemistry, skin sections (prepared as explained in *Histology* and processed as detailed in (Evers *et al.*, 2010) were incubated overnight at 4°C with 5 μg/ml anti-Ki67 antibody followed by incubation with the secondary antibody—donkey anti-mouse conjugated to the fluorophore Cy3—for one hour.

The DeadEnd™ Fluorometric TUNEL kit (Cat. No. G3250, Promega, Madison, WI) was used to label apoptotic cells. Skin sections (having undergone the same processing as above) were heated at 58^{o}C for 15 minutes then deparrafinized, rehydrated, and fixed in 4% PFA for 15 minutes at 23^{o}C. Sections were permeabilized with proteinase K (20 μg/mL), washed, then refixed again in 4% PFA for 5 minutes at 23^{o}C. After a 10 minute, room temperature incubation in Equilibration Buffer, sections were treated with the TdT Reaction mixture at 37^{o}C for 1 hour in the dark. The slides were

then washed with 2X saline-sodium citrate buffer for 15 minutes and counterstained with propidium iodide for 1 hour at 37^{o}C.

Quantitative real-time PCR

Total RNA was prepared from each mouse skin sample individually (n=4 for both groups of control and mutant mice) as outlined before (Liang *et al.*, 2002). This RNA was then used to make cDNA and subjected to quantitative real-time PCR (Liang *et al.*, 2002). All reactions were measured in triplicate and the comparative C_T method was used to calculate the relative amount of all mRNAs. Cyclophilin mRNA was used as the invariant control for all experiments.

RNA in Situ Hybridization

Probe template corresponding to the entire length of Shh cDNA was amplified by PCR and cloned into pCRII-TOPO (Invitrogen, Carlsbad, CA). These cDNA templates were linearized and used to generate ^{35}S-labeled sense and antisense probes via *in vitro* transcription by Sp6 and T7 RNA polymerases, respectively; Maxiscript kit (Ambion, Inc., Austin, TX). Radioisotopic *in situ* hybridization was carried out as outlined in the past (Shelton *et al.*, 2000). Autoradiographic exposure of slides was performed for 21 days at 4°C.

Affymetrix Oligonucleotide Array Hybridization and Data Analysis

Total RNA was prepared from each skin as above, then equal aliquots of total RNA from each of the four mouse skins in each group were pooled (total, 4 μg) and used

for biotin labeling as described in the Affymetrix technical bulletin. Hybridization, washing, scanning, and analysis of the Affymetrix GeneChip Mouse Genome 430 2.0 array (Affymetrix, Santa Clara, CA) were carried out as described (Horton *et al.*, 2003). Data obtained from the microarray hybridizations was processed with MICROARRAY SUITE 5.0 (Affymetrix) software.

Determination of tissue sterol composition

Sterols were measured in the skin of control and Epi-*Insig*-DKO mice at PND4 by gas chromatography-mass spectrometry (Evers *et al.*, 2010). Each sample (n=5 for both groups) was analyzed individually.

Simvastatin treatment of neonatal mice

A solution of simvastatin in 7:3 propylene glycol:ethanol was prepared at a concentration of 6.4 mg/ml, pH 7.4 as detailed (Evers *et al.*, 2010). A mixture of 7:3 propylene glycol:ethanol made in the same manner but without simvastatin was used as a control. As before, entire litters of mice first had acetone rubbed on their dorsal skin followed by application of either 1 mg of simvastatin or vehicle (isovolumetric). Mice were treated daily from PND1 to PND4.

Electron Microscopy

For transmission electron microscopy, skins from the upper back were collected from mice at PND 4 and fixed in a solution of 4% paraformaldehyde, 1% glutaraldehyde and 0.1 M sodium cacodylate buffer for 48 hours at 4°C. The fixed samples were then

treated with 2% osmium tetroxide in PBS for 1 hour at 4°C. After dehydration with ethanol, skins were embedded in epoxy resin (EMBED 812, Electron Microscopy Sciences) and polymerized at 60°C. Though keratinizing tissues are typically refractory to resin penetration, this is less of a problem with skin from neonatal rodents (Morioka, 2009). Ultrathin sections were cut at a thickness of 80 nm, placed on copper grids, and counterstained with uranyl acetate and lead citrate. Sections were examined at 120 kV with a Tecnai G2 Spirit transmission electron microscope (FEI Company), and images were taken by a Gatan USC1000 2k CCD camera.

For scanning electron microscopy, vibrissae from PND4 mice were isolated and affixed to carbon adhesive tabs on aluminum mounts. Samples were then coated with gold using a sputter coater and analyzed at 15kV with an XL30 environmental scanning electron microscope (FEI Company).

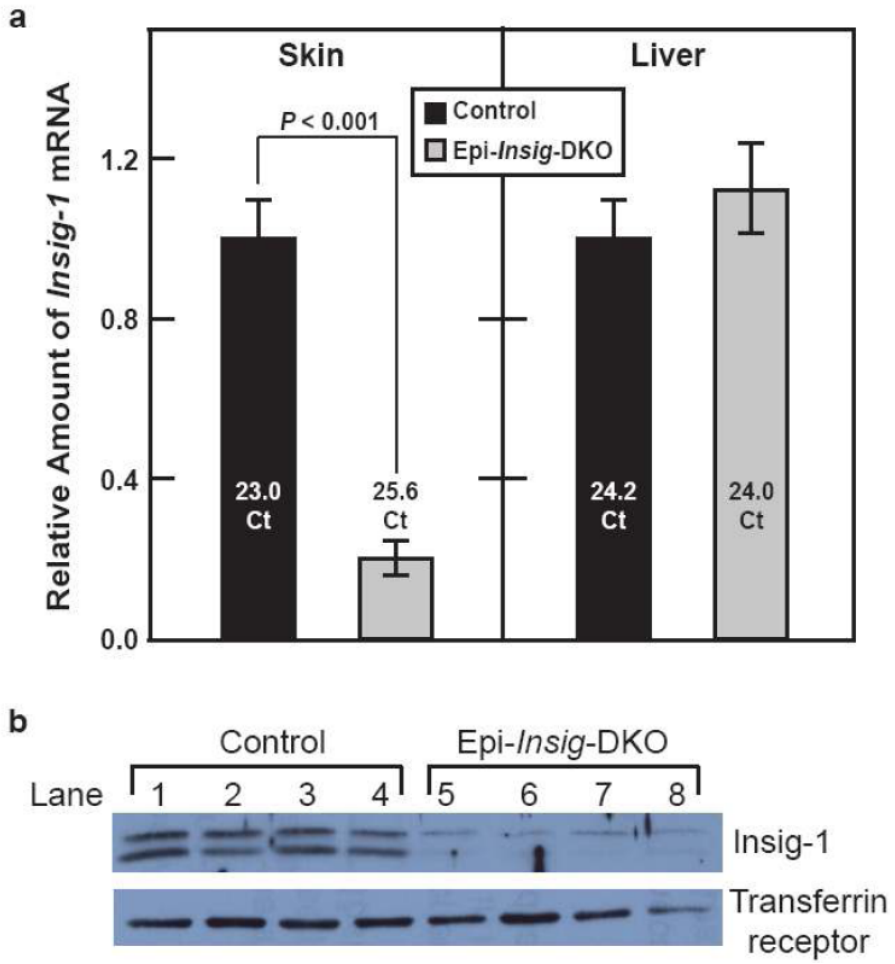

Figure 3-1. Loss of expression of *Insig-1* mRNA and protein. Mice harboring floxed *Insig-1* and null *Insig-2* alleles (*Insig-1*$^{f/f}$*;Insig-2*$^{-/-}$) were bred to mice carrying a *Keratin14-Cre* (*K14-Cre*) transgene to generate epidermal-specific *Insig*-double knockout (Epi-*Insig*-DKO) mice. (**a**) Total RNA was derived from back skins and livers of postnatal day 4 (PND 4) littermate control (*Insig-1*$^{f/f}$*;Insig-2*$^{-/-}$) and Epi-*Insig*-DKO mice (*Krt14-Cre;Insig-1*$^{f/f}$*;Insig-2*$^{-/-}$). The relative amount of *Insig-1* mRNA was measured by quantitative real-time PCR using the comparative C_t method. Each bar represents the mean±SEM of data from four mice. The actual cycle threshold (C_t) numbers are given inside the bars. Statistical analysis was performed with the two-tailed Student's t-test. (**b**) Immunoblot analysis of *Insig-1*. Skins from the upper back of PND 4 control and Epi-*Insig*-DKO mice were used to prepare membrane fractions of protein. Aliquots (30 μg) of these samples were subjected to 12% SDS–PAGE and analyzed by immunoblotting with a rabbit polyclonal antibody against mouse Insig-1 as well as a mouse monoclonal antibody against transferrin receptor to confirm equal loading. The results from four control (lanes 1–4) and four mutant (lanes 5–8) mice are shown.

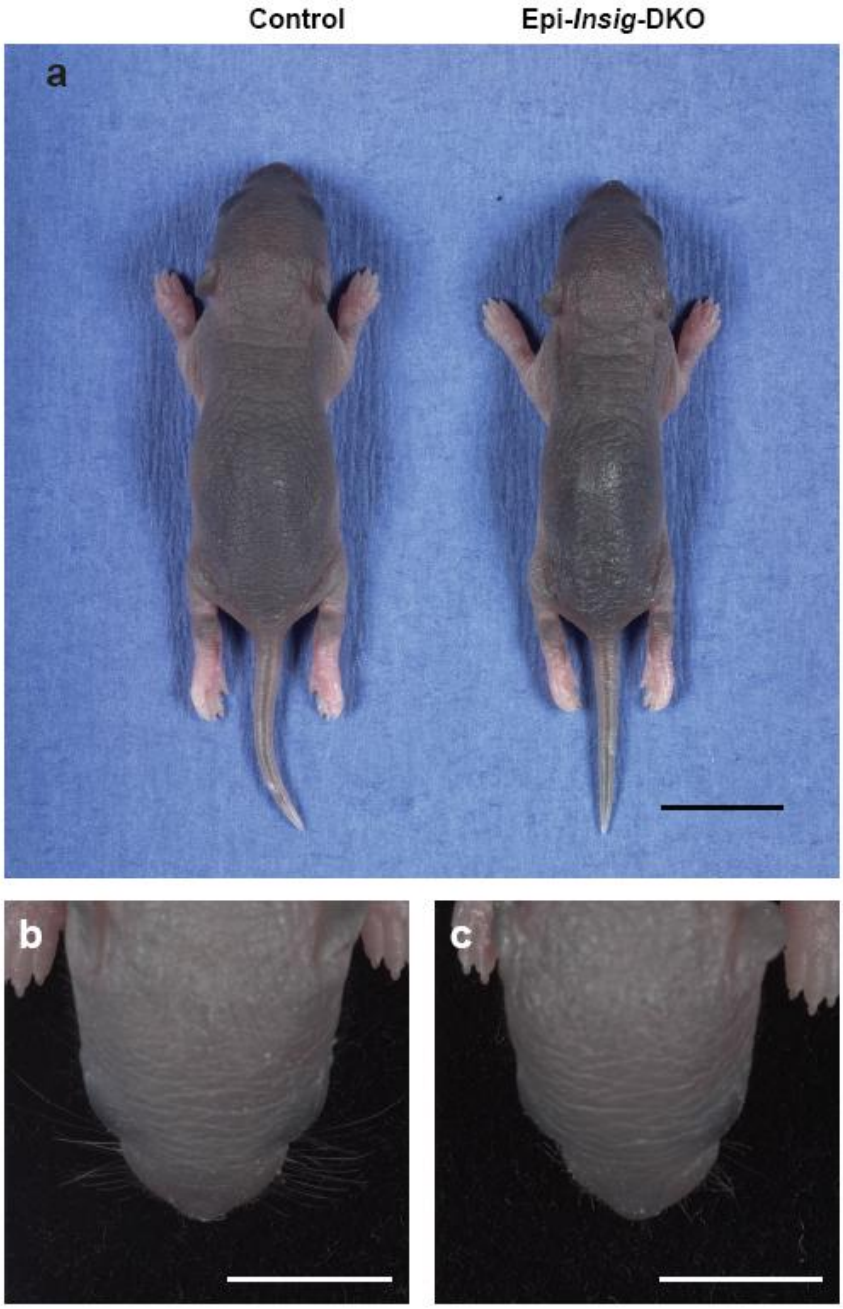

Figure 3-2. Overall appearance of control and Epi-*Insig*-DKO mice. (**a–c**) Representative photographs of control and Epi-*Insig*-DKO littermate mice at PND 4 are shown. The head of each mouse (**b, c**) was photographed closer up with a top-down view on a black background to visualize the vibrissae in relief. Scale bars = 1.0 cm.

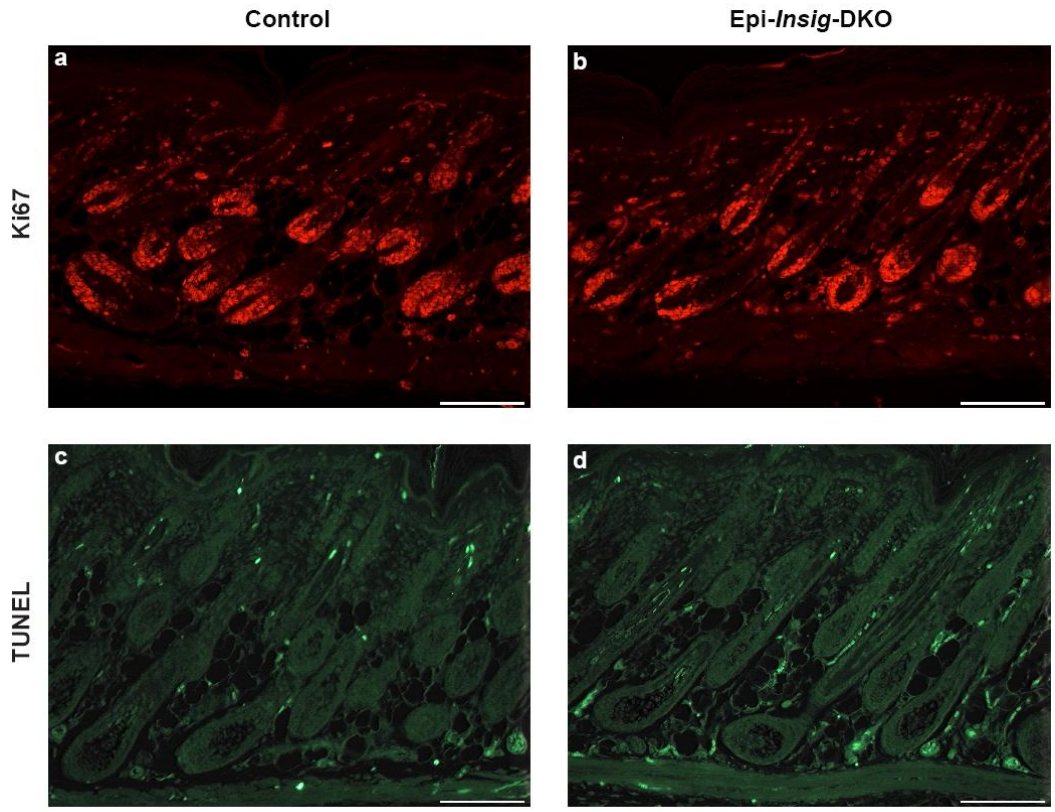

Figure 3-3. Proliferation and apoptosis of hair follicle cells. Skins from the upper back of PND 4 control and Epi-*Insig*-DKO mice were fixed, embedded in paraffin, and sectioned parallel to the hair shaft. (**a, b**) Hair follicle cell proliferation. These sections were then subjected to immunohistochemical staining with a mouse monoclonal antibody to Ki67, a marker for cell proliferation. (**c, d**) Hair follicle cell death. Skin sections from the mice above were also analyzed by terminal deoxynucleotidyl transferase dUTP nick end labeling (TUNEL), which marks cells undergoing apoptosis. Sections representative of the three mice in each group are shown (**a-d**). Scale bars = 0.1 mm.

Table 1

mRNA levels of developmental pathway genes in Epi-Insig-DKO mice relative to control mice, fold change

	PND 4		PND 7	
	Control	Epi-*Insig*-DKO	Control	Epi-*Insig*-DKO
Insig-1	1 ± 0.08	0.22 ± 0.04	1 ± 0.17	0.11 ± 0.02
Shh	1 ± 0.09	0.79 ± 0.07	1 ± 0.02	0.93 ± 0.11
Patched-1	1 ± 0.14	0.90 ± 0.02	1 ± 0.06	0.80 ± 0.09
Smoothened	1 ± 0.09	0.86 ± 0.04	1 ± 0.05	0.99 ± 0.06
Gli-1	1 ± 0.15	0.85 ± 0.04	1 ± 0.04	0.80 ± 0.08
Wnt-5a	1 ± 0.05	0.62 ± 0.10	1 ± 0.07	0.69 ± 0.05
Wnt-10b	1 ± 0.05	0.63 ± 0.12	1 ± 0.11	1.01 ± 0.08
Frizzled-1	1 ± 0.08	0.70 ± 0.10	1 ± 0.07	1.04 ± 0.06
APC	1 ± 0.13	0.87 ± 0.10	1 ± 0.04	1.00 ± 0.04
GSK-3β	1 ± 0.13	0.92 ± 0.08	1 ± 0.04	0.98 ± 0.04
Axin-2	1 ± 0.13	0.81 ± 0.11	1 ± 0.04	0.91 ± 0.05
β-catenin	1 ± 0.21	0.76 ± 0.12	1 ± 0.05	0.85 ± 0.06
Tcf-1	1 ± 0.05	0.85 ± 0.01	1 ± 0.07	0.71 ± 0.03
Lef-1	1 ± 0.04	0.67 ± 0.04	1 ± 0.03	0.60 ± 0.08

Table 3-1. Total RNA was derived from back skins and livers of postnatal day 4 (PND 4) littermate control (*Insig-1*$^{f/f}$*;Insig-2*$^{-/-}$) and Epi-*Insig*-DKO mice (*Krt14-Cre;Insig-1*$^{f/f}$*;Insig-2*$^{-/-}$). The relative amount of each mRNA was measured by quantitative real-time PCR using the comparative C_t method. Each bar represents the mean±SEM of data from four mice. Statistical analysis was performed with the two-tailed Student's t-test.

Table 2

mRNA levels of developmental pathway genes in Epi-Insig-DKO mice relative to control mice, Ct Values

	PND 4		PND 7	
	Control	Epi-*Insig* -DKO	Control	Epi-*Insig* -DKO
Insig-1	23.03	25.59	22.42	25.63
Shh	23.81	24.53	24.42	24.49
Patched-1	23.00	23.44	23.65	23.88
Smoothened	24.12	24.63	24.34	24.25
Gli-1	23.58	24.11	24.34	24.57
Wnt-5a	24.36	25.41	24.38	24.81
Wnt-10b	26.05	27.08	26.40	26.29
Frizzled-1	24.40	25.27	24.46	24.31
APC	23.63	24.24	23.68	23.60
GSK3-β	22.26	22.81	22.36	22.31
Axin-2	24.26	24.97	24.65	24.72
β-catenin	22.36	23.14	22.32	22.56
Tcf-1	24.89	25.50	24.61	25.10
Lef-1	23.23	24.19	23.11	23.85

Table 3-2. Total RNA was derived from back skins and livers of postnatal day 4 (PND 4) littermate control (*Insig-1*$^{f/f}$*;Insig-2*$^{-/-}$) and Epi-*Insig*-DKO mice (*Krt14-Cre;Insig-1*$^{f/f}$*;Insig-2*$^{-/-}$). The actual cycle threshold (C_t) numbers are given; each value represents the average of data from four mice.

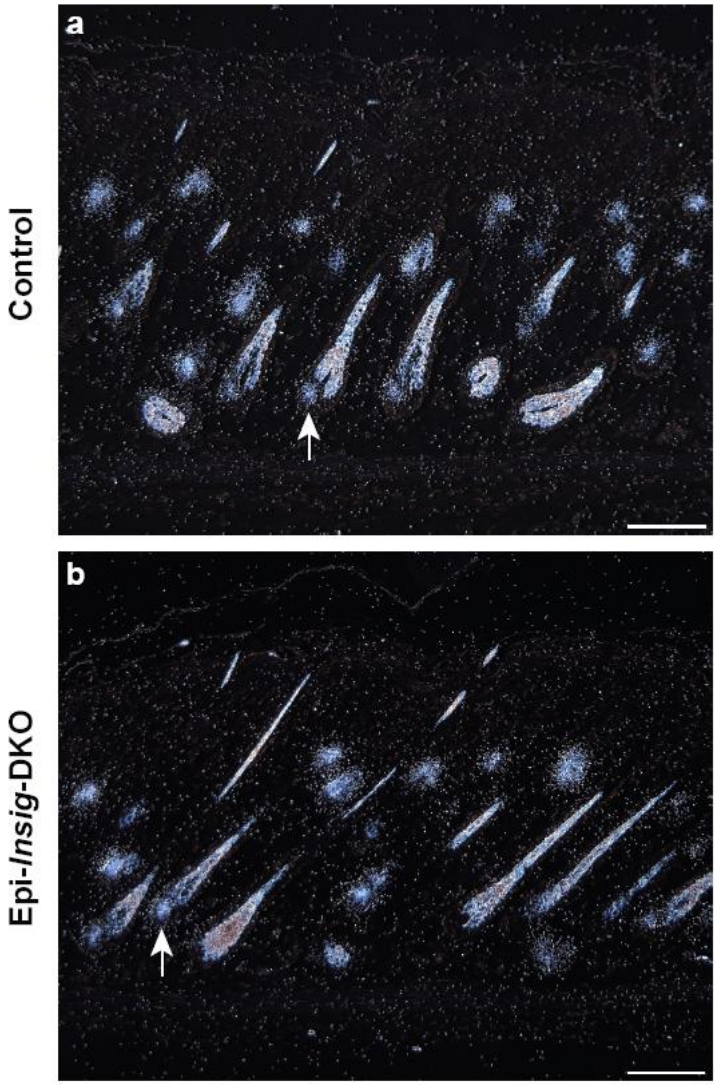

Figure 3-4. *In situ* hybridization of *Sonic hedgehog* mRNA. (**a, b**) Skins from the upper back of PND 4 control and Epi-*Insig*-DKO mice were fixed, embedded, and sectioned parallel to the hair shaft. These slides were then hybridized to a ^{35}S-labeled cRNA probe against Sonic hedgehog (Shh), coated with nuclear emulsion, and developed for 21 days. Low-magnification darkfield images of control (**a**) and mutant (**b**) skin sections representative of the three mice per group are shown. White arrows indicate areas of Shh expression. Scale bars = 0.1mm.

Table 3

List of genes downregulated in Epi-Insig-DKO mice versus control mice

WT Signal	KO Signal	Fold Chg	Gene Symbol	Gene Title
690.2	22.6	0.02	Krtap5-3	keratin associated protein 5-3
6006.6	209.3	0.04	Krtap28-13	keratin associated protein 28-13
3840.4	248.7	0.06	A030005K14	RIKEN cDNA A030005K14 - similar to Krtap5-2
4477.3	220.3	0.06	A030005L19	RIKEN cDNA A030005L19 - similar to Krtap5-2
918.9	49.2	0.08	Krtap5-4	keratin associated protein 5-4
6348.4	497.1	0.08	Krtap6-3	keratin associated protein 6-3
5074.2	680	0.11	665225	predicted gene, 665225 - similar to Krtap5-2
1804.8	169.2	0.12	Krtap5-1	keratin associated protein 5-1
5875	691.5	0.12	Krtap5-2	keratin associated protein 5-2
170.8	15.2	0.13	Hoxc10	homeo box C10
2794.7	369.8	0.13	Unknown	Hypothetical: similar to Krtap 5-5
6075.1	786.2	0.13	A030003K21	RIKEN cDNA A030003K21 - similar to Krtap5-2
1598.6	180	0.16	Krtap5-1	keratin associated protein 5-1
5681.9	981.3	0.18	A030014E15	RIKEN cDNA A030014E15 - similar to Krtap5-2
199.1	38.6	0.22	Crisp1	cysteine-rich secretory protein 1
9556	2154.1	0.22	Krtap16-9	keratin associated protein 16-9
1185.2	254.1	0.27	Tmem87a	transmembrane protein 87A
1548.8	413.8	0.27	Insig1	insulin induced gene 1
900.3	258.2	0.29	Hoxa9	homeo box A9
1456.3	393.8	0.29	Krtap12-1	keratin associated protein 12-1
7319.2	2144.4	0.29	Krtap16-4	keratin associated protein 16-4
9983.9	3095.2	0.29	Krtap6-2	keratin associated protein 6-2
128.4	31.4	0.31	Hoxa10	homeo box A10
277.3	103.8	0.31	Cps1	carbamoyl-phosphate synthetase 1
367.9	123	0.31	Pldn	pallidin

Table 3-3. For each group, total RNA from the skin of four mice (in each group) was pooled and prepared for Affymetrix oligonucleotide hybridization as described in *Methods*. The relative mRNA expression of each transcript in Epi-*Insig*-DKO skin relative to that in control skin is shown. Genes are listed in ascending order from those most decreased to those less decreased.

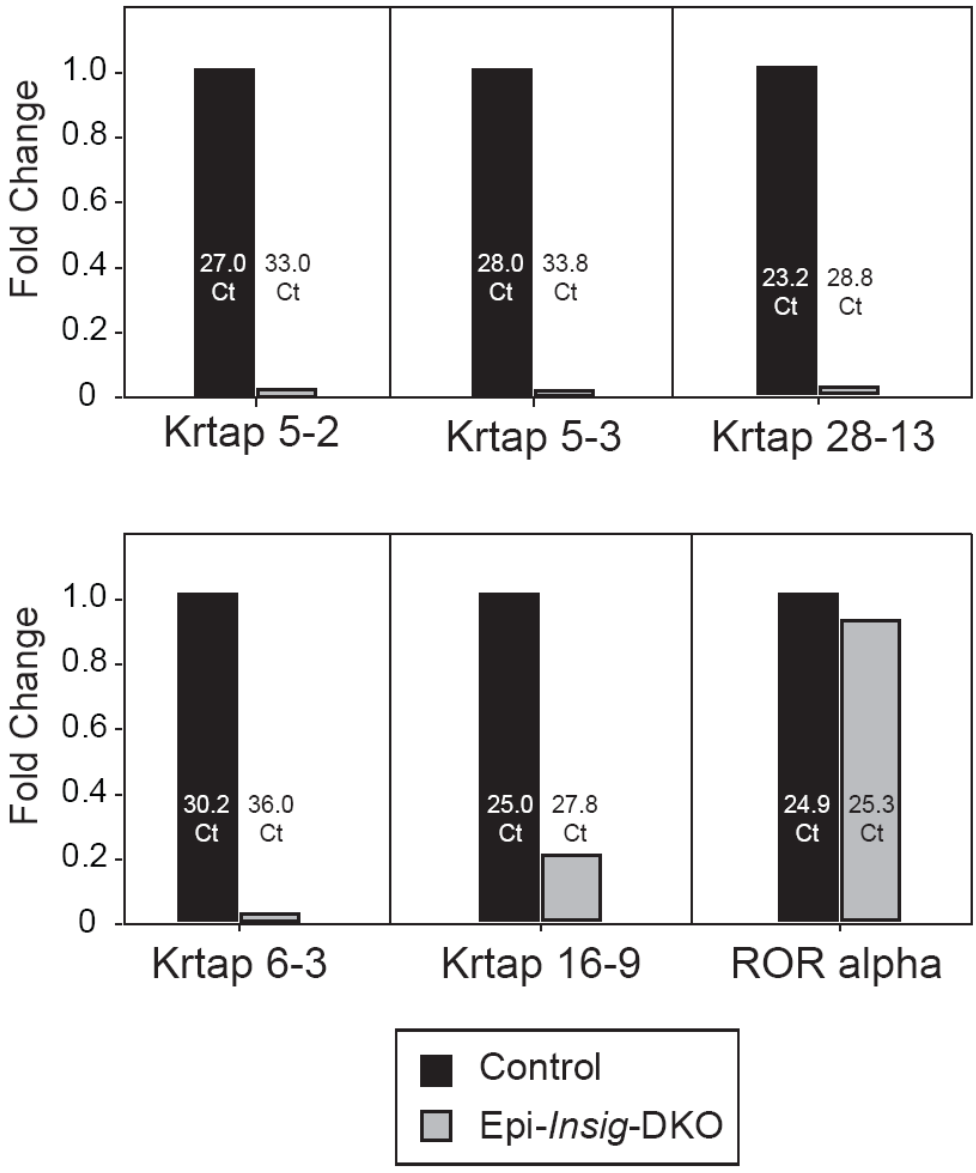

Figure 3-5. mRNA expression of different Krtap family members. Total RNA was isolated from the back skin of PND 4 control and Epi-*Insig*-DKO mice. The relative amount of mRNA of various keratin-associated proteins (Krtaps) was measured by quantitative real-time PCR using the comparative C_t method. Each bar represents the mean of data from four mice. The actual cycle threshold (C_t) numbers are given inside the bars.

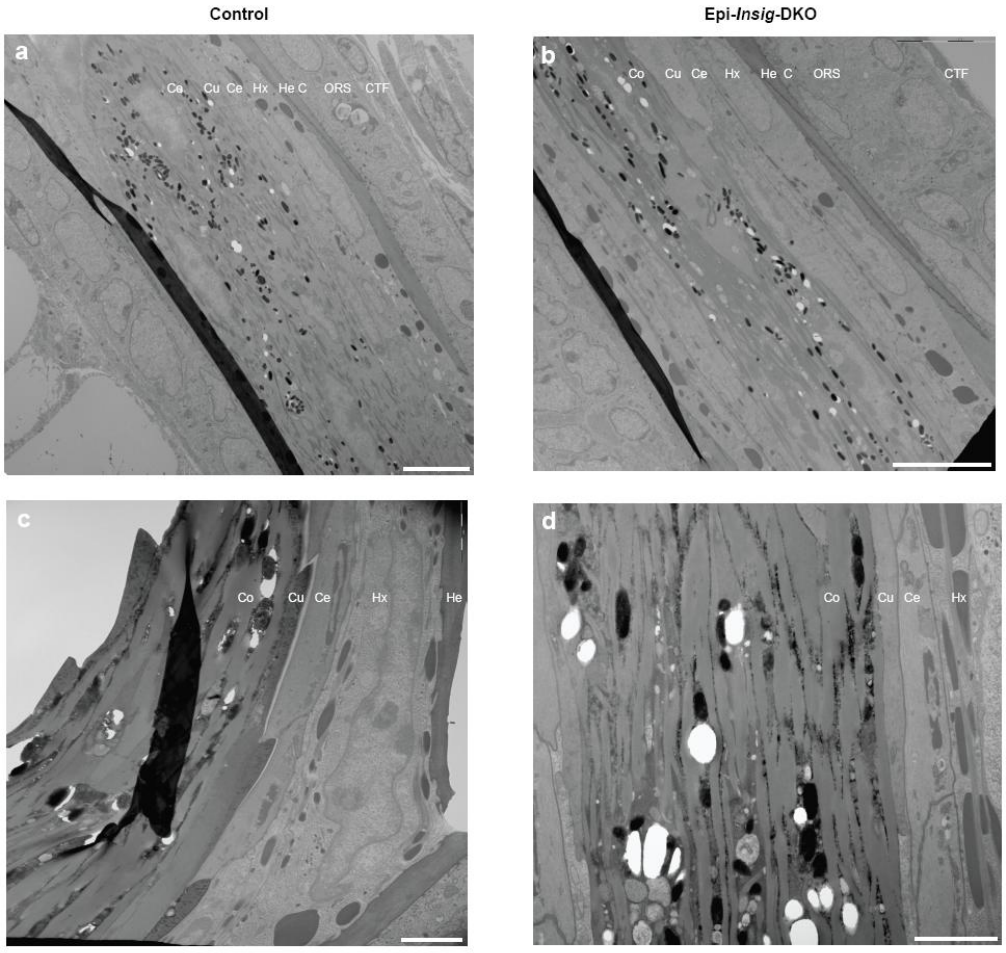

Figure 3-6. Transmission electron microscopy of hair follicles. (a-d) Dorsal skins from PND 4 control and Epi-*Insig*-DKO mice were fixed, treated with osmium tetroxide, and embedded in epoxy resin. Ultrathin sections (parallel to the hair shaft) cut from these samples were then stained with uranyl acetate and lead citrate. Skin sections of control (**a, c**) and mutant (**b, d**) mice are shown. Abbreviations: Co (cortex), Cu (hair cuticle), Ce (IRS cuticle), Hx (Huxley's layer), He (Henle's layer), C (companion layer, ORS (outer root sheath), CTS (connective tissue sheath). Scale bars = 10μm (**a, b**), 2μm (**c, d**).

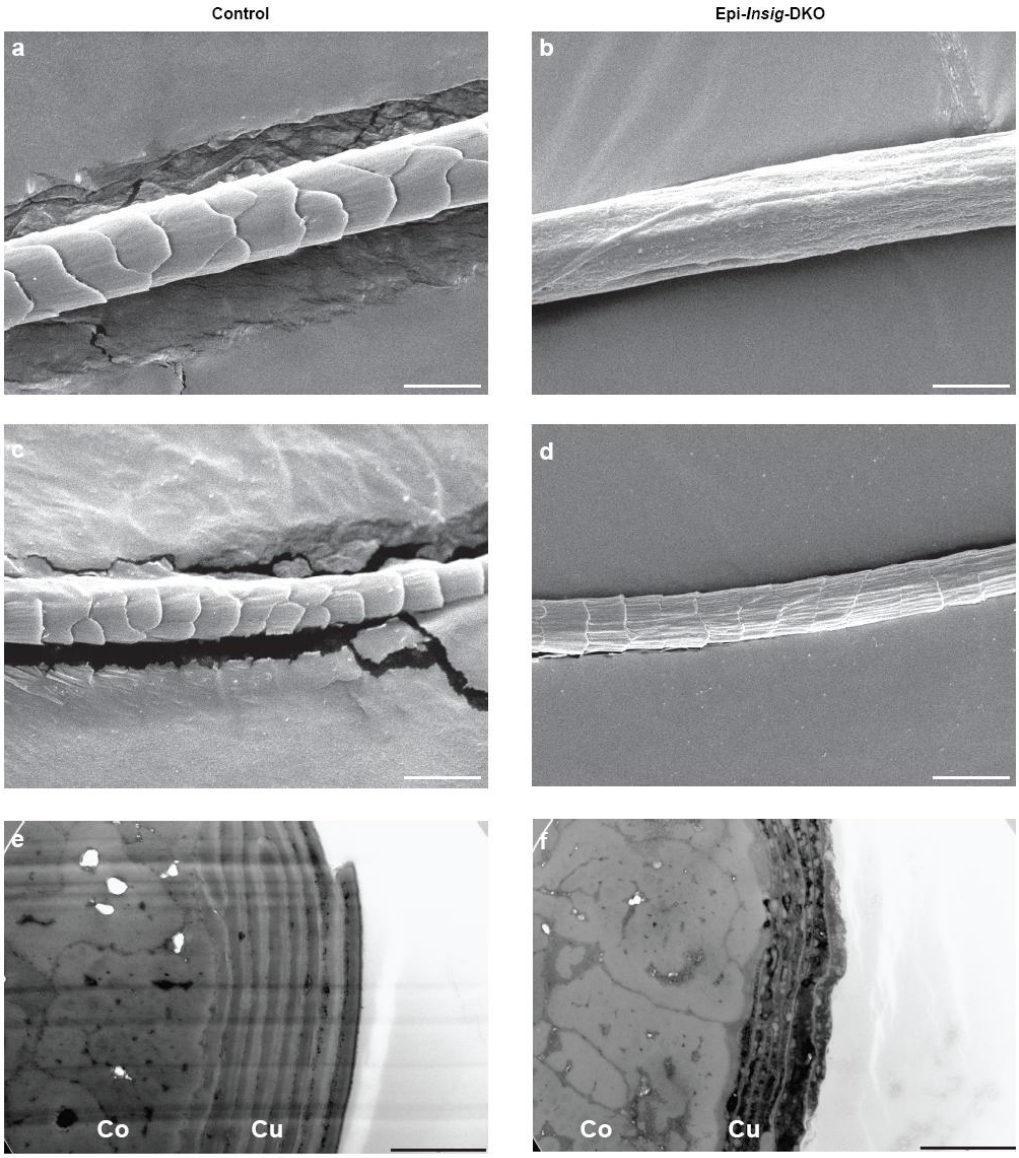

Figure 3-7. Scanning electron microscopy of hair follicles. (a-d) Vibrissae from PND 4 control and Epi-*Insig*-DKO mice were washed with water, air-dried, then coated with gold. Samples were then visualized using a scanning electron microscope. At least three whiskers from each mouse (n=3/group) were analyzed and representative images of vibrissae from control (**a, c**) and Epi-*Insig*-DKO (**b, d**) mice are shown. (**e, f**) Vibrissae were fixed, treated with osmium tetroxide, and embedded in epoxy resin. Ultrathin sections (perpendicular to the hair shaft) cut from these samples were then stained with uranyl acetate and lead citrate. Images of whiskers from control (**e**) and Epi-*Insig*-DKO (**f**) mice are shown. Co (cortex), Cu (hair cuticle). Scale bars = 10μm (**a-d**), 1μm (**e, f**).

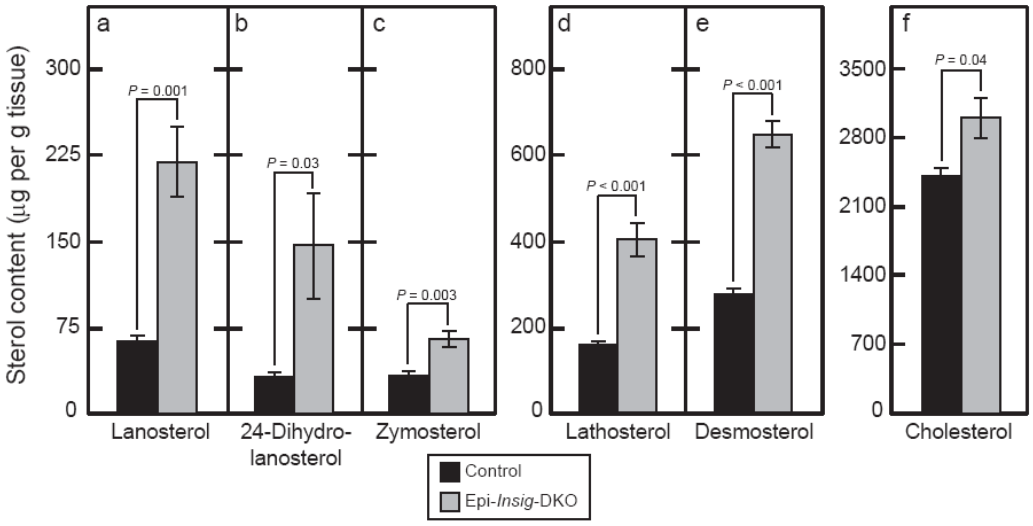

Figure 3-8. Sterol content in the skin of control and Epi-*Insig*-DKO mice. (**a-f**) On PND 4, skin from the upper back was harvested from littermate control and mutant mice. These samples were then processed for and subjected to gas chromatography–mass spectroscopy as described in *Methods*. The amounts of cholesterol and five of the sterol intermediates that precede it were measured. Each bar represents the mean±SEM of data from five mice. Statistical analysis was performed with the two-tailed Student's t-test.

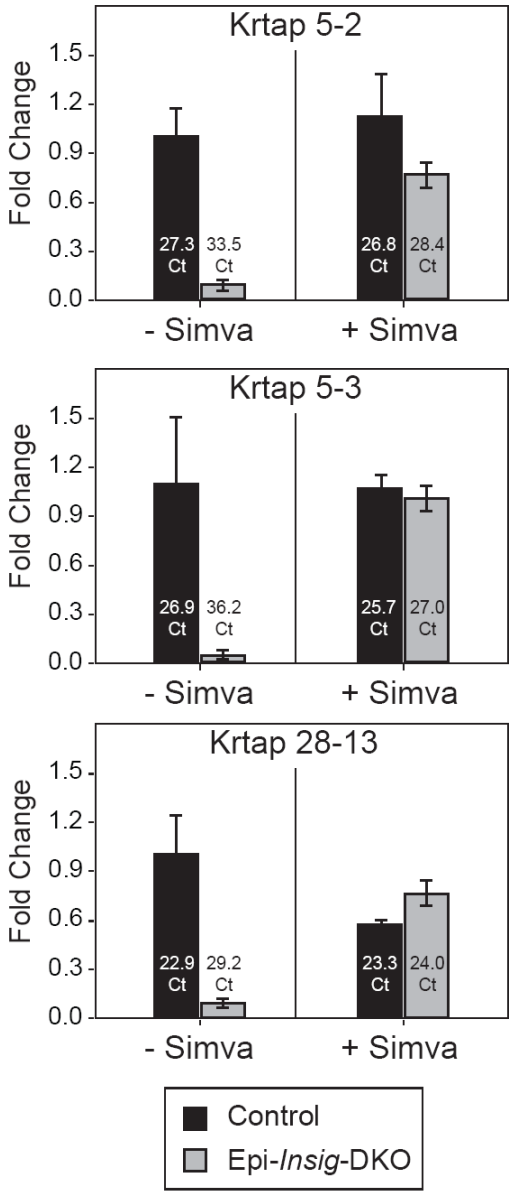

Figure 3-9. mRNA expression of different Krtap family members in control and Epi-*Insig*-DKO mice treated with or without simvastatin. Littermate control and Epi-*Insig*-DKO mice were treated daily with either 1mg simvastatin or vehicle from PND 1 to PND 4. Total RNA was isolated from the back skin of PND 4 control and Epi-*Insig*-DKO mice. The relative amount of mRNA of various keratin-associated proteins (Krtaps) was measured by quantitative real-time PCR using the comparative C_t method. Each bar represents the mean±SEM of data from four mice. The actual cycle threshold (C_t) numbers are shown inside the bars. Statistical analysis was performed with the two-tailed Student's t-test.

CHAPTER FOUR
Conclusion

The studies shown here underscore yet another role, unappreciated up until now, that cholesterol and its biosynthetic sterol intermediates play in mammalian life. It also highlights the importance of the feedback regulatory system that maintains cholesterol homeostasis and how Insigs are critical for this system to operate properly. Indeed, the feedback regulatory system evolved not only to maintain adequate amounts of cholesterol, but also to keep the levels of its precursor sterols in check as not doing so can lead to many developmental consequences.

These adverse effects on development range from alopecia to cleft palate. Since the mechanism by which Insig loss leads to craniofacial defects has been discussed elsewhere (Evers, 2009), the current discussion will focus on the pathogenesis of alopecia in *Insig*-deficient mice and some related phenotypes. Chapter 1 demonstrated that when Insigs were ablated in the epidermis (Epi-*Insig*-DKO), mutant mice failed to grow body hair as their hair follicles arrested in late follicular morphogenesis. Furthermore, sterol intermediates were increased in the skin of mutant mice and could be lowered by topical treatment with simvastatin; doing so completely reversed the hair loss seen in these mice.

Chapter 2 then went on to reveal a molecular change that preceded this defect in hair eruption. The expression of class of genes known as keratin-associated proteins (Krtaps) was lost in the skin of Epi-*Insig*-DKO mice. This deficiency was also associated with accumulation of sterol precursors in mutant epidermis and topical treatment of Epi-*Insig*-DKO mice with simvastatin could restore *Krtap* expression.

The loss of *Krtap* expression was significant as it led to the formation of abnormal hair shaft cuticles in mutant follicles. Importantly, electron microscopic studies showed that a hair shaft cuticle layer was not absent in Epi-*Insig*-DKO hair follicles, but that it failed to completely keratinize and organize into its proper structure. An abnormal hair shaft cuticle helps explain the alopecia in our mutant mice, since this layer typically forms an interlocking structure with the cuticle of the inner root sheath; a partnership essential to the smooth upwards growth and eruption of the hair fiber.

A major question that remains is how Insig-deficiency brings about the loss of *Krtap* expression. We hypothesized that a transcription factor existed which was responsible for the expression of all ultrahigh sulfur *Krtaps* and whose function was altered by sterol accumulation. In an attempt to find this protein, we carried out bioinformatics analysis with the help of one of our colleagues, David Meredith. We searched for common sequence elements in the promoters of genes in the *Krtap5* family as their expression was the most affected out of all the *Krtaps* we examined. One of the elements identified by this study was 'ATTGAGTAGGTCA', a sequence that bore great similarity to the canonical binding site for retinoic acid receptor-related orphan receptor α (RORα): a core nuclear receptor sequence 'RGGTCA' preceded by a 6-base pair AT-rich tract (Giguère *et al.*, 1994). We thereby posited this protein as a major transcriptional activator of the *Krtap5* family.

Many other lines of evidence favored RORα as a candidate. Being a nuclear receptor, RORα could directly bind DNA and activate transcription. However, it could do this only in the presence of a ligand and, intriguingly, two known ligands for RORα included cholesterol and cholesterol sulfate (Kallen *et al.*, 2002). This fact raised the

possibility that Insig-deficiency and sterol intermediate accumulation could lead to potential RORα dysfunction. Furthermore, it was known that mice deficient in this protein had defects in hair growth (Steinmayr *et al.*, 1998). Encouragingly, we confirmed that RORα was expressed in mouse epidermis at PND 4 (Chapter 2, Figure 5).

Next, we tested whether RORα could activate transcription from a *Krtap5* gene promoter *in vitro* (Appendix A); unfortunately, it was unable to do so. Nor were we able to show—in cultured cells—that Insig-deficiency had any adverse effect on RORα function (Appendix B). These experiments make it unlikely that RORα dysfunction is the mechanism by which Insig-deficiency brings about the loss of *Krtap* expression. Nonetheless, given the specificity of ultrahigh sulfur *Krtap* mRNA loss, it is tempting to postulate the existence of a common transcription factor for this class of *Krtap* genes whose function becomes aberrant under conditions of sterol excess.

Discovery of such a protein would also aid in the formal demonstration of the observation that lack of Insigs causes alopecia by decreasing *Krtap* expression, as knocking out this transcription factor should give rise to a very similar phenotype. At present, such an experiment is very difficult to do given the number and functional redundancy amongst *Krtaps*; one would, in essence, have to eliminate expression of entire *Krtap* families. We could however further extend our studies by ablating Insigs specifically in the hair shaft cuticle layer using a Cre protein whose expression was under the control of a hair cuticle-specific keratin promoter. Such experiments would help strengthen the ideas put forth here.

Another observation regarding Epi-*Insig*-DKO mice, touched upon in Chapter 1, was their low body weight and smaller size, which led to them dying intermittently

between birth and weaning. Interestingly, this metabolic phenotype, like the alopecia, could be completely reversed by topical simvastatin treatment (Chapter 1, Fig 7). As this meant the phenotype was linked to Insig-deficiency, we decided to investigate further and began by characterizing the metabolic features of mutant mice in more detail.

We found that Epi-*Insig*-DKO mice were strikingly hypoglycemic as well as hypothermic (Appendix C), with the former manifesting around PND 7 and the latter by PND 14. Upon dissection, stomach weights were also lower in mutant animals implying poor feeding. As *K14-Cre* is expressed in the oral epithelia as well as the tongue (Wang *et al.*, 1997), this raised the question of whether these structures were abnormal in Epi-*Insig*-DKO mice and preventing them from feeding. Gross examination of the palatal and buccal epithelium plus the teeth and tongue revealed no differences between control and mutant mice. We also looked at these same tissues along with the esophagus, stomach, and all three parts of the small intestine histologically and came to the same conclusion.

It is possible though that *K14-Cre* expressed ectopically at some point in development in a place we failed to examine, e.g., a small specific location in the brain. Presumably, loss of Insigs at such a site could cause anomalous feeding behavior. Furthermore, if topically-applied simvastatin could enter the bloodstream, it would be able to reach this tissue and mitigate the effects of Insig loss (being lipophilic, simvastatin could also cross the blood-brain barrier). This scenario is unlikely, as we tested whether simvastatin was present systemically by measuring amounts of HMG-CoA reductase protein in the liver via immunoblotting. If simvastatin could reach all tissues, in the liver it would surely inhibit cholesterol biosynthesis and prompt upregulation of HMG-CoA reductase expression. However, there was no difference in levels of reductase

protein between livers of control mice given either vehicle or simvastatin; the same was true of livers of Epi-*Insig*-DKO mice.

A more likely possibility is that mutant mice feed poorly due to the fact that they have abnormal vibrissae. It has been shown that whisker removal increases the latency period for nipple attachment in rat neonates (Sullivan *et al.*, 2003), so such a scenario is not difficult to envision. It would also fit with why the metabolic defects were still seen in Epi-*Insig*-DKO even when litter sizes were small and they did not have to compete for food; they themselves are unable to feed well. Furthermore, given the proximity of the pups to one another during statin treatment, one can imagine some of the topical simvastatin solution finding its way onto the vibrissal pad.

It is my feeling that the metabolic phenotype of Epi-*Insig*-DKO is tied to the hair phenotype. I think that mutant mice feed less well than their siblings because of their abnormal vibrissae and that this causes them to become hypoglycemic soon after birth. The hypoglycemia prompts Epi-*Insig*-DKO mice to become hypothermic (as can happen in human patients), which is exacerbated when they develop alopecia. The increased energy required to generate body heat then causes these mice to become more hypoglycemic, which in turn further promotes their hypothermia, prompting a vicious cycle leading to their demise.

In all, this work furnishes insight into the abnormalities of hair and skin that are seen in human patients with inborn errors of cholesterol metabolism, diseases in which sterol precursors accumulate due to enzymatic defects in the cholesterol biosynthetic pathway. It is my hope that better treatments will be available for these patients in the future.

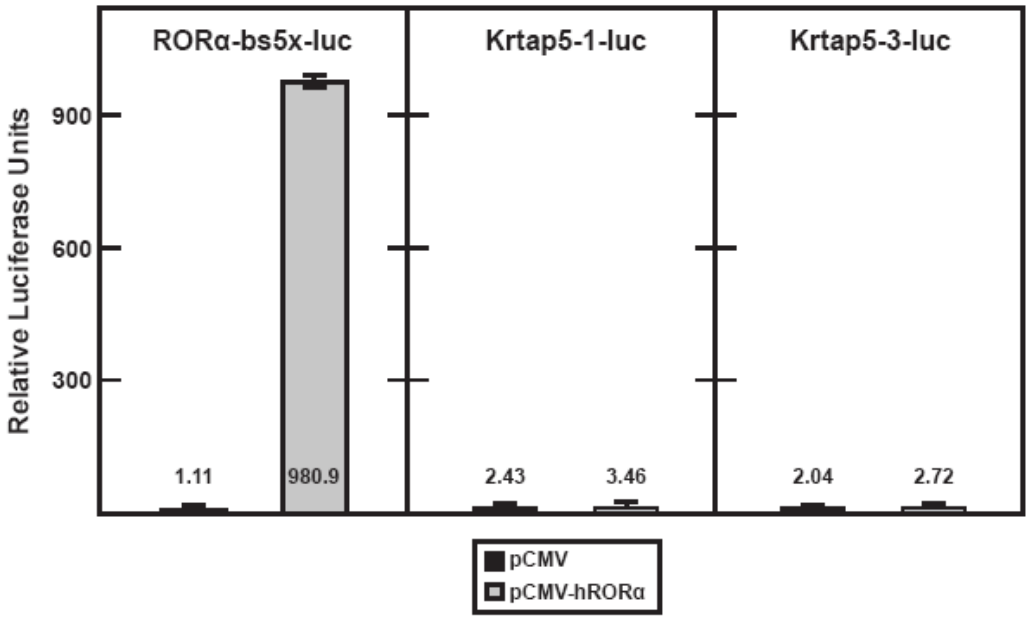

Figure 4-1. **RORα does not transactivate Krtap5 family promoters linked to luciferase *in vitro*.** An approximately 1000-base pair sequence that lay immediately upstream of the translational start site for Krtap5-1 was cloned and placed into a luciferase reporter vector (pGL4.10, Promega, Madison, WI); the same was done for Krtap5-3 (Krtap5-1-luc and Krtap5-3-luc). As a positive control, five copies of the canonical RORα binding site (arrayed in tandem) were placed into a luciferase reporter vector as well (RORα-5xbs-luc). These constructs were transfected into Cos-7 cells either with or without a human RORα expression vector (SC123126, OriGene, Rockville, MD). Twenty-four hours after transfection, cells were harvested in passive lysis buffer (Promega) and measured for dual luciferase activities with the Dual-Luciferase reporter assay system (Promega). Relative luciferase units were calculated as the ratio of firefly luciferase activity to Renilla luciferase activity. Each value represents the mean of two transfection experiments (each assayed in triplicate).

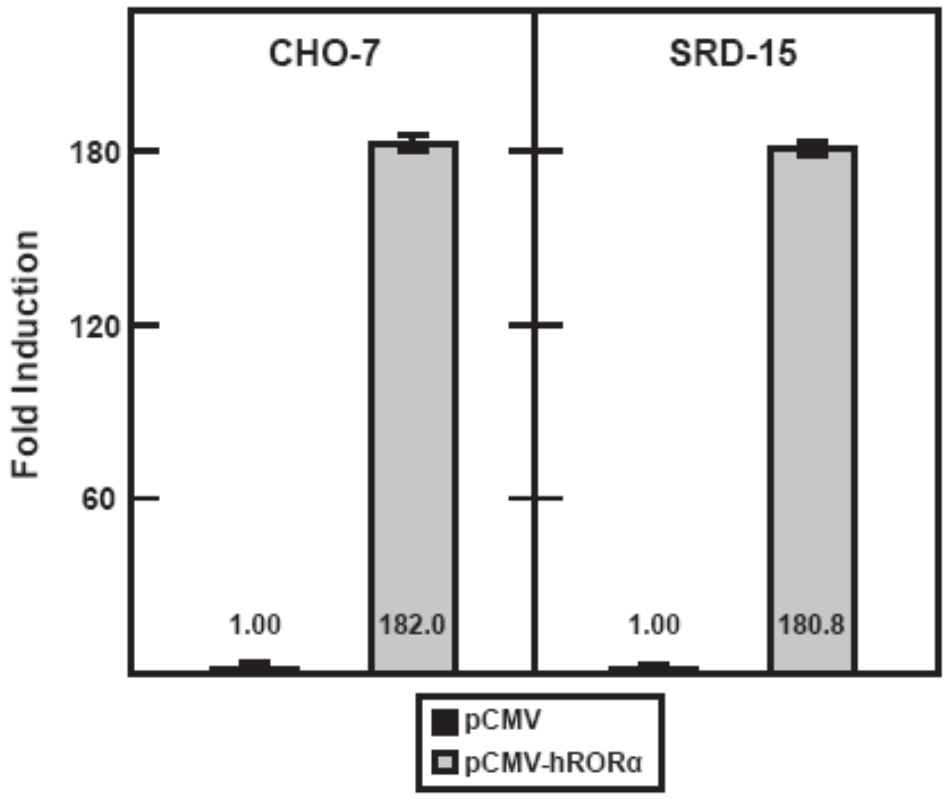

Figure 4-2 Insig-deficiency does not affect the transcriptional activity of RORα *in vitro*. The positive control RORα-5xbs-luc was transfected either with or without a human RORα expression vector into a CHO-7 cell line deficient in both Insig-1 and Insig-2 (SRD-15) as well as normal CHO-7 cells. Twenty-four hours after transfection, cells were harvested in passive lysis buffer (Promega) and measured for dual luciferase activities with the Dual-Luciferase reporter assay system (Promega). The fold induction was calculated as the ratio of normalized luciferase activity in the presence of hRORα to that in the absence of hRORα. Each value represents the mean of two transfection experiments (each assayed in duplicate).

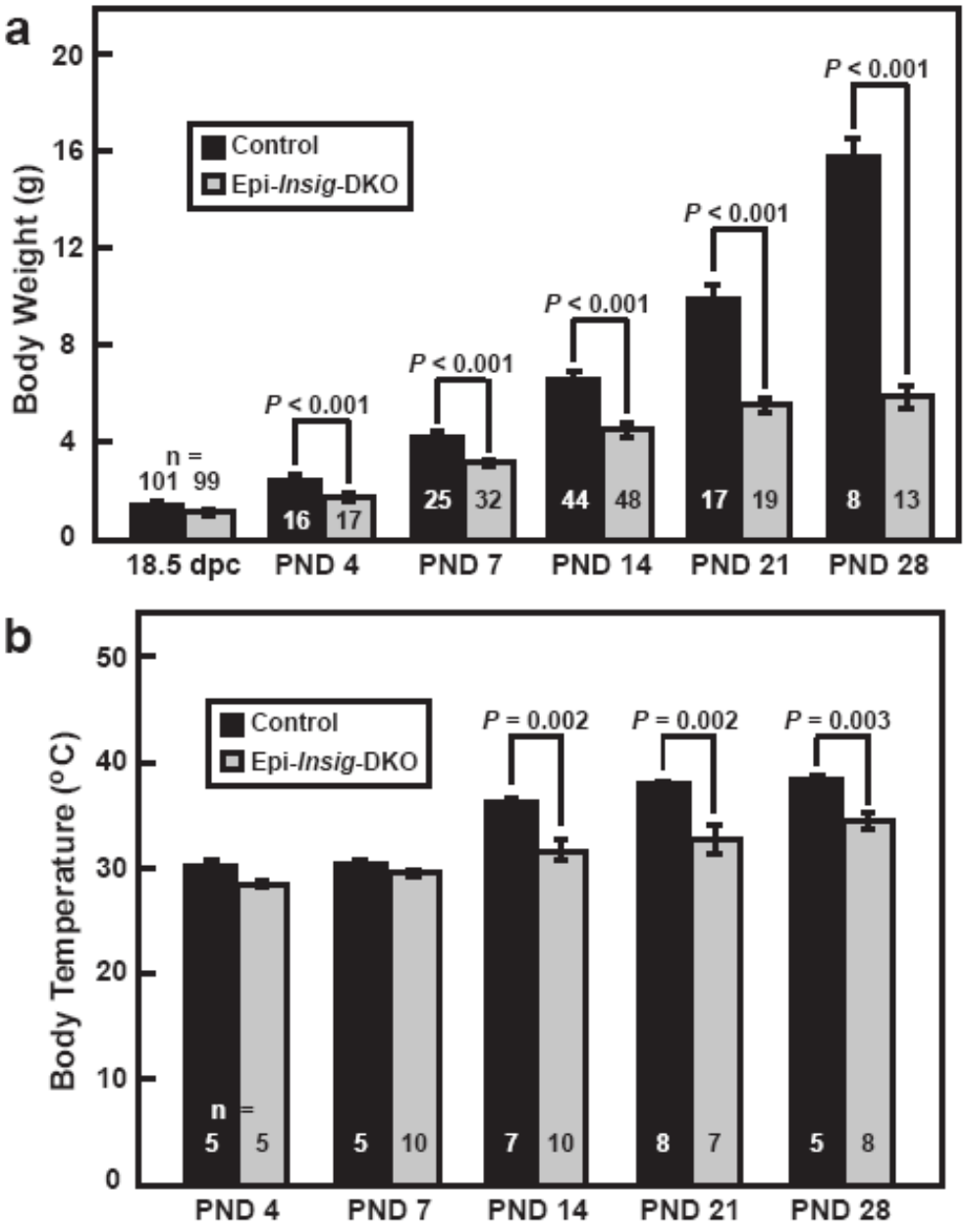

Figure 4-3. **Select metabolic parameters of control and Epi-*Insig*-DKO mice.** Body weights and temperatures of littermate control and Epi-*Insig*-DKO mice measured at various ages are shown (**a, b**). Each bar represents the mean±SEM of data from the indicated number of mice. Statistical analysis was performed with the two-tailed Student's t-test.

BIBLIOGRAPHY

Adams CM, Reitz J, De Brabander JK, Feramisco JD, Li L, Brown MS, Goldstein JL (2004) Cholesterol and 25-hydroxycholesterol inhibit activation of SREBPs by different mechanisms, both involving SCAP and Insigs. J. Biol. Chem 279:52772-52780

Alonso L, Fuchs E (2006) The hair cycle. J Cell Sci 119:391-393

Andersson HC, Kratz L, Kelley R (2002) Desmosterolosis presenting with multiple congenital anomalies and profound developmental delay. Am. J. Med. Genet 113:315-319

Anstey A (2006) School in photodermatology: Smith-Lemli-Opitz syndrome. Photodermatol Photoimmunol Photomed 22:200-204

Benavides F, Oberyszyn TM, VanBuskirk AM, Reeve VE, Kusewitt DF (2009) The hairless mouse in skin research. J. Dermatol. Sci 53:10-18

Blanpain C, Fuchs E (2006) Epidermal Stem Cells of the Skin. Annu Rev Cell Dev Biol 22:339-373

Blanpain C, Fuchs E (2009) Epidermal homeostasis: a balancing act of stem cells in the skin. Nat Rev Mol Cell Biol 10:207-217

Bloch K (1965) The biological synthesis of cholesterol. Science 150:19-28

Botchkarev VA, Sharov AA (2004) BMP signaling in the control of skin development and hair follicle growth. Differentiation 72:512-526

Bourne GH, Danielli J (1979) International review of cytology. Academic Press.

Brown MS, Ye J, Rawson RB, Goldstein JL (2000) Regulated intramembrane proteolysis: a control mechanism conserved from bacteria to humans. Cell 100:391-398

Brown MS, Goldstein JL (2009) Cholesterol feedback: from Schoenheimer's bottle to Scap's MELADL. J. Lipid Res 50 Suppl:S15-27

Buhaescu I, Izzedine H (2007) Mevalonate pathway: A review of clinical and therapeutical implications. Clinical Biochemistry 40:575-584

Chiang C, Swan RZ, Grachtchouk M, Bolinger M, Litingtung Y, Robertson EK, Cooper MK, Gaffield W, Westphal H, Beachy PA, Dlugosz AA (1999) Essential role for Sonic hedgehog during hair follicle morphogenesis. Dev. Biol 205:1-9

Dassule HR, Lewis P, Bei M, Maas R, McMahon AP (2000) Sonic hedgehog regulates growth and morphogenesis of the tooth. Development 127:4775-4785

Davidson P, Hardy MH (1952) The development of mouse vibrissae in vivo and in vitro. J. Anat 86:342-356

DeBose-Boyd RA, Brown MS, Li WP, Nohturfft A, Goldstein JL, Espenshade PJ (1999) Transport-dependent proteolysis of SREBP: relocation of site-1 protease from Golgi to ER obviates the need for SREBP transport to Golgi. Cell 99:703-712

DeBose-Boyd RA (2008) Feedback Regulation of Cholesterol Synthesis. Cell Res 18:609-621

Denecke J, Kranz C (2009) Hypoglycosylation due to dolichol metabolism defects. Biochimica et Biophysica Acta (BBA) - Molecular Basis of Disease 1792:888-895

Elias ER, Irons MB, Hurley AD, Tint GS, Salen G (1997) Clinical effects of cholesterol supplementation in six patients with the Smith-Lemli-Opitz syndrome (SLOS). Am. J. Med. Genet 68:305-310

Endo A (2010) A historical perspective on the discovery of statins. Proc. Jpn. Acad., Ser. B, Phys. Biol. Sci 86:484-493

Engelking LJ, Evers BM, Richardson JA, Goldstein JL, Brown MS, Liang G (2006) Severe facial clefting in Insig-deficient mouse embryos caused by sterol accumulation and reversed by lovastatin. J. Clin. Invest 116:2356-2365

Engelking LJ, Liang G, Hammer RE, Takaishi K, Kuriyama H, Evers BM, Li W, Horton JD, Goldstein JL, Brown MS (2005a) Schoenheimer effect explained--feedback regulation of cholesterol synthesis in mice mediated by Insig proteins. J. Clin. Invest 115:2489-2498

Engelking LJ, Liang G, Hammer RE, Takaishi K, Kuriyama H, Evers BM, Li W, Horton JD, Goldstein JL, Brown MS (2005b) Schoenheimer effect explained--feedback regulation of cholesterol synthesis in mice mediated by Insig proteins. J. Clin. Invest 115:2489-2498

Espenshade PJ, Cheng D, Goldstein JL, Brown MS (1999) Autocatalytic processing of site-1 protease removes propeptide and permits cleavage of sterol regulatory element-binding proteins. J. Biol. Chem 274:22795-22804

Espenshade PJ, Hughes AL (2007) Regulation of sterol synthesis in eukaryotes. Annu. Rev. Genet 41:401-427

Estrach S, Ambler CA, Lo Celso C, Hozumi K, Watt FM (2006) Jagged 1 is a beta-catenin target gene required for ectopic hair follicle formation in adult epidermis. Development 133:4427-4438

Evers BM (2009) Role of Insig-Mediated Cholesterol Homeostasis in the Development of the Palate and Hair Follicles in Mice. Ph.D. Dissertation. University of Texas Southwestern Medical Center, Dallas, Texas.

Evers BM, Farooqi MS, Shelton JM, Richardson JA, Goldstein JL, Brown MS, Liang G (2010) Hair growth defects in Insig-deficient mice caused by cholesterol precursor accumulation and reversed by simvastatin. J. Invest. Dermatol 130:1237-1248

Feingold KR, Man MQ, Menon GK, Cho SS, Brown BE, Elias PM (1990) Cholesterol synthesis is required for cutaneous barrier function in mice. J. Clin. Invest 86:1738-1745

Feingold KR (2009) The outer frontier: the importance of lipid metabolism in the skin. J. Lipid Res 50 Suppl:S417-422

Fraser A (1951) Growth of the mouse coat. Journal of Experimental Zoology 117:15-29

Funda DP, Houstěk J, Holub M, Kazdová L, Michalský M, Burýsek L, Cervinková M, Síma P (1998) Differences in thermoregulation between immunocompetent and immunodeficient hairless mice exposed to mild cold. Folia Microbiol. (Praha) 43:487-489

Gibson DM, Parker RA, Stewart CS, Evenson KJ (1982) Short-term regulation of hydroxymethylglutaryl coenzyme A reductase by reversible phosphorylation: modulation of reductase phosphatase in rat hepatocytes. Adv. Enzyme Regul 20:263-283

Giguère V, Tini M, Flock G, Ong E, Evans RM, Otulakowski G (1994) Isoform-specific amino-terminal domains dictate DNA-binding properties of ROR alpha, a novel family of orphan hormone nuclear receptors. Genes Dev 8:538-553

Gil G, Faust JR, Chin DJ, Goldstein JL, Brown MS (1985) Membrane-bound domain of HMG CoA reductase is required for sterol-enhanced degradation of the enzyme. Cell 41:249-258

Goldstein JL, Brown MS (1990) Regulation of the mevalonate pathway. Nature 343:425-430

Goldstein JL, Brown MS (2009) The LDL receptor. Arterioscler. Thromb. Vasc. Biol 29:431-438

Goldstein JL, DeBose-Boyd RA, Brown MS (2006) Protein sensors for membrane sterols. Cell 124:35-46

Gritli-Linde A (2007) Molecular control of secondary palate development. Dev. Biol 301:309-326

Gritli-Linde A, Hallberg K, Harfe BD, Reyahi A, Kannius-Janson M, Nilsson J, Cobourne MT, Sharpe PT, McMahon AP, Linde A (2007) Abnormal hair development and apparent follicular transformation to mammary gland in the absence of hedgehog signaling. Dev. Cell 12:99-112

Hardman MJ, Sisi P, Banbury DN, Byrne C (1998) Patterned acquisition of skin barrier function during development. Development 125:1541-1552

Herman GE (2003) Disorders of cholesterol biosynthesis: prototypic metabolic malformation syndromes. Hum. Mol. Genet 12 Spec No 1:R75-88

Horton JD, Goldstein JL, Brown MS (2002) SREBPs: activators of the complete program of cholesterol and fatty acid synthesis in the liver. J. Clin. Invest 109:1125-1131

Horton JD, Shah NA, Warrington JA, Anderson NN, Park SW, Brown MS, Goldstein JL (2003) Combined analysis of oligonucleotide microarray data from transgenic and knockout mice identifies direct SREBP target genes. Proc. Natl. Acad. Sci. U.S.A 100:12027-12032

Ikeda Y, Demartino GN, Brown MS, Lee JN, Goldstein JL, Ye J (2009) Regulated endoplasmic reticulum-associated degradation of a polytopic protein: p97 recruits proteasomes to Insig-1 before extraction from membranes. J. Biol. Chem 284:34889-34900

Jamora C, DasGupta R, Kocieniewski P, Fuchs E (2003) Links between signal transduction, transcription and adhesion in epithelial bud development. Nature 422:317-322

Jones LN, Rivett DE (1997) The role of 18-methyleicosanoic acid in the structure and formation of mammalian hair fibres. Micron 28:469-485

Kallen JA, Schlaeppi J, Bitsch F, Geisse S, Geiser M, Delhon I, Fournier B (2002) X-ray structure of the hRORalpha LBD at 1.63 A: structural and functional data that cholesterol or a cholesterol derivative is the natural ligand of RORalpha. Structure 10:1697-1707

Kelley RI, Herman GE (2001) Inborn errors of sterol biosynthesis. Annu Rev Genomics Hum Genet 2:299-341

Kim JB, Spotts GD, Halvorsen YD, Shih HM, Ellenberger T, Towle HC, Spiegelman BM (1995) Dual DNA binding specificity of ADD1/SREBP1 controlled by a single amino acid in the basic helix-loop-helix domain. Mol. Cell. Biol 15:2582-2588

Kiso M, Tanaka S, Saba R, Matsuda S, Shimizu A, Ohyama M, Okano HJ, Shiroishi T, Okano H, Saga Y (2009) The disruption of Sox21-mediated hair shaft cuticle differentiation causes cyclic alopecia in mice. Proceedings of the National Academy of Sciences 106:9292 -9297

Kurek D, Garinis GA, van Doorninck JH, van der Wees J, Grosveld FG (2007) Transcriptome and phenotypic analysis reveals Gata3-dependent signalling pathways in murine hair follicles. Development 134:261 -272

Li B, Mackay DR, Dai Q, Li TWH, Nair M, Fallahi M, Schonbaum CP, Fantes J, Mahowald AP, Waterman ML, Fuchs E, Dai X (2002) The LEF1/beta -catenin complex activates movo1, a mouse homolog of Drosophila ovo required for epidermal appendage differentiation. Proc. Natl. Acad. Sci. U.S.A 99:6064-6069

Liang G, Yang J, Horton JD, Hammer RE, Goldstein JL, Brown MS (2002) Diminished Hepatic Response to Fasting/Refeeding and Liver X Receptor Agonists in Mice with Selective Deficiency of Sterol Regulatory Element-binding Protein-1c. Journal of Biological Chemistry 277:9520 -9528

Liu XY, Dangel AW, Kelley RI, Zhao W, Denny P, Botcherby M, Cattanach B, Peters J, Hunsicker PR, Mallon AM, Strivens MA, Bate R, Miller W, Rhodes M, Brown SD, Herman GE (1999a) The gene mutated in bare patches and striated mice encodes a novel 3beta-hydroxysteroid dehydrogenase. Nat. Genet 22:182-187

Liu XY, Dangel AW, Kelley RI, Zhao W, Denny P, Botcherby M, Cattanach B, Peters J, Hunsicker PR, Mallon AM, Strivens MA, Bate R, Miller W, Rhodes M, Brown SD, Herman GE (1999b) The gene mutated in bare patches and striated mice encodes a novel 3beta-hydroxysteroid dehydrogenase. Nat. Genet 22:182-187

Logan CY, Nusse R (2004) The Wnt signaling pathway in development and disease. Annu. Rev. Cell Dev. Biol 20:781-810

Mathers CD, Loncar D (2006) Projections of Global Mortality and Burden of Disease from 2002 to 2030. PLoS Med 3:e442

McNamara JR, Warnick GR, Cooper GR (2006) A brief history of lipid and lipoprotein measurements and their contribution to clinical chemistry. Clinica Chimica Acta 369:158-167

Mirza R, Hayasaka S, Takagishi Y, Kambe F, Ohmori S, Maki K, Yamamoto M, Murakami K, Kaji T, Zadworny D, Murata Y, Seo H (2006) DHCR24 gene knockout mice demonstrate lethal dermopathy with differentiation and maturation defects in the epidermis. J. Invest. Dermatol 126:638-647

Miyai M, Tanaka YG, Kamitani A, Hamada M, Takahashi S, Kataoka K (2010) c-Maf and MafB transcription factors are differentially expressed in Huxley's and Henle's layers of the inner root sheath of the hair follicle and regulate cuticle formation. J. Dermatol. Sci 57:178-182

Morioka K (2004) *Hair follicle: differentiation under electron microscope : an atlas.* Springer-Verlag: Tokyo, 152pp.

Morioka K (2009) A guide to hair follicle analysis by transmission electron microscopy: technique and practice. Exp. Dermatol 18:577-582

Muller-Rover S, Handjiski B, van der Veen C, Eichmuller S, Foitzik K, McKay IA, Stenn KS, Paus R (2001) A Comprehensive Guide for the Accurate Classification of Murine Hair Follicles in Distinct Hair Cycle Stages. 117:3-15

Murray RK, Granner DK, Rodwell VW (2006) Harper's illustrated biochemistry. Lange Medical Books/McGraw-Hill.

Nohturfft A, Brown MS, Goldstein JL (1998) Topology of SREBP Cleavage-activating Protein, a Polytopic Membrane Protein with a Sterol-sensing Domain. Journal of Biological Chemistry 273:17243 -17250

Ohnemus U, Uenalan M, Inzuna J, Gustafsson JA, Paus R (2006) The hair follicle as an estrogen target and source . Endocr Rev 27: 677-706.

Oro AE, Higgins K (2003) Hair cycle regulation of Hedgehog signal reception. Developmental Biology 255:238-248

Panico R, International Union of Pure and Applied Chemistry. (1993) A guide to IUPAC nomenclature of organic compounds : recommendations 1993. Oxford ;;Boston ;Boca Raton Fla.: Blackwell Scientific Publications ;;CRC Press [distributor].

Paus R, Muller-Rover S, van der Veen C, Maurer M, Eichmuller S, Ling G, Hofmann U, Foitzik K, Mecklenburg L, Handjiski B (1999) A Comprehensive Guide for the Recognition and Classification of Distinct Stages of Hair Follicle Morphogenesis. 113:523-532

Persson B, Esberg B, Ólafsson Ó, Björk G (1994) Synthesis and function of isopentenyl adenosine derivatives in tRNA. Biochimie 76:1152-1160

Porter FD (2003) Human malformation syndromes due to inborn errors of cholesterol synthesis. Curr. Opin. Pediatr 15:607-613

Porter FD (2002) Malformation syndromes due to inborn errors of cholesterol synthesis. J Clin Invest 110:715-724

Porter JA, Young KE, Beachy PA (1996) Cholesterol modification of hedgehog signaling proteins in animal development. Science 274:255-259

Posnett DN, McGrath H, Tam JP (1988) A novel method for producing anti-peptide antibodies. Production of site-specific antibodies to the T cell antigen receptor beta-chain. J. Biol. Chem 263:1719-1725

Potter CS, Peterson RL, Barth JL, Pruett ND, Jacobs DF, Kern MJ, Argraves WS, Sundberg JP, Awgulewitsch A (2006) Evidence that the satin hair mutant gene Foxq1 is among multiple and functionally diverse regulatory targets for Hoxc13 during hair follicle differentiation. J. Biol. Chem 281:29245-29255

Radhakrishnan A, Ikeda Y, Kwon HJ, Brown MS, Goldstein JL (2007) Sterol-regulated transport of SREBPs from endoplasmic reticulum to Golgi: oxysterols block transport by binding to Insig. Proc. Natl. Acad. Sci. U.S.A 104:6511-6518

Radhakrishnan A, Sun L, Kwon HJ, Brown MS, Goldstein JL (2004) Direct Binding of Cholesterol to the Purified Membrane Region of SCAP: Mechanism for a Sterol-Sensing Domain. Molecular Cell 15:259-268

Rogers GE (2004) Hair follicle differentiation and regulation. Int. J. Dev. Biol 48:163-170

Sakai J, Rawson RB, Espenshade PJ, Cheng D, Seegmiller AC, Goldstein JL, Brown MS (1998) Molecular identification of the sterol-regulated luminal protease that cleaves SREBPs and controls lipid composition of animal cells. Mol. Cell 2:505-514

Schlake T (2007) Determination of hair structure and shape. Seminars in Cell & Developmental Biology 18:267-273

Schmidt-Ullrich R, Paus R (2005) Molecular principles of hair follicle induction and morphogenesis. Bioessays 27:247-261

Schneider MR, Schmidt-Ullrich R, Paus R (2009) The hair follicle as a dynamic miniorgan. Curr. Biol 19:R132-142

Seabra MC, Brown MS, Goldstein JL (1993) Retinal degeneration in choroideremia: deficiency of rab geranylgeranyl transferase. Science 259:377-381

Sever N, Song B, Yabe D, Goldstein JL, Brown MS, DeBose-Boyd RA (2003) Insig-dependent Ubiquitination and Degradation of Mammalian 3-Hydroxy-3-methylglutaryl-CoA Reductase Stimulated by Sterols and Geranylgeraniol. Journal of Biological Chemistry 278:52479 -52490

Shelton JM, Lee M, Richardson JA, Patel SB (2000) Microsomal triglyceride transfer protein expression during mouse development. J. Lipid Res. 41:532-537

Shimomura I, Shimano H, Horton JD, Goldstein JL, Brown MS (1997) Differential expression of exons 1a and 1c in mRNAs for sterol regulatory element binding protein-1 in human and mouse organs and cultured cells. J. Clin. Invest 99:838-845

Shimomura Y, Aoki N, Rogers MA, Langbein L, Schweizer J, Ito M (2003) Characterization of Human Keratin-Associated Protein 1 Family Members. J Investig Dermatol Symp Proc 8:96-99

Smith JR, Osborne TF, Goldstein JL, Brown MS (1990) Identification of nucleotides responsible for enhancer activity of sterol regulatory element in low density lipoprotein receptor gene. J. Biol. Chem 265:2306-2310

Soma T, Ishimatsu-Tsuji Y, Tajima M, Kishimoto J (2006) Runx1 transcription factor is involved in the regulation of KAP5 gene expression in human hair follicles. J. Dermatol. Sci 41:221-224

Steinmayr M, André E, Conquet F, Rondi-Reig L, Delhaye-Bouchaud N, Auclair N, Daniel H, Crépel F, Mariani J, Sotelo C, Becker-André M (1998) staggerer phenotype in retinoid-related orphan receptor alpha-deficient mice. Proc. Natl. Acad. Sci. U.S.A 95:3960-3965

Stenn KS, Paus R (2001) Controls of Hair Follicle Cycling. Physiol. Rev. 81:449-494

St-Jacques B, Dassule HR, Karavanova I, Botchkarev VA, Li J, Danielian PS, McMahon JA, Lewis PM, Paus R, McMahon AP (1998) Sonic hedgehog signaling is essential for hair development. Curr. Biol 8:1058-1068

Sullivan RM, Landers MS, Flemming J, Vaught C, Young TA, Jonathan Polan H (2003) Characterizing the functional significance of the neonatal rat vibrissae prior to the onset of whisking. Somatosens Mot Res 20:157-162

Sun L, Seemann J, Goldstein JL, Brown MS (2007) Sterol-regulated transport of SREBPs from endoplasmic reticulum to Golgi: Insig renders sorting signal in Scap inaccessible to COPII proteins. Proc. Natl. Acad. Sci. U.S.A 104:6519-6526

Sundberg JP, Boggess D, Sundberg BA, Eilertsen K, Parimoo S, Filippi M, Stenn K (2000) Asebia-2J (Scd1ab2J): A New Allele and a Model for Scarring Alopecia. Am J Pathol 156:2067-2075

Sundberg JP (1994) *Handbook of mouse mutations with skin and hair abnormalities.* CRC Press: Tokyo, 544 pp.

Tauchi M, Fuchs TA, Kellenberger AJ, Woodward DF, Paus R, Lütjen-Drecoll E (2010) Characterization of an in vivo model for the study of eyelash biology and trichomegaly: mouse eyelash morphology, development, growth cycle, and anagen prolongation by bimatoprost. Br J Dermatol Available at: http://www.ncbi.nlm.nih.gov/pubmed/20346040 [Accessed August 14, 2010].

Wang X, Zinkel S, Polonsky K, Fuchs E (1997) Transgenic studies with a keratin promoter-driven growth hormone transgene: Prospects for gene therapy. Proceedings of the National Academy of Sciences of the United States of America 94:219 -226

Wang X, Bolotin D, Chu DH, Polak L, Williams T, Fuchs E (2006) AP-2alpha: a regulator of EGF receptor signaling and proliferation in skin epidermis. J. Cell Biol 172:409-421

Wang Y, McMahon AP, Allen BL (2007) Shifting paradigms in Hedgehog signaling. Curr. Opin. Cell Biol 19:159-165

Wu D, Irwin D, Zhang Y (2008) Molecular evolution of the keratin associated protein gene family in mammals, role in the evolution of mammalian hair. BMC Evolutionary Biology 8:241

Yabe D, Komuro R, Liang G, Goldstein JL, Brown MS (2003) Liver-specific mRNA for Insig-2 down-regulated by insulin: implications for fatty acid synthesis. Proc. Natl. Acad. Sci. U.S.A 100:3155-3160

Yang C, Cotsarelis G (2010) Review of hair follicle dermal cells. J. Dermatol. Sci 57:2-11

Zelenski NG, Rawson RB, Brown MS, Goldstein JL (1999) Membrane Topology of S2P, a Protein Required for Intramembranous Cleavage of Sterol Regulatory Element-binding Proteins. Journal of Biological Chemistry 274:21973 -2198